



NTNU – Trondheim
Norwegian University of
Science and Technology

Nucleation kinetics and polymorphism of calcium carbonate particles in natural gas production

Astrid Odland Barland

Chemical Engineering and Biotechnology

Submission date: June 2012

Supervisor: Jens-Petter Andreassen, IKP

Co-supervisor: Margrethe Nergaard, IKP

Norwegian University of Science and Technology
Department of Chemical Engineering

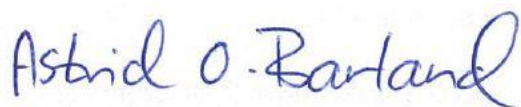
Preface

This master thesis was a mandatory part of the fifth year in the Chemical Engineering and Biotechnology Master's Degree Program at the Norwegian University of Science and Technology, NTNU. The master thesis was written the spring of 2012 on behalf of the Institute of Chemical Engineering (IKP). The title of the project was "*Nucleation kinetics and polymorphism of calcium carbonate particles in natural gas production*", and it was based on experimental work.

When working with a project of this extent, there are many people involved in the process that deserves a big thank. Firstly, I want to thank my supervisor, Jens-Petter Andreassen for good academic support throughout the semester. Then I would like to thank my co-supervisor, Margrethe Nergaard, for a close and inspiring cooperation - she always had time to listen to my ideas and worries concerning the project and supported me either in the lab, SEM or XRD. Other crucial key persons I would like to thank are the engineers Julian Tolchard introducing me to SEM and Geir Finnøy who helped me out in the laboratory when the technical equipment failed.

At last, but not least, I want to thank my two fellow students, Charlotte Kleven Krossholm and Torunn Kvam, for all the time we have spent together in the laboratory and in the working room. All the days we spent in the laboratory working and listening to feel-good music are worth the times of frustration during the semester!

I declare that this is an independent work according to the exam regulations of the Norwegian University of Science and Technology,



Astrid Odland Barland

Abstract

Precipitation of calcium carbonate in pipes and process equipment is a widespread problem in natural gas production as we know it today. Studies of calcium carbonate systems are crucial to prevent this problem.

When the mixture of natural gas and well water is to be transported towards the on shore facility, mono ethylene glycol (MEG) and sodium hydroxide (NaOH) are injected at the well head to prevent respectively plugs of hydrates in the pipelines and corrosion. Calcium-ions from the reservoir and iron-ions from corrosion in the steel pipelines can react with carbonate in the water/MEG-mixture and form particles. To prevent further precipitation and growth of calcium carbonate in process equipment, the particles are removed from the bulk in the MEG pre-treatment in the MEG regeneration loop. To know which conditions are optimal in removal of the nucleated particles, different aspects of the nucleation mechanism must be investigated.

The objective of this master thesis was to investigate the *kinetics* and *polymorphism* in a calcium carbonate system at varying parameters. The varying parameters were supersaturation, temperature and weight percent of MEG, and the experiments were denoted by (SR, T, w% MEG). The supersaturation was varied from 20 to 100, the temperature between 40 and 70 °C and the content of MEG between 0, 40 and 80 w%. Also variation in stoichiometry was investigated.

The nucleation rates were calculated on the basis of the induction times, which were determined experimentally. The induction time is defined as the time it takes before a supersaturated system starts to precipitate detectable crystals. Two different methods were tested to measure the induction time, the pH measurement method and the conductivity measurement method. The method chosen to determine the induction times in all the experiments was the pH measurement method because of the more stable results. It was found that induction time decreased with increasing supersaturation and/or temperature, while it increased with increasing content of MEG in the solution. When the activity ratio between calcium and carbonate was varied in the 40-40-0 experiment, it was found that the induction time increased when the ratio became > 1 .

The polymorphism obtained in the experiments were studied and characterized in a Scanning Electron Microscope (SEM) and by powder X-Ray Diffraction (powder-XRD). MEG decreased the size of the particles in the solutions, and only affected the polymorphism at the high MEG content of 80 w%. Variations in supersaturation and/or temperature gave different polymorphism in the experiments. Especially the polymorph *vaterite* changed morphologies when the supersaturation and/or the temperature was changed, and appeared as *flowers* at supersaturations ≥ 30 and a temperature of 40 °C and as *stars* at supersaturations ≥ 30 and a temperature of 70 °C.

Sammendrag

Utfelling av kalsiumkarbonat i rør og prosessutstyr er et omfattende problem i naturgassproduksjon slik vi kjenner det i dag. Studier av kalsiumkarbonatsystemer er nødvendige for å prøve å unngå dette problemet.

Når en miks av naturgass og brønnvann skal transporteres til et prosessanlegg på land, injiseres mono etylen glykol (MEG) og natriumhydroksid (NaOH) ved brønnhodet for å unngå henholdsvis plugging av gasshydrater og korrosjon i rørene. Kalsiumioner fra reservoaret og jernioner fra korrosjon i stålrørene kan reagere med karbonat i vann/MEG-blandingen og danne partikler. For å unngå utfelling av kalsiumkarbonat i prosessutstyr, separeres de utfelte partiklene fra bulken i forhåndsbehandlingen av MEG i MEG-regenereringsloopen. For å finne de optimale betingelsene for fjerning partiklene, må forskjellige aspekter ved nukleeringsmekanismen undersøkes.

Hensikten med denne masteroppgaven var å undersøke *kinetikk* og *polymorfisme* i et kalsiumkarbonatsystem ved varierende betingelser. De varierende betingelsene var overmetning, temperatur og vektprosent MEG, og eksperimentene ble angitt med parameterne (SR, T, v% MEG). Overmetningen ble variert fra 20 til 100, temperaturen mellom 40 og 70 °C og innholdet av MEG mellom 0, 40 og 80 v%. Også variasjon i støkiometrien mellom kalsium og karbonat ble undersøkt.

Nukleeringsratene ble kalkulert på grunnlag av induksjonstider som ble funnet eksperimentelt. Induksjonstid er definert som tiden det tar før et system starter å felle ut detekterbare partikler. To forskjellige metoder ble brukt for å måle induksjonstider, nemlig pH målinger og ledningsevne målinger. Metoden valgt til å bestemme induksjonstider var pH-metoden, da denne gav mest stabile resultater. Det ble funnet at induksjonstiden sank med økende overmetning og/eller temperatur, mens den økte med økende innhold av MEG i løsningen. Når aktivitetsbrøken mellom kalsium og karbonat ble endret i 40-40-0 forsøket, økte induksjonstiden når forholdet > 1.

Polymorfismen dannet i eksperimentene ble undersøkt i elektronmikroskop (SEM) og pulverrøntgen diffraksjon (pulver-XRD). MEG reduserte størrelsen på partiklene som ble utfelt, og påvirket kun polymorfismen ved det høye MEG-innholdet på 80 v%. Variasjon i overmetning og/eller temperatur gav endring i polymorfismen i eksperimentene. Særsilt polymorfen *vateritt* endret morfologi når overmetning og/eller temperatur ble variert, og dukket opp som *blomster* ved overmetninger ≥ 30 og temperatur på 40 °C og som *stjerner* ved overmetninger ≥ 30 og temperatur på 70 °C.

Table of contents

Preface.....	i
Abstract	ii
Sammendrag	iii
Table of contents.....	v
1 Introduction	1
2 Theory	3
2.1 Thermodynamics	3
2.1.1 The nucleation driving force	3
2.1.2 Thermodynamics in a solution	3
2.1.3 Thermodynamics in a carbonate system	4
2.2 Nucleation.....	9
2.2.1 Homogeneous nucleation	9
2.2.2 Heterogeneous nucleation.....	12
2.2.3 Induction time and nucleation rate	13
2.3 Crystal growth.....	19
2.3.1 Diffusion-reaction theories	19
2.4 Polymorphism.....	23
2.5 Addition of co-solvents and inhibitors	27
3 Experimental	29
3.1 Apparatus	29
3.2 Experiments with varying SR, T and w% MEG	31
3.3 Experiments with varying stoichiometry.....	33
3.3.1 Experiments with CO ₂ -bubbling.....	33
3.3.2 Experiments at high pH	33
4 Results and Discussion	35
4.1 Validation of the induction time measurement methods.....	35
4.2 Varying SR, T and w% MEG.....	37
4.2.1 Variation of SR.....	37
4.2.2 Variation of w% MEG	38

4.2.3	Induction times.....	39
4.2.4	Polymorphism in the experiments.....	40
4.2.5	Nucleation rates in the experiments.....	49
4.3	Variation of stoichiometry.....	57
4.3.1	Induction times and polymorphism in CO ₂ -bubbling experiments.....	57
4.3.2	Induction times and polymorphism in high pH experiments.....	61
5	Conclusions.....	63
6	Further recommendations.....	65
7	References.....	67
	List of symbols.....	71
	Appendix A: Raw data for all experiments.....	I
	Appendix B: Chemical data and lab calculations.....	III
	Appendix C: Extended results.....	V
	Appendix D: Uncertainties in the experiments.....	XI
	Appendix E: XRD results.....	XVII
	Appendix F: Calculations.....	XIX
	Appendix G: Analysis equipment.....	XXIII
	Appendix H: Risk assessment form.....	XXV

1 Introduction

A crystal is a solid material where constituent atoms, molecules, or ions are arranged in a repeating pattern or lattice (Mullin, 2001). The arrangements of the different ions or planes in a crystal, depends mainly on the surrounding temperature, supersaturation, composition or pH, as these factors change the activity of the ions in the solution.

Calcium carbonate is a common substance found in rocks in all parts of the world, and is the main component of shells of marine organisms. Calcium carbonate is also the cause to hard water and widely used in medical purposes. In industrial context, like the oil- and gas industry, calcium carbonate causes problems, because nucleation and growth of the calcium carbonate particles result in difficulties in the industrial production and processing.

Transportation and processing of gas and liquids from subsea tie-ins require hydrate prevention, corrosion control and a minimal risk of mineral precipitation. When natural gas is extracted from reservoirs, MEG is injected at the well-head to prevent plugs of gas hydrates during the transport in pipelines towards the onshore facility. Calcium-ions from the reservoir and iron-ions from corrosion in the steel pipelines can react with carbonate in the water/MEG-mixture and form particles. The probability of precipitation increases when the MEG is alkaline, and MEG is made alkaline to promote the formation of an FeCO_3 film on the pipeline surface and thereby control pipeline corrosion (Flaten et al., 2010b).

When the mixture of gas, MEG and water reaches the shore, the MEG is being regenerated in a regeneration-loop. A problem then occurring is the separation of CaCO_3 and FeCO_3 particles from the MEG. The size and amount of particles are important factors on the efficiency of the separation. Thus depends on the *nucleation rate* and *growth rate* of the particles at the surrounding conditions, where temperature and concentration are being the most important factors.

There are two main problems concerning precipitation of calcium carbonate particles in natural gas production and processing. The first one is when particles nucleate in the *bulk phase* during transport where separation of the particles from the MEG is the problem. The other problem is when the supersaturated solution of calcium carbonate hits the hot equipment in the on-shore facility leading to *scaling*. When this happen, the scale must be removed which give delay in the process. The kinetics being investigated in this master-thesis is concerning the calcium carbonate particles in the bulk phase.

Polymorphism describes when a solid structure has the ability of existing in more than one form or crystal structure. Calcium carbonate crystallizes in three different anhydrous polymorphs, calcite, aragonite and vaterite. The three polymorphs have different solubility, and the polymorph created depends on supersaturation, temperature, presence of additives

or inhibitors and the mechanics in the solution (Wang et al., 1999). The *morphology* describes the shape and size of the polymorphs.

It is important to investigate issues concerning precipitation of calcium carbonate, particularly with regard to the lost productivity associated with removal of scale from equipment or separation of particles from the bulk phase in natural gas production. Therefore, studies must be done to increase the understanding of the nucleation mechanism of calcium carbonate.

In this master thesis, the kinetics and polymorphism of calcium carbonate will be studied at different conditions. The variables controlled are supersaturation, temperature and content of MEG in the solution. Another variable will be investigated towards the end, namely the activity ratio between calcium and carbonate in the solution, and how this ratio affects the kinetics and polymorphism. The objective is to increase the knowledge of the kinetics and the resulting polymorphism at different conditions which reflect real conditions in natural gas production.

There have been many earlier studies on kinetics and polymorphism in a calcium carbonate system, but not many of those contained the co-solvent MEG. Flaten performed experiments with calcium carbonate systems containing MEG, using conductivity measurements to measure the induction time (2010). The results extracted in this master thesis are compared with the results obtained by Flaten.

The nucleation rate is calculated from the induction time. The induction time is defined as the time it takes before a supersaturated system starts to precipitate detectable crystals. There are different ways to measure the induction time, the most used methods by date is the conductivity measurement method and the pH measurement method. Both these methods are used in this master thesis to determine the induction time. The polymorphism obtained in the experiments is determined by powder X-Ray Diffraction (powder-XRD) and by Scanning Electron Microscope (SEM).

2 Theory

2.1 Thermodynamics

2.1.1 The nucleation driving force

The driving force for crystallization is the change in chemical potential between two states. In crystallization, this is the difference in chemical potential between the crystal state and the solution (Mullin, 2001). The expression for difference in chemical potential can be written as,

$$\Delta\mu = \mu_1 - \mu_2 \quad (2.1)$$

Where state 1 is the state in the solution and state 2 is the crystalline state. The chemical potential, μ , is defined in terms of the activity, a , and the standard potential, μ_0 , as

$$\mu = \mu_0 + RT \ln a \quad (2.2)$$

where R is the universal gas constant and T the absolute temperature.

By combining Equation (2.1) and Equation (2.2), the fundamental driving force for crystallization may be expressed dimensionless, as

$$\frac{\Delta\mu}{RT} = \ln\left(\frac{a}{a^*}\right) = \ln S \quad (2.3)$$

where S is the supersaturation and a^* is the activity in a supersaturated solution. As seen from Equation (2.3), the change in chemical potential depends on temperature, T , and supersaturation, S . Consequently, crystallization in a solution is induced by these factors.

2.1.2 Thermodynamics in a solution

The activity in a solution depends on how the molecules behave when different components are mixed together. How ions act in a solution, mainly depends on present electrostatic forces (Helbæk and Kjelstrup, 2006). In an ideal mixture, the concentration term, c , can be used instead of the activity term, a . But when there is a deviation from ideality, the concentrations are being modified by an activity coefficient, γ . The theory of Debye and Hückel describes this deviation based on electrostatic forces in a solution. The correlation between concentration and activity for component i , is described as

$$a_i = \gamma \cdot c_i \quad (2.4)$$

It is not possible to determine the activity coefficient for one ion alone, therefore a mean activity coefficient, γ_{\pm} , for the electrolyte is used (Helbæk and Kjelstrup, 2006):

$$\gamma_{\pm} = \left[\gamma_+^{(v_+)} \cdot \gamma_-^{(v_-)} \right]^{\frac{1}{(v_+)+(v_-)}} \quad (2.5)$$

In Equation (2.5), v_+ is the number of moles of positive charged ions in one mole of solution and v_- is the number of moles of negative charged ions in one mole of solution. For an univalent electrolyte, as the calcium carbonate solution, the mean activity coefficient, γ_{\pm} , is expressed by,

$$\gamma_{\pm} = \sqrt{\gamma_+ \cdot \gamma_-} \quad (2.6)$$

Based on quantified work by Max Born in 1920, Debye and Hückel developed an expression for the mean activity coefficient, γ_{\pm} . This will be demonstrated in what follows. The activity coefficient can be described as,

$$\log \gamma_i = z_i^2 \cdot A \cdot \sqrt{I} \quad (2.7)$$

Where A is a proportional constant and z is the number of charge.

The ionic strength, I , in Equation (2.7) is expressed by,

$$I = \frac{1}{2} \cdot \sum_i c_i z_i^2 \quad (2.8)$$

The mean activity coefficient from Equation (2.6) is incorporated into Equation (2.7), and since the mean values of positive and negative ions now are used, the expression is written with the absolute values of the ions' number of charge:

$$\log \gamma_{\pm} = -|z_+| |z_-| \cdot A \cdot \sqrt{I} \quad (2.9)$$

Equation (2.9) is called the *Debye-Hückel limiting law*, and can only be used for electrolytes with low ionic strength (Helbæk and Kjelstrup, 2006). The mean activity coefficient can also be found by using known data of supersaturation, K_{sp} and the concentrations of the ions in the solution. This will be demonstrated in the following section.

2.1.3 Thermodynamics in a carbonate system

The following criteria decide whether precipitation of calcium carbonate will occur or not, (Sandengen, 2006):

SR>1: Precipitation may occur due to supersaturation

SR=1: At equilibrium, concentration is the same as the activity in the solution

SR<1: The solution is undersaturated

In Figure 2.1, the different regions of solubility are shown.

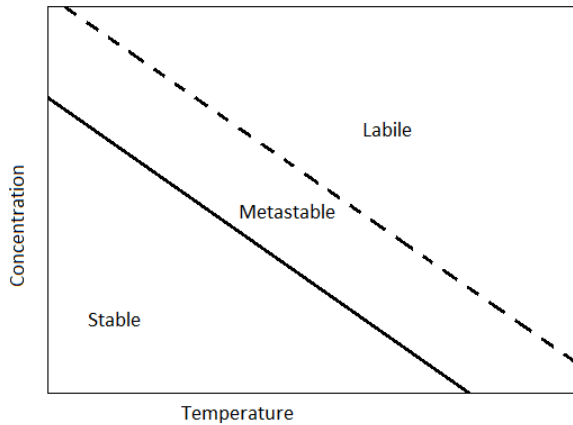
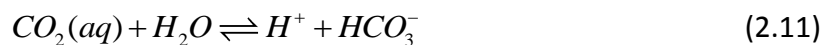


Figure 2.1: Different regions of solubility in a solution

In the *stable* region, the solution is undersaturated and no nucleation will occur. In the *metastable* region nucleation is not very likely, but crystal growth will occur if there is a surface available. The *labile* region is to the right of the super solubility curve, and here the solution is supersaturated. Spontaneous crystallization will occur in the labile region. As seen from the graph, solubility highly depends on temperature and concentration in the solution. Figure 2.1 shows the solubility curves for a calcium carbonate system, which has a so-called *opposite solubility*. That basically means that precipitation of crystals increases with temperature which is opposite to most systems.

The equilibrium equations for precipitation of calcium carbonate in an aqueous solution are as follows (Sandengen, 2006):



There are more equilibrium equations concerning the calcium carbonate system, which the simulation tool, MultiScale uses in calculations, but these are not shown here. Some of the calcium-ions will be used in different complexes and the calcium left to react with carbonate to form $CaCO_3(s)$, will be referred to as the *free concentration of calcium*, $c_{Ca^{2+},free}$.

On behalf of equations (2.10)-(2.13), an expression of supersaturation ratio, S , can be developed. S is based on the ionic activity product in a supersaturated solution compared to the solubility product in a saturated solution of calcium carbonate and can be written like,

$$S = \sqrt{\frac{IAP}{K_{sp}(CaCO_3)}} = \sqrt{\frac{a_{Ca^{2+}} \cdot a_{CO_3^{2-}}}{K_{sp}(CaCO_3)}} \quad (2.14)$$

Where IAP is the ionic activity product. Equation (2.14) can also be written in terms of the supersaturation ratio, SR :

$$SR = \frac{a_{CaCO_3}}{K_{sp}(CaCO_3)} \quad (2.15)$$

In this master thesis, SR is the term that will be used concerning supersaturation.

When replacing the activity-term in Equation (2.15) by the expression of activity in Equation (2.4) and the mean activity coefficient in Equation (2.5), SR can be written like,

$$SR = \frac{c_{Ca^{2+},free} \cdot c_{CO_3^{2-}} \cdot \gamma_{\pm}^2}{K_{sp}} \quad (2.16)$$

The mean activity coefficient, γ_{\pm} , is expressed by rearranging Equation (2.16),

$$\gamma_{\pm} = \sqrt{\frac{K_{sp} \cdot SR}{c_{Ca^{2+},free} \cdot c_{CO_3^{2-}}}} \quad (2.17)$$

By using a simulation tool like MultiScale, the different values in Equation (2.17) can be found and the mean activity coefficient can be determined. MultiScale is further described in Appendix G.

pH depends on temperature, and when the temperature increases, the activity of the H^+ ions also increases, and the pH will decrease. This can be illustrated by the Nernst equation (Zumdahl, 2005):

$$E = E_0 - kT(-\log a_{H^+}) \quad (2.18)$$

Here E is the electrical potential of a pH-electrode, E_0 is the standard electrode potential, k is the Boltzmann constant and T is the temperature in Kelvin. Equation (2.18) can also be written in terms of pH:

$$E = E_0 - kT \cdot pH \quad (2.19)$$

In Figure 2.2, the different compounds from equation (2.10)-(2.13) favored at different pH are shown.

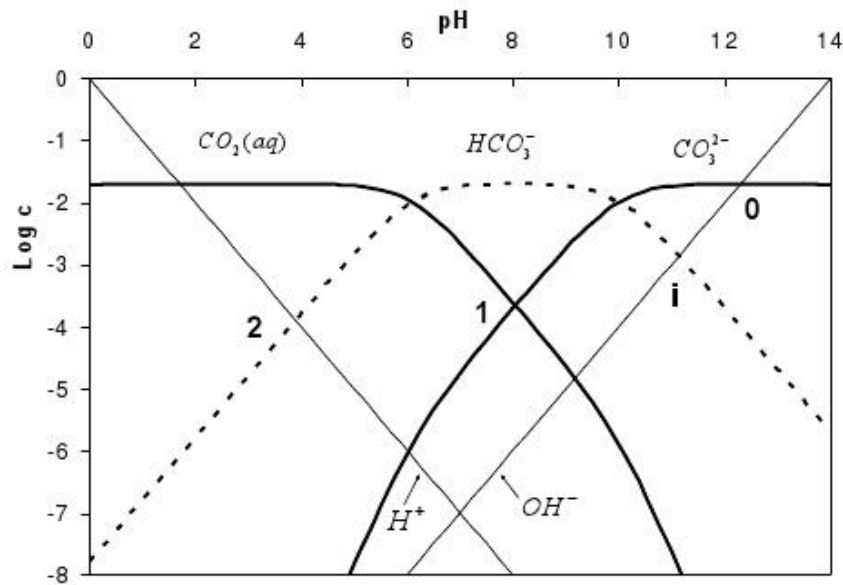


Figure 2.2: Alkalinity in relation to pH (Kaasa, 1998)

As seen from Figure 2.2, the existing complexes in the solution depend on the pH on the solution. From the figure it can also be seen that the concentration of carbonate increases with increasing pH and this also applies to the activity of carbonate due to the relation between concentration and activity shown in Equation (2.4).

When precipitation of calcium carbonate starts, carbonate will be removed from the solution, and the equilibrium in Equation (2.12) will be shifted towards the right. Because pH is the negative logarithm of the activity of H^+ -ions in a solution, the pH in the solution will consequently decrease.

Alkalinity is defined as the sum of bases that can be titrated (Kaasa, 1998) or a systems ability to resist a change in pH by neutralizing H^+ to the equivalent point of carbonate or bicarbonate. The electro neutrality equation for the calcium carbonate system is written like:

$$m_{Na^+} + 2 \cdot m_{Ca^{2+}} + m_{H^+} = m_{OH^-} + 2 \cdot m_{CO_3^{2-}} + m_{HCO_3^-} + m_{Cl^-} \quad (2.20)$$

Where m is the molality in mmol/kg solvent.

The species contributing to alkalinity can be identified:

$$Alkalinity = m_{OH^-} - m_{H^+} + 2 \cdot m_{CO_3^{2-}} + m_{HCO_3^-} + 2 \cdot m_{CaCO_3^0} + m_{CaHCO_3^+} \quad (2.21)$$

All the species and complexes in Equation (2.21) are contributing to the alkalinity in a calcium carbonate solution.

When sodium carbonate is the source of carbonate, the initial source to alkalinity is carbonate.

$$\text{Alkalinity} = 2 \cdot m_{\text{CO}_3^{2-}} \quad (2.22)$$

Experiments using sodium carbonate as the source of carbonate have an initial pH around 10. From Figure 2.2, the main complexes in the solution at this pH are CO_3^{2-} and HCO_3^- .

When sodium hydroxide bubbled with CO_2 is the source of carbonate, the initial source to alkalinity is hydroxide.

$$\text{Alkalinity} = m_{\text{OH}^-} \quad (2.23)$$

Experiments using sodium hydroxide as the source of carbonate have an initial pH around 7. From Figure 2.2, the main complexes in the solution at this pH are HCO_3^- , $\text{CO}_2(\text{aq})$ and CO_3^{2-} .

When the solutions of calcium and carbonate are mixed together, all the complexes in Equation (2.21) will be present.

The alkalinity required to maintain a desired supersaturation, can be calculated on the basis of the molality of either carbonate or hydroxide, and thermodynamic calculation programs such as MultiScale can be used.

2.2 Nucleation

There are two different types of nucleation mechanisms; primary nucleation and secondary nucleation. Primary nucleation occurs in supersaturated systems that do not contain crystalline matter, while secondary nucleation occurs when a supersaturated solution is in contact with particles of the crystallizing compound (Mullin, 2001).

In this master thesis, only primary nucleation is investigated. This type of nucleation has an exponential dependence on supersaturation and very large metastable zone widths, and can be divided into two groups; heterogeneous- and homogeneous nucleation. In Figure 2.3, the different types of nucleation are shown:

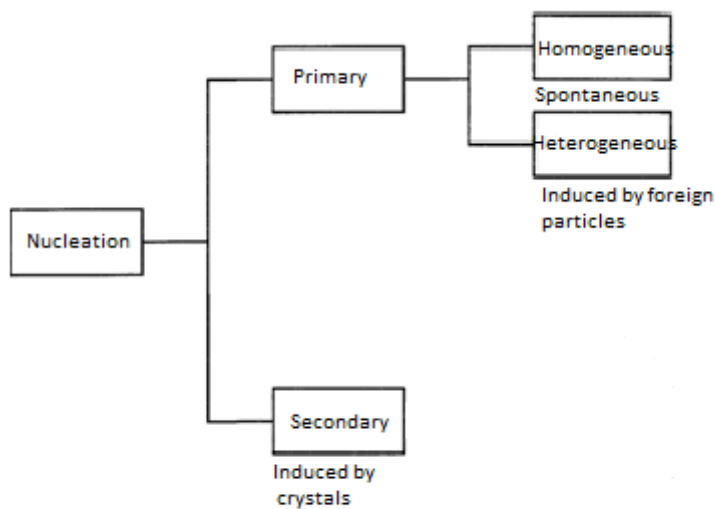


Figure 2.3: Schematic representation of the two different nucleation mechanisms

2.2.1 Homogeneous nucleation

Homogeneous nucleation occurs at the boundaries of a new phase. The formation of crystals could arise from the sequence of bimolecular additions,



After numerous additions to the critical cluster, A_n , nucleation will occur and subsequent crystal growth. If the nucleus exceeds a specific critical size, it becomes stable in the surrounding supersaturated bulk fluid.

The nucleation rate from classical nucleation theory is derived from changes in the Gibbs free energy for solid formation,

$$\Delta G = \Delta G_s + \Delta G_v \quad (2.25)$$

In Equation (2.25), ΔG_s , represents the excess free energy between the bulk of the particle and the surface of the particle. ΔG_v represents the excess free energy between a very large particle ($r=\infty$) and the solute in solution. ΔG_s is proportional to r^2 (assuming that the particle is a sphere) and in a supersaturated solution, ΔG_v is a negative quantity proportional to r^3 . Writing Equation (2.25) in terms of radius of a sphere, gives,

$$\Delta G = 4\pi r^2 \gamma + \frac{4}{3} \pi r^3 \Delta G_v \quad (2.26)$$

Here, γ , is the interfacial tension between the developing crystalline surface and the supersaturated solution and ΔG_v the free energy change of the transformation per unit volume.

For a nucleolus to be formed, it needs to overcome a maximum in the free energy, ΔG_{crit} , corresponding to the critical radius of the nuclei, r_{crit} . The free energy diagram for nucleation is shown in Figure 2.4.

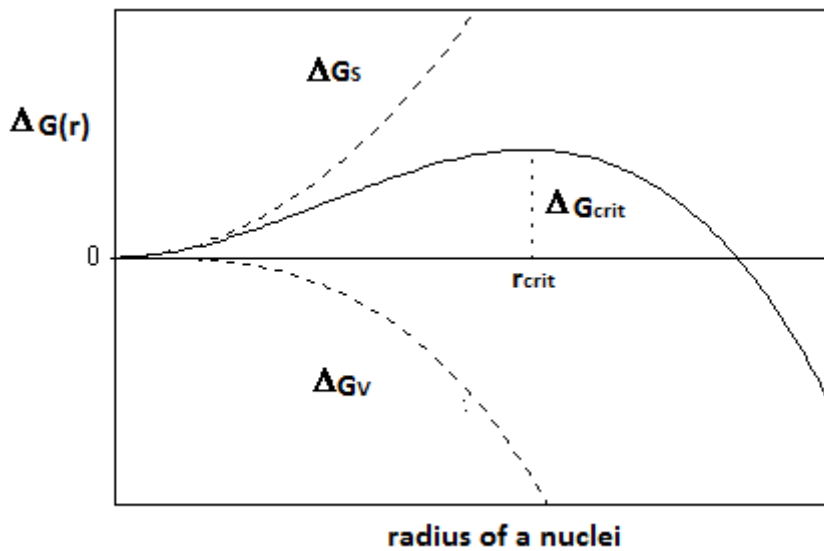


Figure 2.4: Free energy diagram for nucleation and critical size, r_c of a nucleus

When assuming a spherical nuclei,

$$\frac{\partial}{\partial r}(\Delta G) \Big|_{r=r_{crit}} = 0 \quad (2.27)$$

$$r_{crit} = \frac{-2\gamma}{\Delta G_v} \quad (2.28)$$

With this expression of r_{crit} Equation (2.26) can be rewritten for ΔG_{crit}

$$\Delta G_{crit} = \frac{16\pi\gamma^3}{3(\Delta G_v)^2} = \frac{4}{3}\pi r_{crit}\gamma \quad (2.29)$$

Thus, particles with radius smaller than r_{crit} will dissolve in a supersaturated solution, while particles with radius bigger than r_{crit} will continue to grow. Since ΔG_v is equal to the driving force, it can be written from the Gibbs-Thomson relation like

$$-\Delta G_v = \frac{kT \ln S}{v} \quad (2.30)$$

where k is the Boltzmann constant and v is the molecular volume. When combining Equation (2.29) and Equation (2.30), ΔG_{crit} can be expressed as,

$$\Delta G_{crit} = \frac{16\pi\gamma^3 v^2}{3(kT \ln S)^2} \quad (2.31)$$

The smaller the critical energy, ΔG_{crit} , the easier it is for a critical cluster to form. When a system is kept under a given temperature-pressure range, stable phases will form at thermodynamic equilibrium. But it is not always easy to form stable phases at the beginning of an experiment. Then metastable phases will appear at nucleation, which is different from the stable phase. This can be described as a competition between the interface free energy terms and the driving force. If the driving force term is small, the contribution of the surface energy term becomes more important. That is why a metastable phase will occur prior to the stable phase expected. After a certain time, the metastable phase will dissolve or transform into the stable phase. But if the conditions are maintained, the metastable phase will act like a stable phase and actually become stable (Sunagawa, 2005). This can be linked to the carbonate system – metastable vaterite and aragonite can be formed prior to the stable calcite at certain conditions. This will be further described in section 2.4.

As mentioned earlier in this chapter, the nucleation rate, J , has an exponential dependence on the supersaturation, S . The rate of nucleation can be expressed in terms of the general Arrhenius reaction velocity equation,

$$J = A \exp\left(\frac{-\Delta G}{kT}\right) \quad (2.32)$$

A is a strictly S -dependent kinetic pre-exponential factor. When introducing Gibbs-Thomson relationship and combining Equation (2.31) and Equation (2.32), the nucleation rate, J , can be written as,

$$J = A \exp\left(\frac{16\pi\gamma^3 v^2}{3k^3 T^3 (\ln S)^2}\right) \quad (2.33)$$

As made visible by Equation (2.33), the nucleation rate is affected by temperature, T , supersaturation, S , and the interfacial tension, γ .

Turnbull and Fisher (1949) quantified Equation (2.33) and included a ‘viscosity’ term,

$$J = A' \exp\left(-\frac{16\pi\gamma^3 v^2}{3k^3 T^3 (\ln S)^2} + \frac{\Delta G'}{kT}\right) \quad (2.34)$$

When the $\Delta G'$ is exceptionally large, as for highly viscous liquids, the other exponential term is small because the supersaturation is generally very large under these circumstances. Then $\Delta G'$ becomes the dominant factor in the expression, and this leads to a decrease in the nucleation rate, J (Mullin, 2001).

2.2.2 Heterogeneous nucleation

Heterogeneous nucleation defines nucleation on foreign particles that act as substrates of nucleation. This nucleation often occurs in industrial scale and in laboratories unless the solutions are filtered carefully. The factor φ , changes the critical energy for nucleation by the availability for a solid surface to nucleate on.

$$\Delta G_{crit,hetr} = \varphi \Delta G_{crit,hom} \quad (2.35)$$

The factor φ , can be defined by general angle theory,

$$\varphi = \frac{1}{4} (2 + \cos \theta)(1 - \cos \theta)^2 \quad (2.36)$$

As described earlier in this section, interfacial tension is one of the factors deciding the rate of nucleation. A relationship between the interfacial tensions between different phases and the contact angle, θ , can be seen from Young’s equation. This phenomenon is referred to as *wetting*,

$$\cos \theta_C = \frac{\gamma_{sl} - \gamma_{cs}}{\gamma_{cl}} \quad (2.37)$$

In Equation (2.37), γ_{sl} is the interfacial tension between another solid surface, s , and the liquid, γ_{cs} is the interfacial tension between the solid crystalline and the foreign solid surface and γ_{cl} is the interfacial tension between the solid crystalline and the liquid. If total wetting occurs, $\theta = 180^\circ$, the critical free energy in heterogeneous nucleation is the same as in a homogeneous nucleation system (Mullin, 2001).

In Figure 2.5 , the different surface tensions dependent on θ_c are shown.

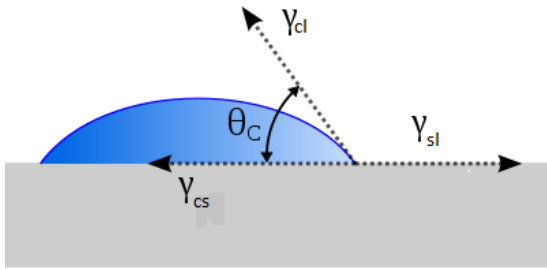


Figure 2.5: Wetting angle, θ_c

Primary heterogeneous nucleation always takes place in early stages of unseeded batch processes when the rate of supersaturation generation is higher than the capacity of the system to absorb it through simply crystal growth (Andreassen). In real systems, most nucleation processes are heterogeneous, because this type of nucleation requires much less driving force than homogeneous nucleation to occur (Sunagawa, 2005).

2.2.3 Induction time and nucleation rate

The difficulty of counting the instantaneous large numbers of nuclei precipitated by nucleation has motivated indirect measurements of the nucleation rate, like e.g. measurements of the *induction time*.

Induction time

There will be a certain time before a supersaturated solution starts to produce detectable crystals. This time period is called the *induction period*. The induction time is the time necessary to produce N particles with sufficient size, so that they can be observed in the system. Induction time depends on the level of supersaturation, temperature, viscosity, agitation and foreign particles. According to Mullin, the induction period, t_{ind} , consists of three different time contributions when it is assumed that the crystal growth is due to diffusion (2001):

$$t_{ind} = t_r + t_n + t_g \quad (2.38)$$

Figure 2.6 describes the different time contributions from Equation (2.38).

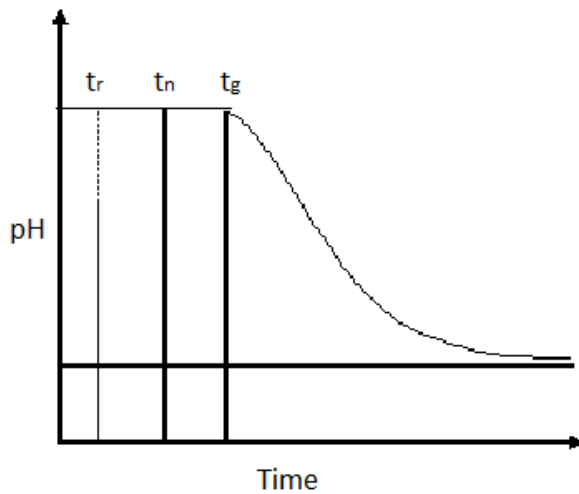


Figure 2.6: The different time contributions describing the induction time, t_{ind}

The term t_r is the relaxation time, the time the system takes to achieve quasi-steady-state distribution of molecular clusters. This contribution was negligible in this work; consequently this term is excluded in the results. The term t_n describes the time for a stable nucleus to be formed. This is the desired time contribution describing when the first nucleus is precipitated in the system. Because of the small volume the first nucleus represents, it is impossible to measure this time. Therefore, one last term is included in Equation (2.38) called t_g , which describes the time it takes for a nucleus to grow to a detectable size. Consequently, the sum of the time-contributions is the time measured and called t_{ind} .

From Figure 2.6 it can be seen that the curve can be separated in three different parts; the plateau, the decreasing part and the part where the curve flattens out. The plateau describes the time it takes for the supersaturated system to start nucleate, as described in the preceding paragraph. The decreasing part of the curve is where the particles grow bigger from the supersaturation left in the solution. The flattening part of the curve is where the supersaturation in the solution is consumed, and the system becomes saturated.

As described in section 2.1.3, tools for measuring changes in pH are suitable to detect when the calcium carbonate system starts to precipitate crystals. This method has been used in earlier experiments to measure the induction time, among others by Lindenberg and Mazzotti. In 2009, they determined the effect of temperature on the nucleation kinetics of α L-glutamic acid, by pH measurements. Also Gómez-Morales et al. used pH as the measurement tool when they in 1996 investigated the nucleation of calcium carbonate at different initial pH-conditions .

Another used method to measure induction time from experimental data is the conductivity measurement method. The electrical conductivity is the ability of a solution to transfer

electric current. It is the reciprocal of *electrical resistivity* (ohms). Ions have either a positive or negative electric charge, which allows current to pass between electrodes in a solution when an electric field is applied (Zumdahl, 2005). Electric conductivity can therefore be used to measure the concentration of ions in a solution. This method was used in earlier experiments to determine the induction time of calcium carbonate in MEG and water (Flaten et al., 2010b). Also Zeppenfeld used this method in 2010 to determine the induction time of calcite precipitation from aqueous solutions with different calcium and hydrogen carbonate concentrations.

There are several methods to measure the induction time, and the last one to be mentioned here is the one where the decreasing concentration of calcium in an experiment is measured. This is done by titration of samples taken during the experiment. This method has earlier been used to determine the growth rate of the calcium carbonate polymorph vaterite in mixtures of water and ethylene glycol at conditions of gas processing (Flaten et al., 2010a).

When using any of the three methods described in the preceding paragraphs, the induction time can be found from experimental data as the intersection between the plateau of the curve and the decreasing part of the curve. This is found by plotting either pH, conductivity or the decreasing concentration of calcium in a supersaturated solution as a function of time.

In Figure 2.7, the method used to find the induction time is shown in a pH plot.

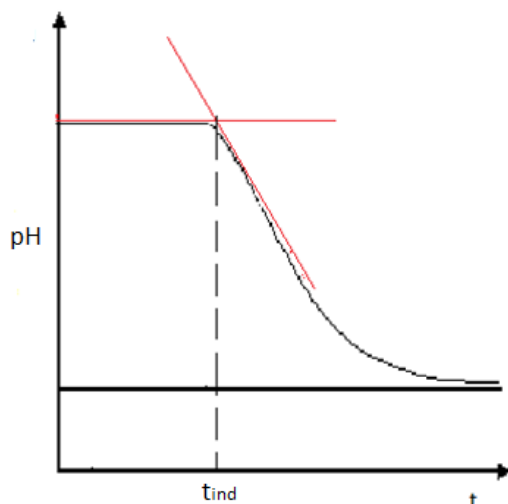


Figure 2.7: How induction time can be found from experimental data

In this master thesis, it was determined that the decreasing part of the curve should have at least three points decreasing at the same rate to be used as an intersection line, while the plateau should represent the average value before the curve started to decrease. The intersection between these two parts (marked with red in Figure 2.7), determined the induction time of the experiment. If there were two parts decreasing with different rates

close to the plateau of the curve, an uncertainty was associated with the induction time value.

Nucleation rate

In order to calculate the correct nucleation rate, the induction time desired is the time when the *first* particle nucleates in the system. This time is impossible to measure, because the volume of the first precipitated nucleus is too small to detect. Consequently, the induction time from Equation (2.38) consists of several time contributions, but t_n is the desired time to be used for nucleation rate calculations. Kashchiev and Rosmalen introduced an expression including both induction time, J , and growth rate, G . It is hard to separate the *nucleation period* from the *induction period*, as growth time varies along with the other parameters, see Equation (2.38). By introducing growth rate, the nucleation rate found is based on an induction time being the nucleation period, consisting of t_n and t_r , because the growth rate describes the growth in t_g . The expression introduced was based on the assumptions that a spherical crystal was created and that the nucleation was stationary (Kashchiev and Rosmalen, 2003):

$$t_{ind} = \left(\frac{3\alpha}{\pi G^3 J} \right)^{\frac{1}{4}} \quad (2.39)$$

Or expressed by the nucleation rate, J :

$$J = \frac{3\alpha}{\pi G^3 t_{ind}^4} \quad (2.40)$$

In Equation (2.40), $\alpha = V_{min}/V$, and depends on the measurement technique used to detect the induction time. α takes values in the range of 10^{-6} - 10^{-8} (Verdoes et al., 1992). V_{min} represents 5-10 % mass precipitated, or the first detectable volume of the precipitated crystals, while V is the volume of the solution. G is the growth rate of the nuclei formed is described more detailed in section 2.3. When the growth rates are known and the induction time found from experimental data, the nucleation rates can be calculated.

Equation (2.39) can only be used when induction time data, t_i , are obtained by an experimental technique which can detect the appearance of a certain overall volume of nucleating crystallites.

Another way to find the nucleation rate is to count particles in a time interval and divide the amount of particles by the induction time, t_{ind} :

$$J \sim \frac{N}{t_{ind}} \quad (2.41)$$

This counting can be done by a Coulter Counter and has been done in earlier studies to determine the nucleation rate when the induction time was found by conductivity measurements (Flaten et al., 2010b). An assumption made in the experiments using Equation (2.41) to determine the induction time, was that the number of counted crystals in

the end of the experiment, were originating from steady state nucleation during the induction time. This assumption gave an uncertainty, as it has been proved that the induction time is highly affected by growth.

2.3 Crystal growth

When nuclei have formed, they continue to grow as long as the surrounding solution is supersaturated. The growth of a crystal can be defined as,

$$G = \frac{dL}{dt} \quad (2.42)$$

assuming that the nucleus grows in a length, L .

2.3.1 Diffusion-reaction theories

Berthoud and Valetton suggested that there are two steps in the mass deposition; a diffusion process followed by a first-order reaction. In the diffusion process, solute molecules are transported from the bulk of the fluid phase to the solid phase. In the reaction, the solute molecules arrange themselves into crystal lattice. In Figure 2.8, the diffusion-reaction process is shown with concentration as driving force.

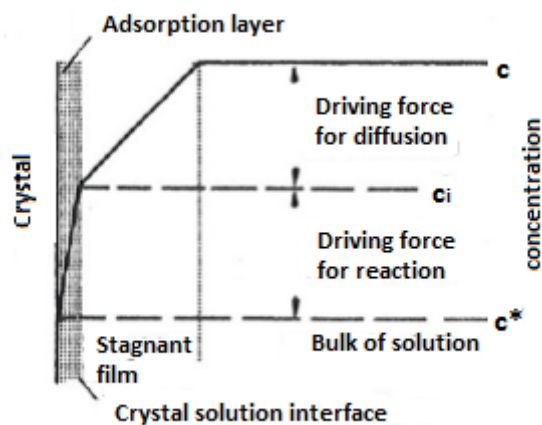


Figure 2.8: Simple diffusion-reaction model (Mullin, 2001)

The growth rate based on mass can be expressed like,

$$\frac{dm}{dt} = k_m A(c - c^*) \quad (2.43)$$

Where k_m is the coefficient of mass transfer, A is the surface area of the crystal, c is the concentration in the solution and c^* the equilibrium saturation concentration.

For the diffusion-process, the mass growth in Equation (2.43) can be expressed as,

$$\frac{dm}{dt} = k_d A(c - c_i) \quad (2.44)$$

where k_d is the coefficient of mass transfer by diffusion and c_i is the solute concentration in the solution at the crystal-solution interface. For the reaction, the mass growth can be expressed as,

$$\frac{dm}{dt} = k_r A (c_i - c^*) \quad (2.45)$$

The overall mass growth can then be written as,

$$\frac{1}{A} \frac{dm}{dt} = K_G (c - c^*)^g \quad (2.46)$$

To obtain a general growth rate, G , c_i is eliminated. The term g is the growth rate order.

The growth rate can also be expressed by relative supersaturation (Flaten et al., 2010a):

$$G = k_r (S - 1)^g \quad (2.47)$$

Growth depends on the polymorphism achieved in the experiment, and based on Equation (2.47), Flaten obtained an expression or model based on growth of vaterite in seeded experiments (2010):

$$G(T, w\%MEG) = (-4,8 \cdot 10^{-9} + 2,6 \cdot 10^{-11} \cdot T - 2,3 \cdot 10^{-11} \cdot w\%MEG) \cdot (S_v - 1)^2 \quad (2.48)$$

The model is only valid for temperatures between 40 and 70 °C and with contents of MEG between 0 and 70 w%. The growth rate order was set to be 2.

For a crystal to grow, atoms, ions or molecules will link at active centers, *kinks*, into the lattice positions where the attractive forces are greatest, shown in Figure 2.9.

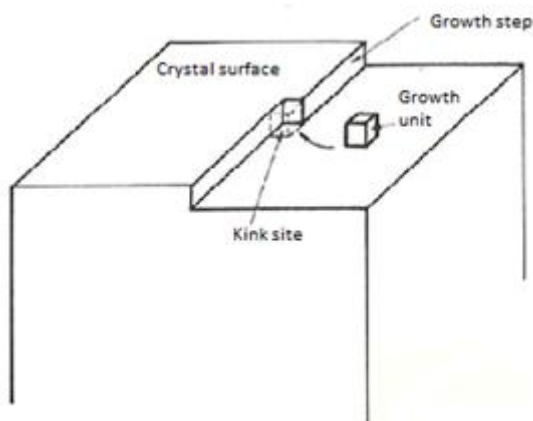


Figure 2.9: Growth of a crystal surface (Mullin, 2001)

As shown in Figure 2.8, the type of growth is determined by two main mechanisms: the reaction rate determining mechanism and the diffusion rate determining mechanism.

There are two main types of growth when the reaction is the rate determining mechanism:

- Spiral growth: Occurs at relatively low supersaturations. Kinks are made from dislocations on the faces, which promote growth. Screw dislocations give the possibility for growth in a “spiral staircase”. The growth rate order, g , is here 2.
- 2D-nucleation growth: Occurs in relatively large supersaturations. The nucleation appears at the crystal surface, and generates the necessary kinks for further growth. If the lateral growth rate is larger than the nucleation growth rate, the crystal grows in smooth layers. In this type of growth, the growth rate order, g , is larger than 2.

In Figure 2.10, the two different reaction rate determining mechanisms of growth are displayed.

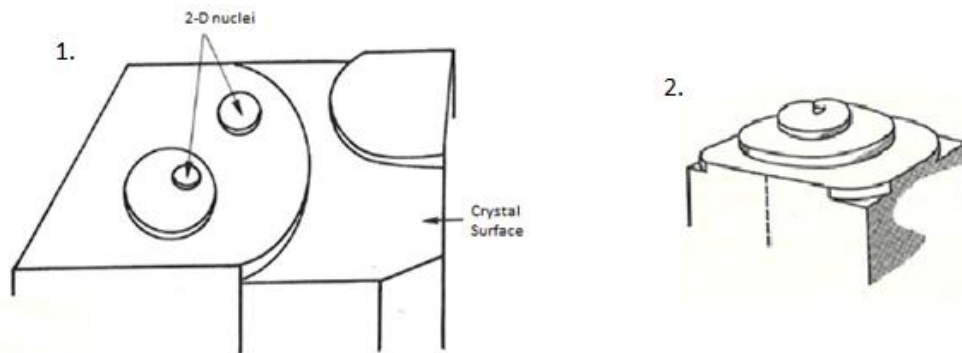


Figure 2.10: Reaction controlled growth rate mechanisms, 1: 2D- growth, 2: Spiral growth (Mullin, 2001)

When the driving force increases, the growth mechanism will change from the reaction- to the diffusion rate determining mechanism:

- Rough growth: Occurs at high supersaturations which allow growth units to attach anywhere on the crystal surface (terraces, kinks and steps). Nucleation on the surface is fast and the surface becomes rough. Here the growth rate order, g , is 1.

The rough growth is an adhesive type of growth, that may lead to *dendritic* growth of planes or corners closer to the supersaturation in the bulk (Sunagawa, 2005). This phenomena is typical for snow crystals crystallizing at low temperatures (Uyeda and Kikuchi, 1990), but also observed in the calcium carbonate system.

In Figure 2.11, the different growth mechanisms are shown.

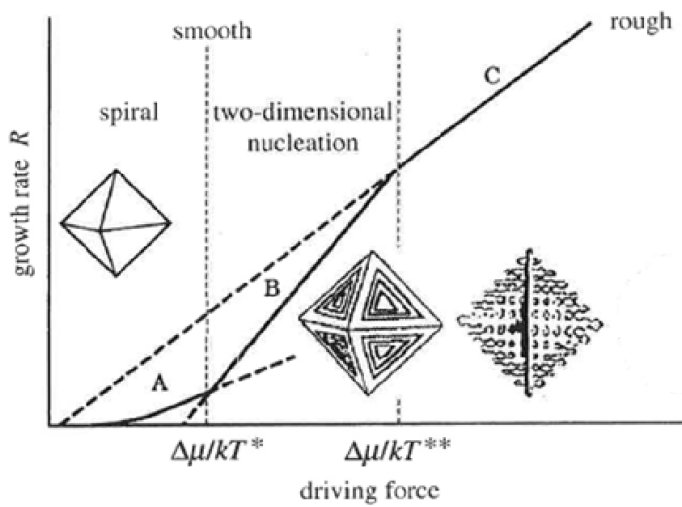


Figure 2.11: Growth rate as a function of driving force (Sunagawa, 2005)

In phase A and phase B the growth is exponential and reaction is the rate determining mechanism. In phase C the diffusion is the rate determining mechanism, which gives linear growth.

2.4 Polymorphism

As mentioned in the introduction, calcium carbonate crystallizes in three different anhydrous polymorphs; calcite, aragonite and vaterite. The polymorph created depends on both thermodynamics and kinetics, where calcite has the highest stability and vaterite the least. Vaterite has a hexagonal unit cell which often results in spherulites, aragonite has an orthorhombic unit cell which result it needle-like crystals and calcite has a rhombohedral unit cell which results in cubic crystals (Flaten et al., 2010a). The abundance of polymorphs formed by homogeneous precipitation strongly depends on temperature. Calcite usually forms at lower temperatures and aragonite at higher temperatures. In Figure 2.12, the polymorphic abundance can be seen as a function of temperature.

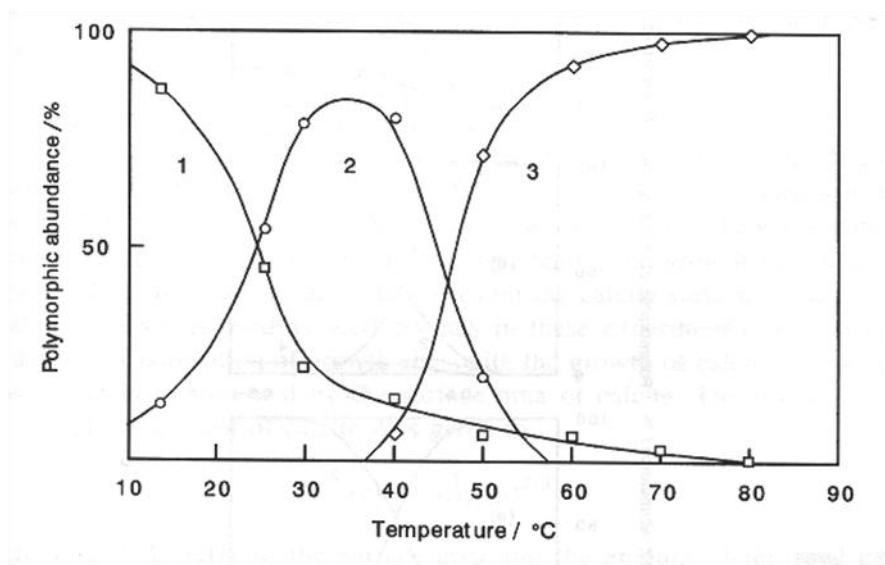


Figure 2.12: Polymorphic abundance in relation to temperature. 1: Calcite, 2: Vaterite, 3: Aragonite (Ohtaki, 1998)

The polymorphs created in the supersaturated solution will by time transform by dissolution and re-precipitation into the thermodynamically stable calcite, shown in Figure 2.13.

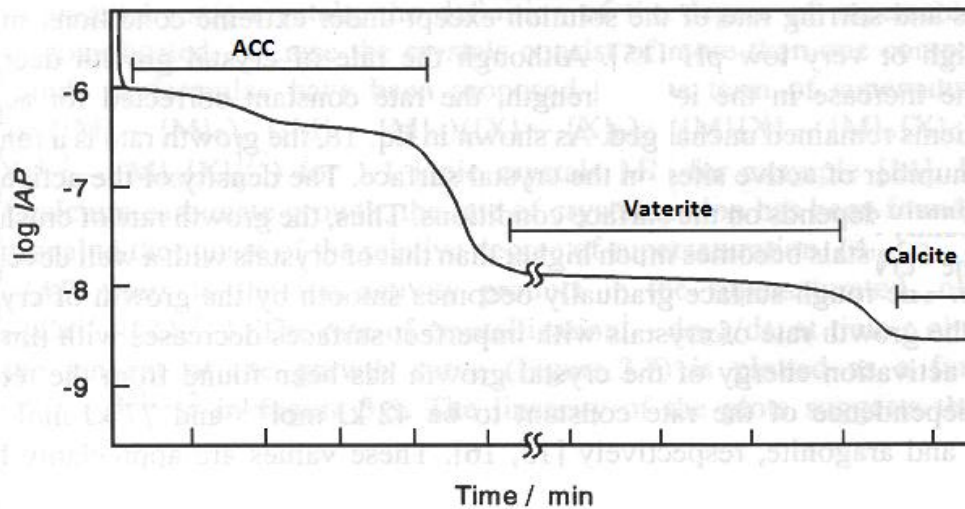


Figure 2.13: Transformation from unstable phase via a metastable phase into the stable phase (Ohtaki, 1998)

If the supersaturation is very high, an amorphous phase, ACC, is created, and will transform into the metastable phases vaterite and/or aragonite, and by time further into the stable calcite.

Vaterite usually forms at higher levels of supersaturation and earlier studies show that vaterite can take different morphologies depending on the surrounding conditions. As described in the preceding paragraph, vaterite usually forms into spherulites, but Wang et al. claimed that morphologies of flower-like vaterite were created when solutions of CaCl_2 and urea was rapidly mixed together (1999). These flower-like structures of vaterite was up for discussion again when Andreassen et al. claimed that these structures could be created in absence of biomolecular additives, just by controlling the supersaturation in the solution at different temperatures (2012b). Also morphologies of vaterite looking like discs and hexagonal plates have been recorded in earlier studies (Beck and Andreassen, 2011).

The three different polymorphs are displayed in Figure 2.14.

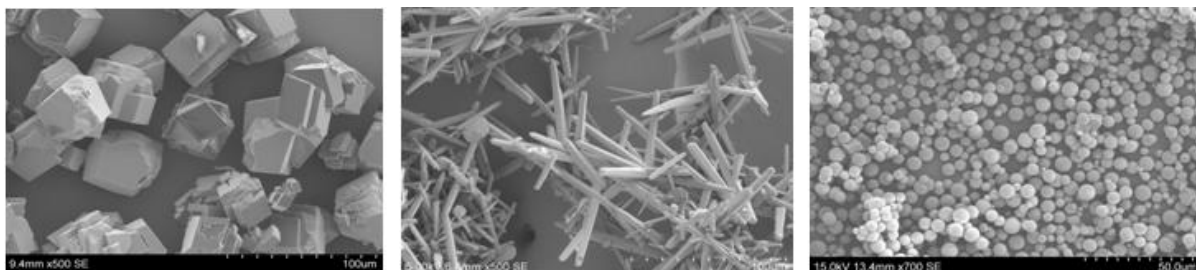


Figure 2.14: Polymorphism of CaCO_3 determined by XRD. From the left: Calcite, aragonite and vaterite (Andreassen, 2010)

The polymorph created in the experiment also depends on the composition of the solution, and addition of co-solvents and/or inhibitors. Flaten et al. observed that the solubility in the calcium carbonate solution decreases with increasing content of the co-solvent MEG (2010b), and this will be further described in the next section.

The solubility of the different polymorphs of CaCO₃ can be found by using the relation between solubility and temperature (Plummer and Busenberg, 1982):

$$\log K_{sp,calcite} = -171.9065 - 0.077993 \cdot T + \frac{2839.319}{T} + 71.595 \cdot \log T \quad (2.49)$$

$$\log K_{sp,aragonite} = -171.9773 - 0.077993 \cdot T + \frac{2903.293}{T} + 71.595 \cdot \log T \quad (2.50)$$

$$\log K_{sp,vaterite} = -172.1295 - 0.077993 \cdot T + \frac{3074.688}{T} + 71.595 \cdot \log T \quad (2.51)$$

Where T is the absolute temperature.

The solubility products from equations (2.49) to (2.51) can be plotted as curves based on IAP and $temperature$, see Figure 2.15.

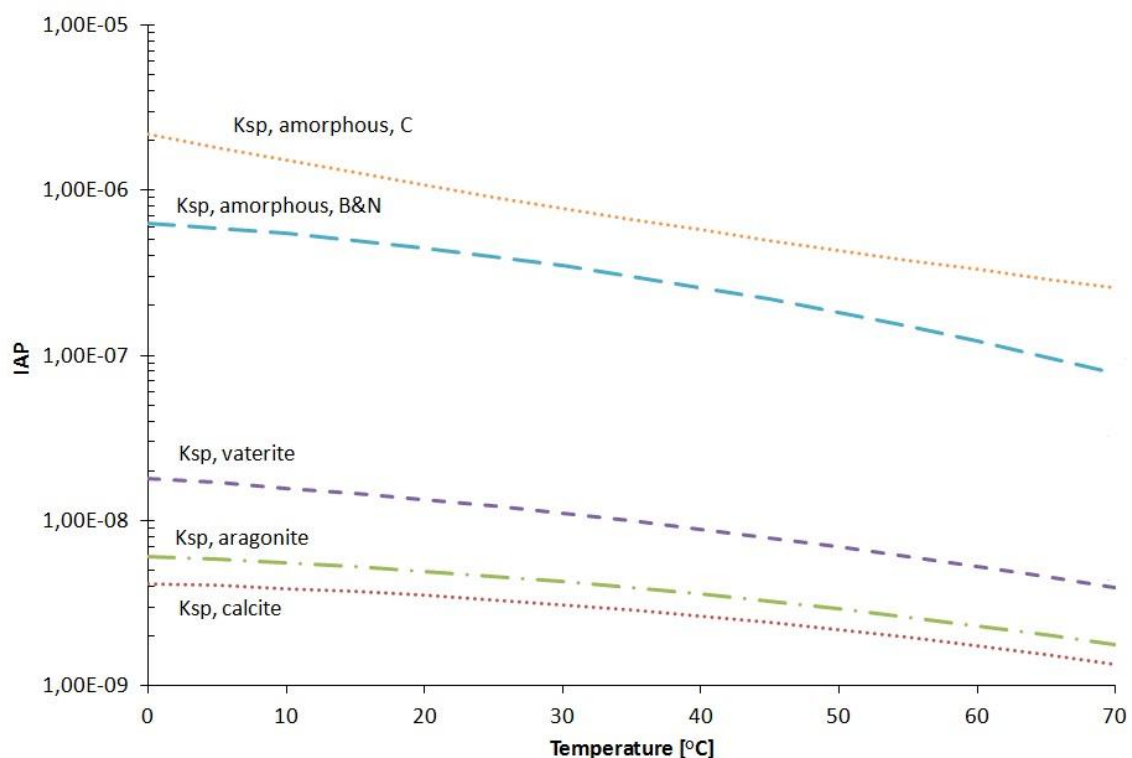


Figure 2.15: Solubility curves of calcium carbonate in a plot of IAP as a function of temperature (Andreassen et al., 2012a)

There is a disagreement concerning the placement of the solubility curve of the amorphous phase, and two different types are included in the diagram in Figure 2.15. In 1989, Brečević and Nielsen introduced a solubility curve of the amorphous phase. But in 1992, Clarkson et al. claimed that the solubility curve of the amorphous phase lies higher than the solubility curve Brečević and Nielsen. Both curves are shown in the diagram.

By using the relationship between the solubility products of the different polymorphs, the supersaturation with respect to the each of the different polymorphs can be calculated:

$$S_1 = S_2 \cdot \sqrt{\frac{K_2}{K_1}} \quad (2.52)$$

2.5 Addition of co-solvents and inhibitors

Experiments have shown that when additives or inhibitors are added to a supersaturated solution, the kinetics in the solution changes. Flaten et al. showed that the induction time of precipitation of calcium carbonate is highly effected when the co-solvent MEG is added to the solution. The induction time increased, the interfacial tension was reduced and the nucleation rate was increased in the presence of MEG (2010b).

Inhibitors and additives also have an effect on crystal growth in the calcium carbonate system. When the inhibitor hydroxyethylidene-1,1-diphosphonic acid (HEDP) was added to a calcium carbonate system, the growth decreased with increasing amount of organic substances added to the system (Sunagawa, 2005). This has also been shown in experiments where co-solvents have been added to the solution. Flaten et al. showed that MEG had a decreasing effect on crystal growth in a calcium carbonate system (2010b). MEG decreases the solubility of calcium carbonate (calcite), and precipitation will be favored in these type of system due to the elevated alkalinity (Kaasa et al., 2004).

The polymorphic system in a calcium carbonate system is also affected by addition of MEG. The morphology of the crystals, the crystal size distribution and the transformation of calcium carbonate are all affected by this co-solvent. Experiments have indicated that vaterite is the most favored polymorph with increasing MEG content in the solution (Flaten et al., 2009). Also in a slurry system, the influence of MEG as a co-solvent in a calcium carbonate system was studied. Konopacka-Lyskawa and Lackowski concluded that addition of MEG decreased the size of the particles in such a system (2010).

3 Experimental

An experimental batch-setup was designed for the specialization project last semester. The setup controlled the temperature during the experiments, while different measurement probes measured and logged data on a computer. The same setup was used for the work in the master thesis.

The experiments were carried out in the 1 L batch reactor of glass and a total of 32 experiments at different conditions were conducted. All experiments were reproduced at least once to check the reproducibility of the pH drop recorded in the experiments. As described in the Abstract, the experiments were labeled with three variables in the following order; SR, temperature and w% MEG. The temperatures were chosen to be 40 °C and 70 °C, and the content of MEG was chosen to be 0, 40 and 80 w%.

The parameters were chosen to reflect the realistic conditions in natural gas production and are the same as used in some of the work by Flaten (2010). The supersaturations were determined by operator to vary between 20 and 100.

The complete list of the experiments done in this master thesis can be found in Appendix A.

3.1 Apparatus

The batch reactor can be seen from above in Figure 3.1.

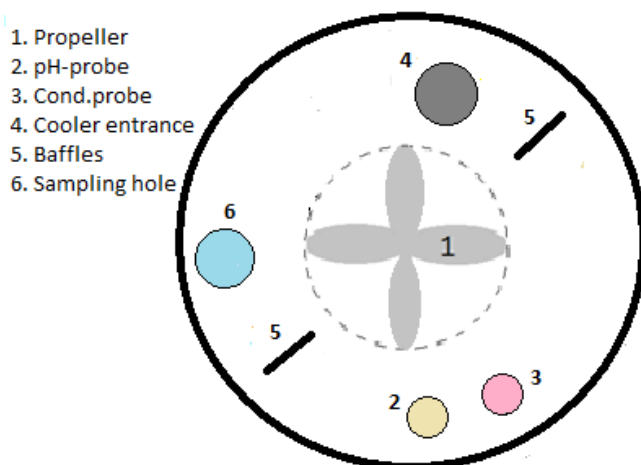


Figure 3.1: The reactor seen from above

The reactor vessel was jacketed for a constant temperature control and a constant stirring of 500 rpm by a four-blade propeller made sure that the mixing was uniform. The propeller was placed 3 cm from the bottom of the reactor. The baffles, propeller and rod were made of Teflon, to avoid corrosion in the reactor. The measurement probes were placed in the

reactor through two holes in the reactor lid. Two other holes in the reactor lid were used as entrances sampling and for a small cooler. The volume of the cooler was small to minimize the loss of liquid due to evaporation. The gas leaving the reactor through the cooler passed a water trap.

In Figure 3.2, a picture of the reactor is displayed.

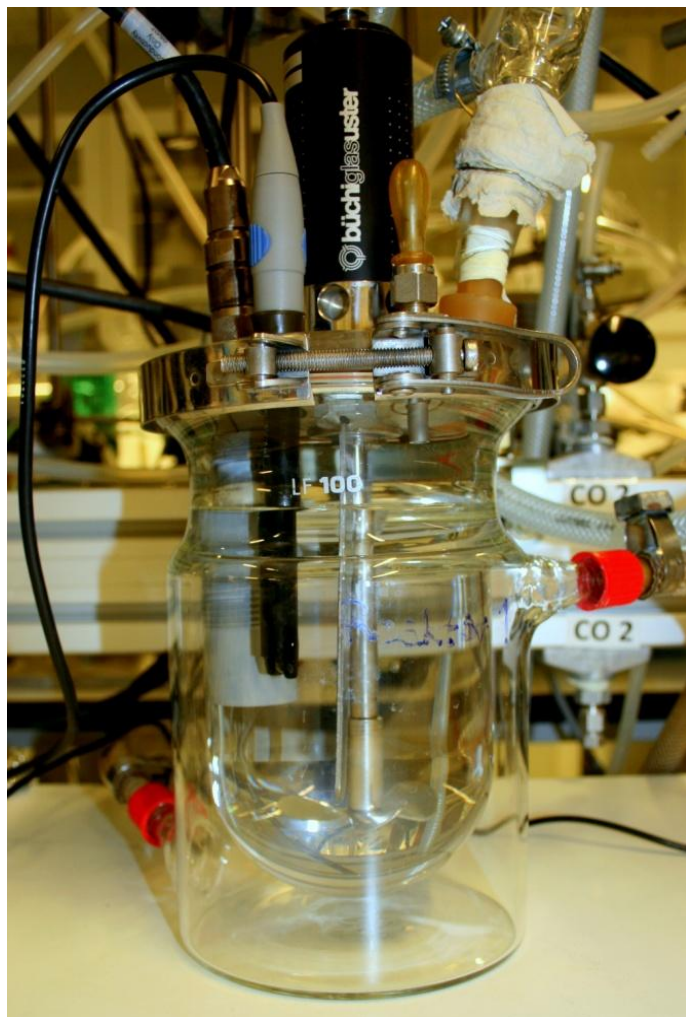


Figure 3.2: Picture of the reactor

The pH-measurements were done by a pH-meter from Mettler-Toledo SevenEasy which gives the pH in three decimal places. The conductivity measurements were done by a Mettler-Toledo Sensor InPro M300.

3.2 Experiments with varying SR, T and w% MEG

The liquid level was chosen to be 1 L which was the maximum amount the reactor could contain. This decision was made to minimize the volume of the gas phase in the reactor. The calcium source was 500 mL of a solution containing CaCl₂ and the carbonate source was 500 mL of a solution containing NaOH bubbled with CO₂. Both solutions were extracted from parent solutions. The solutions were preheated to the desired temperature in separate water baths and bubbled with CO₂ until equilibrium was reached and the pH was stable. The initial pH in the experiments varied between 6,7 and 7,7. CO₂ was continuously added to the gas phase of the reactor. This procedure was chosen to reflect the real conditions of natural gas production. The initial concentration of Ca²⁺ was 5 mmol/kg solvent in all these experiments.

The lab matrix for the experiments done with an initial concentration of Ca²⁺ of 5 mmol/kg solvent and CO₂-bubbling can be seen in Table 3.1.

Table 3.1: Experimental conditions for experiments with varying SR, T and w% MEG. CO₂-bubbling

w% MEG	T=40 °C			T=70 °C		
	SR	C _{NaOH} [mmol/kg solv]	Initial pH	SR	C _{NaOH} [mmol/kg solv]	Initial pH
0	20	118,0	6,90	20	38,5	6,79
	25	141,0	6,97			
	30	164,5	7,03	30	51,5	6,91
	35	187,5	7,08			
	40	211,5	7,12	40	64,1	7,00
	70	363,5	7,33	70	102,9	7,18
	93 (max)	498,5	7,44			
40	20	74,0	7,01	20	23,6	6,90
	30	100,5	7,13	30	31	7,01
	40	126,5	7,22	40	37,8	7,09
	70	206,0	7,40	70	57,4	7,26
	100 (max)	292	7,54			
80	40	60,5	7,48	40	20,0	7,36
	70	92,2	7,65	70	29,1	7,51

The experimental conditions from Table 3.1 can be plotted into Figure 2.15, and give following result:

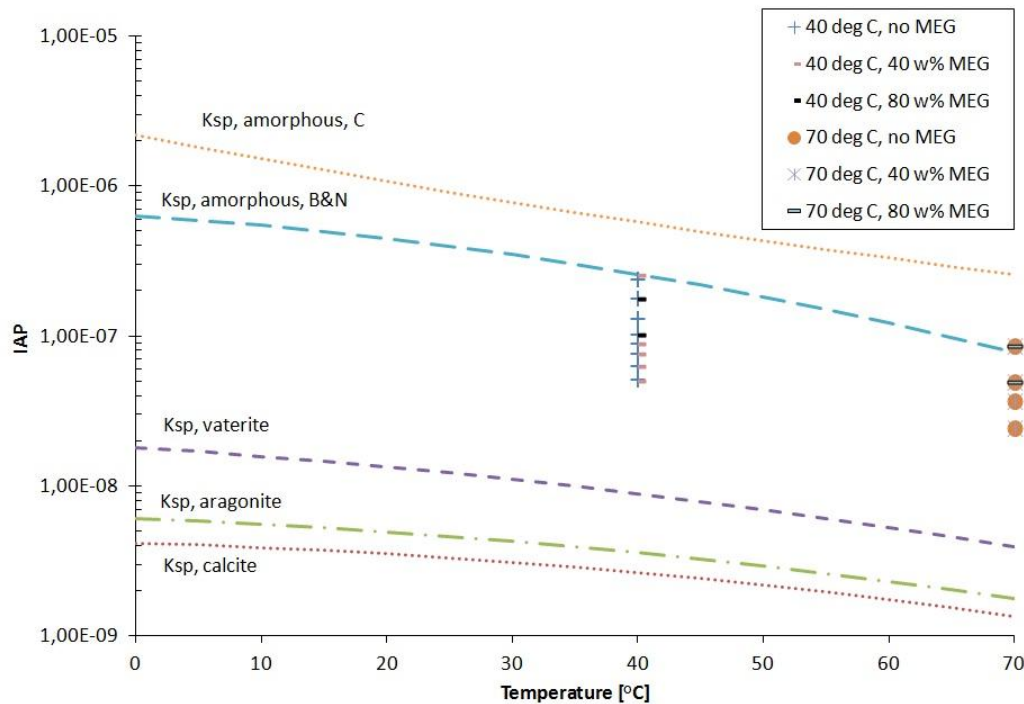


Figure 3.3: The experiments with CO₂-bubbling performed in this master thesis plotted in the solubility plot

From Figure 3.3 it can be seen that the start *IAP* values in the experiments ended up in the same area; between the solubility curve of the vaterite phase and the solubility curve of the amorphous phase by Brečević and Nielsen. This basically means that a metastable phase could be created in the beginning of the experiments, and the polymorphism depended on the *IAP* value at the end of the experiments. Three experiments, 70-70-0, 70-70-40 and 70-70-80, were placed slightly above the solubility curve of Brečević and Nielsen, indicating that an amorphous phase may have been created in the start of these three experiments.

Samples of 30 mL were taken by syringe and tubing every five minutes for all experiments at 40 °C and no content of MEG. The same procedure was conducted for the respective experiments with a SR of 40 and 70. The samples were diluted with 100 mL deionized water to avoid spontaneous secondary nucleation when the supersaturated solution hit the filter paper. At the end of every experiment, a final sample was taken where all the solution in the reactor was filtered, washed with ethanol and set to dry. The dried particles were coated with conducting gold to prevent charge build-up on the electrically insulating sample, and then the polymorphism was investigated in SEM. Six samples were also tested in XRD.

Samples for titration were taken in the 40-40-0 experiment to verify that the decrease in Ca²⁺-concentration correlates with the precipitation detected by the pH measurement probe.

A description of the analysis measurement equipment can be found in Appendix G.

3.3 Experiments with varying stoichiometry

In the preceding experiments, the three varying parameters were supersaturation, temperature and w% MEG in the solution. Another variable was further investigated, namely the stoichiometry between calcium and carbonate in the solution. The experiments with varying stoichiometry were conducted at a temperature of 40 °C and a fixed SR of 40. The ratio between the activity of Ca^{2+} and the activity of CO_3^{2-} was changed, and pH was used as the measurement method to determine the induction time. Also in these experiments samples were taken every five minutes, as described in section 3.2. Further, the polymorphs created were examined by SEM.

3.3.1 Experiments with CO_2 -bubbling

The experiments with varying stoichiometry and CO_2 -bubbling were done with the same procedure as described in section 3.2.

The initial pH in the experiments varied between 6,7 and 7,7.

The lab matrix for the experiments done with CO_2 -bubbling and varying stoichiometry can be investigated in Table 3.2.

Table 3.2: Experimental conditions for the 40-40-0 experiments with varying stoichiometry. CO_2 -bubbling

$C_{\text{Ca}^{2+}}$ [mmol/kg solv]	Alkalinity	Initial pH	$a_{\text{Ca}^{2+}}/a_{\text{CO}_3^{2-}}$
1,38	850,0	7,64	0,110
2,46	424,0	7,39	1,00
5,00	211,5	7,12	9,60
13,0	103,5	6,83	116
20,0	81,50	6,74	269

To achieve an alkalinity of 850 and a total volume in the reactor of 1 L, the volumes in the start bulbs were changed: 850 mL of the NaOH solution was used, and 150 mL of the CaCl_2 solution was used. The amount taken from the parent solutions to achieve an alkalinity of 850, was calculated.

3.3.2 Experiments at high pH

The source of carbonate was changed from NaOH saturated with CO_2 to Na_2CO_3 . This was done in order to see if the source of carbonate affected the induction time and polymorphism in the experiments.

pH measurements are very sensitive for interactions between the gas phase in the reactor and the atmosphere outside of the reactor. In order to minimize these interactions, the reactor was kept as tight as possible during the experiments done at high pH.

The liquid level was chosen to be 1 L which was the maximum amount the reactor could contain. This decision was made to minimize the exchange of CO₂ between gas and liquid phase. The calcium source was 500 mL of a solution containing CaCl₂ and the carbonate source was 500 mL of a solution containing Na₂CO₃, both solutions were extracted from parent solutions. The two solutions were pre-heated separately in water baths to the desired temperature was reached and then mixed together in the reactor. The initial pH in the experiments varied between 10,0 and 10,2.

The lab matrix for the experiments done at high pH and varying stoichiometry can be seen in Table 3.3.

Table 3.3: Conditions for the 40-40-0 experiment with varying stoichiometry. High pH

$C_{Ca^{2+}}$ [mmol/kg solv]	Alkalinity	Initial pH	$a_{Ca^{2+}}/a_{CO_3^{2-}}$
0,38	5,05	10,43	0,09
0,66	2,18	10,12	1,00
1,60	1,26	9,88	9,39
6,00	0,87	9,61	103

Chemical data and calculations concerning the experimental procedure can be found in Appendix B.

4 Results and Discussion

4.1 Validation of the induction time measurement methods

To decide which method was most suitable to determine the induction times in the experiments, two of the different methods mentioned in section 2.2.3 were tested in several experiments. The conductivity measurements were only stable and usable in the high pH-experiments, and too noisy to be used in the CO₂-bubbling experiments. It was obvious that the CO₂-bubbling gave disturbances in the conductivity measurements. The results from the comparable measurements can be further investigated in Appendix C. On the basis of the observations, pH was chosen as the most suitable method to measure the induction time, and this method was further compared with measurements of the decreasing calcium concentration in the experiment. The pH probe had a certainty of 3 decimal places.

As mentioned in section 3.2, titration samples were taken in the 40-40-0 experiment, to verify whether the registered drop in pH was related to the decreasing calcium concentration in the solution throughout the experiment. 16 samples were taken, but only 10 gave results. The two plotted curves can be seen in Figure 4.1.

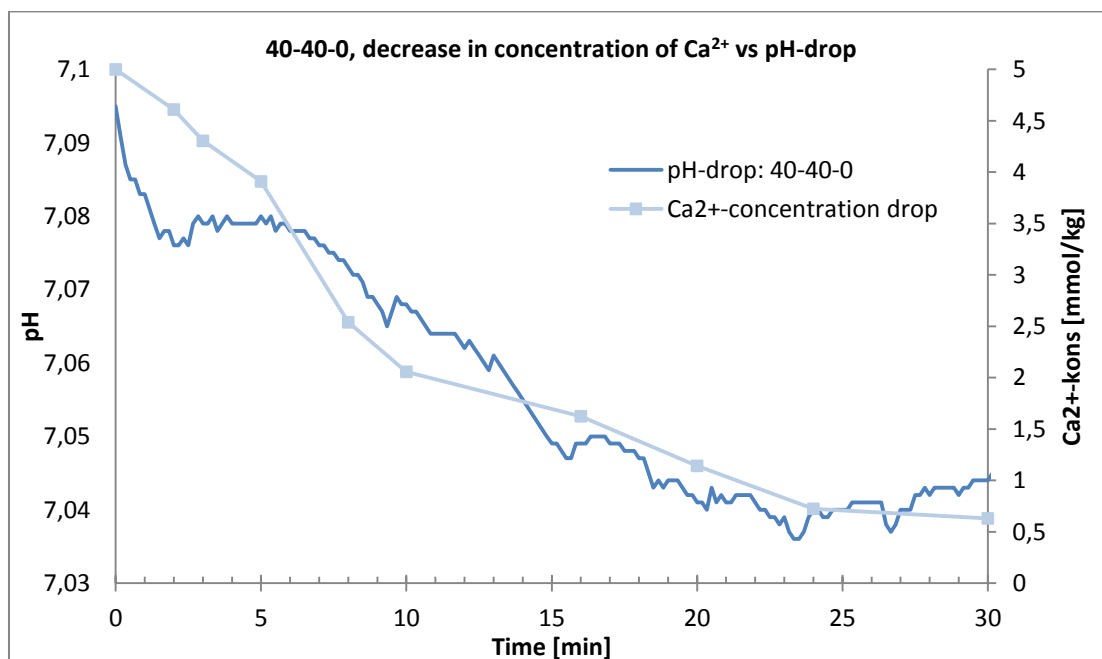


Figure 4.1: The 40-40-0 experiment. Drop in pH related to decreasing concentration of Ca²⁺

The titration values should decrease by time, as the concentration of calcium decreases when calcium carbonate is created. Figure 4.1 shows that the drop in pH was related to the decreasing concentration of calcium in the solution, because the two curves were decreasing at \approx the same rate. The curve representing the drop of calcium did not have a plateau in the beginning of the experiment. This observation indicated that these types of measurements are unsuitable to determine the induction time. To obtain the plateau in the beginning

before the precipitation starts to occur, many samples must be taken early in the experiment to be able to see it. This is very capacity demanding, and made this method unsuitable for induction time measurements. However, it was a good method to verify whether the drop in pH is due to precipitation of calcium carbonate. On the basis of the preceding observations, it was decided that pH was suitable as tool for determination of induction times in the experiments done in this master thesis.

4.2 Varying SR, T and w% MEG

It was found that the induction time decreased as the supersaturation, SR , was increased in all the experiments. The induction time also decreased with increasing temperature, T . Addition of MEG to the solution increased the induction time, and this effect got more evident at high contents of MEG at low temperatures. These observations match earlier studies (Flaten et al., 2010b).

4.2.1 Variation of SR

When the supersaturation is increased, the driving force for nucleation also increases, leading to a higher probability of precipitation. From the Gibbs-Thomson relation described in Equation (2.30), it can be seen that the driving force, ΔG_v , increases with increasing supersaturation and temperature, which was demonstrated in these experiments.

To easier compare the different induction times at different SR, all the pH curves were shifted from the respective initial pH-values to a pH=7. This could be done because it was the *change* of the slope and when it occurred which was interesting, and not the initial pH. An example of such a pH plot is shown in Figure 4.2. To explore the unedited raw data obtained for a pH plot, go to Appendix C.

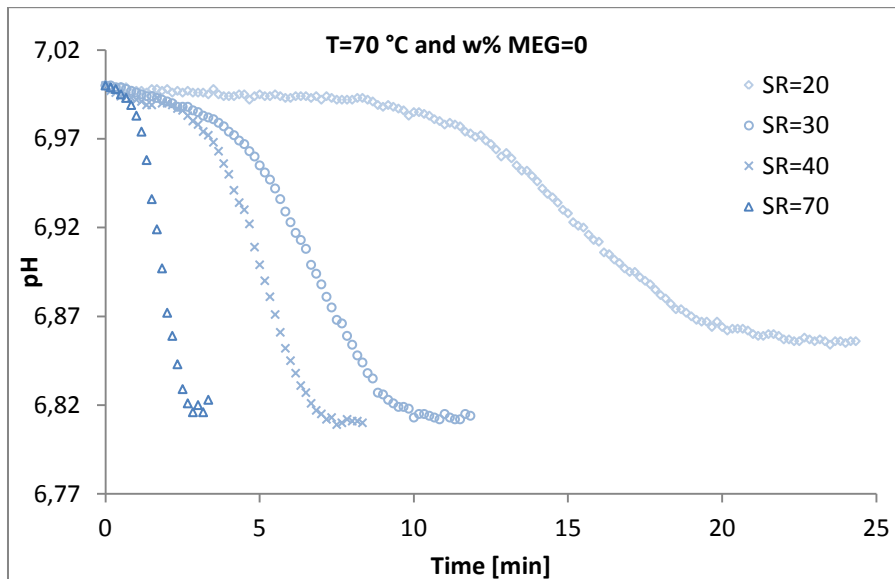


Figure 4.2: Drop in pH at 70 °C and w% MEG=0

The rest of the plots describing drop in pH during the experiments can be seen in Appendix C. The induction times shown later in section 4.2.3, were determined on the basis of these pH plots.

4.2.2 Variation of w% MEG

When the co-solvent MEG was added to the experiments, the induction time increased with increasing content of MEG added. Addition of MEG to a solution changes the interfacial tension because of the variation of the solvent composition. In earlier studies it was shown that the interfacial tension decreases with increasing content of MEG in the solution (Flaten et al., 2010b).

Plots describing the decrease in pH were made the same way as described in section 4.2.1. An example of a pH plot showing the effect of MEG with constant SR and temperature can be seen in Figure 4.3. The pH curves were shifted from the respective initial pH-values to pH=7.

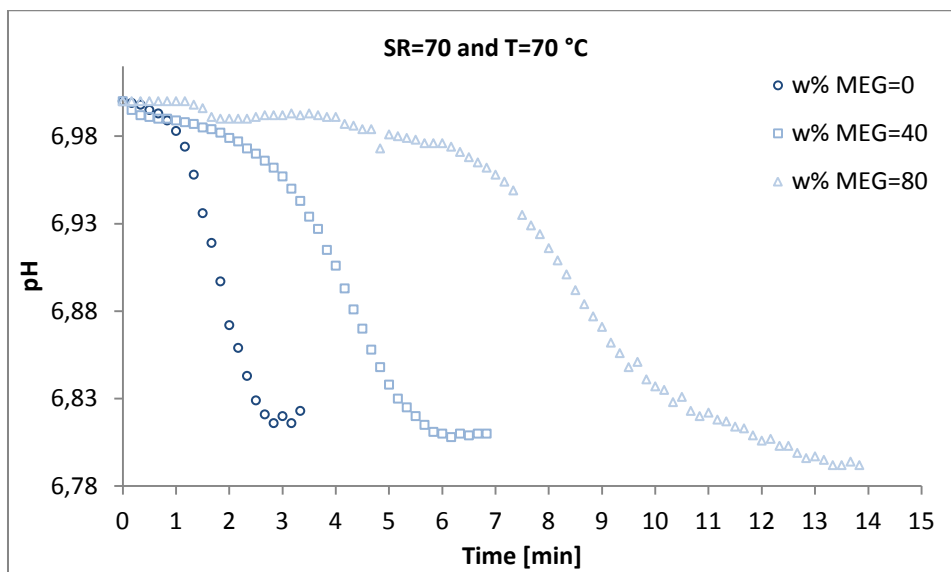


Figure 4.3: Effect of MEG on induction time in experiments. SR=70 and T=70 °C

As seen from Figure 4.3, the induction time increased with increasing content of MEG, the same trend as Flaten showed (2010b). One observation made from this figure was that the decrease in pH during the whole experiments, seem to be nearly the same for all the three experiments. Apparently MEG changed the induction time, but the difference in pH between start and end, seemed to be the same.

MEG added to a calcium carbonate system decreases the growth rate of the particles in the solution. Therefore, the reason why the induction time increased when MEG was added to the system can be seen from Equation (2.39). When G becomes smaller, t_{ind} increases, which was determined experimentally and shown in Figure 4.3. This has been reported in earlier studies where it was shown that the particles grew at a slower rate when MEG was added to a calcium carbonate system (Flaten et al., 2010a).

4.2.3 Induction times

Based on the method of determining the induction time in section 2.2.3, the induction times were found in all the experiments. An example of how the induction time was determined from experimental data in this master thesis can be seen in Appendix C.

The resulting induction times are displayed in Table 4.1.

Table 4.1: Induction times with uncertainties for experiments with initial concentration of $\text{Ca}^{2+}=5 \text{ mmol/kg solv}$

w% MEG	T=40 °C		T=70 °C	
	SR	Induction time [min]	SR	Induction time [min]
0	20	$39 \pm 0,5$	20	$11 \pm 0,5$
	25	$14,5 \pm 0,5$		
	30	$13 \pm 0,5$	30	$3,5 \pm 0,4$
	35	$12 \pm 0,4$		
	40	$5 \pm 0,5$	40	$2,2 \pm 0,2$
	70	$0,5 \pm 0,1$	70	$0,5 \pm 0,1$
	93	0		
40	20	40 ± 1	20	$10,5 \pm 0,5$
	30	35 ± 1	30	$5,5 \pm 0,5$
	40	10 ± 1	40	$2,5 \pm 0,2$
	70	$1 \pm 0,2$	70	$1,5 \pm 0,1$
	100	0		
80	40	> 120	40	$8 \pm 0,3$
	70	$16 \pm 0,6$	70	$6 \pm 0,3$

The 40-40-80 experiment did not have any response in pH for 120 minutes. Accordingly, the induction time was larger than 120 minutes, but set to be 120 minutes to be able to do calculations on the nucleation rate.

The induction times in Table 4.1 are based on pH plots for single experiments done at the varying conditions. The uncertainties associated with the induction times are as mentioned in section 2.2.3, when the decreasing part of the pH curve had two possible slopes. This uncertainty came from the *reading method* when determining the intersection between parts of the curve.

Based on the induction times found experimentally and shown in Table 4.1, a plot was made to compare the induction times with the three varying contents of MEG. This applied to the experiments with SR=40 and SR=70, see Figure 4.4.

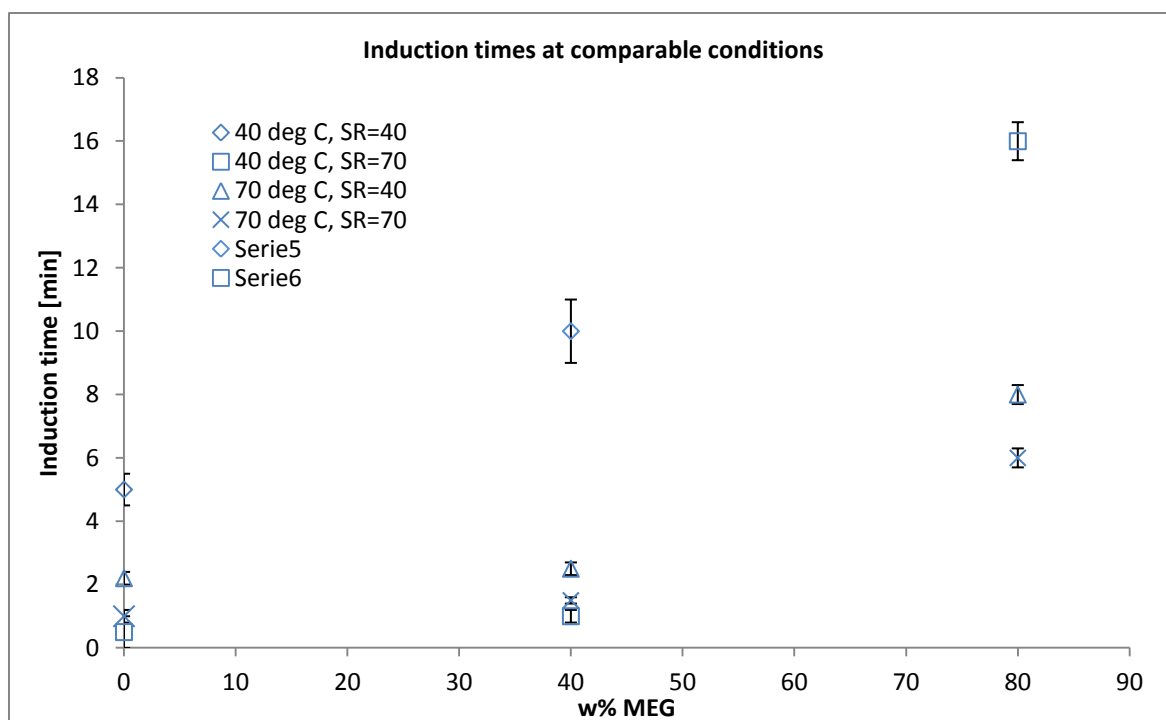


Figure 4.4: Induction times at comparable SR at 40 and 70 °C with different MEG contents

From Figure 4.4 it can be seen that the induction times increased with increasing content of MEG. It can also be seen that the induction times decreased with increasing SR. The different experiments are plotted as points with an associated uncertainty given in minutes. Each point describes one experiment and the uncertainty came from the reading method. This uncertainty is further described in section 4.2.5.

A plot showing all the induction times from Table 4.1 can be seen in Appendix C.

4.2.4 Polymorphism in the experiments

In order to calculate the nucleation rates from the induction times found in the previous section, the polymorphism obtained in the experiments had to be determined. SEM and XRD were the analysis equipment used for this matter and information about these equipments can be found in Appendix G.

Samples for SEM and XRD were taken in the end of each experiment when the supersaturation was consumed and the slope starting to flatten out $\pm 10\%$. See examples when such samples were taken in Figure 4.8 and Figure 4.10.

In most the experiments, there was too little precipitate for XRD to be used. But six experiments with high enough precipitate were chosen to be investigated by XRD. The temperature was 40 °C in three of the experiments and 70 °C in the other three. The SR varied between 20 and 70 and there was no content of MEG present.

The XRD was done to verify if the polymorphism found by using SEM was the same as determined by XRD. The XRD results obtained can be found in Appendix E. The results of this comparison can be seen in Table 4.3.

Table 4.2: Polymorphism in experiments with no MEG, detected by XRD and SEM

Experiment	Sample taken [min]	Polymorphism XRD	Polymorphism SEM
25-40-0	30	c + a	c + a
40-40-0	20	c + v + a	c + v + a
70-40-0	20	c + v + a	c + v + a
20-70-0	25	c + a	c + a
40-70-0	8	v + a	v + a
70-70-0	4	c + v + a	c + v + a

The results from the two different analysis equipment show that SEM was a reliable equipment to determine polymorphism in the rest of the experiments done in this master thesis. The polymorphism found by SEM in the rest of the experiments can be seen in Table 4.3.

Table 4.3: Polymorphism in experiments found by SEM

w% MEG	T=40 °C			T=70 °C		
	SR	Sample taken [min]	Polymorphism SEM	SR	Sample taken [min]	Polymorphism SEM
0	20	100	c + a	20	25	c + a
	25	30	c + a			
	30	30	c + v + a	30	12	v + a
	35	30	c + v + a			
	40	20	c + v + a	40	8	v + a
	70	12	c + v + a	70	4	c + v + a
	93	4	c + v + a			
40	20	120	c + a	20	35	c + a
	30	65	c + v	30	18	c + v + a
	40	40	c + v + a	40	11	c + v + a
	70	12	c + v + a	70	8	c + v + a
	100	8	c + a			
80	40	120	c	40	25	a
	70	60	c + a	70	15	c + a

A collage showing the polymorphism for all experiments at 40 °C can be seen in Figure 4.5. The SEM pictures are taken with the same settings and a magnification of 1500x, resulting in a scalebar of 30 µm. The background of the samples must not be mistaken for particles; some samples are shown on a polymer filter, while some are taped directly onto the carbon tape. E.g. the three samples from SR=40 are situated on polymer filters. From Figure 2.12 it can be seen that all the three polymorphs can be expected at 40 °C and the supersaturations chosen.

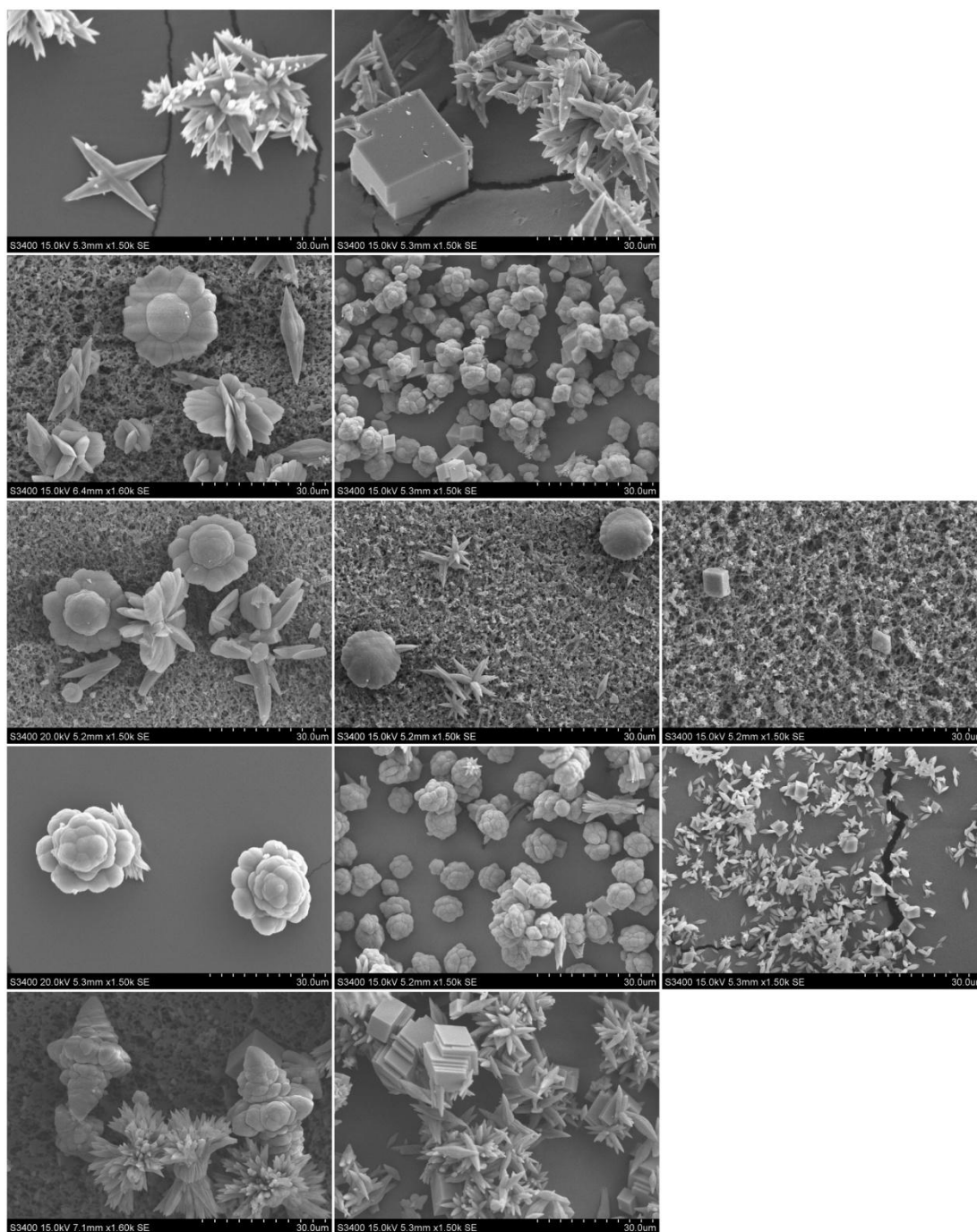


Figure 4.5: Polymorphism in experiments at 40 °C, showing increasing SR downwards (SR=20, 30, 40, 70 and 93) and increasing MEG content rightwards (0, 40 and 80 w% MEG)

As seen from Figure 4.5, the size of the particles decreases with increasing content of MEG. According to the theory in section 0, this is a right observation; the growth rate of calcium carbonate decreases with increasing content of MEG.

At a temperature of 40 °C, the morphology of vaterite is unique and looks like *flowers*. When the supersaturation was increased from 20 to 30, vaterite appeared as a flower with *flower petals* surrounding a *flower bud* in the middle. The same shape reappeared as the supersaturation was increased further. The only experiment where vaterite was not created was when the supersaturation was 20. This result is in accordance with the theory claiming that vaterite is created at high supersaturations, while calcite is created at lower supersaturations, see section 2.4. But in the rest of the experiments performed at 40 °C, morphologies of the flower-like vaterite were created. When the supersaturation was increased, the flower-shape of vaterite changed. It seems like the flower bud increases lateral with increasing supersaturation. The flower bud also seems to be more *gnarled* at supersaturations of 70 and 93.

Aragonite appears mainly at the maximum supersaturation of 93. When there was no content of MEG in the solution, all the three polymorphs were created. The aragonite appears much curved and looks like *sheaf of wheat*. When this experiment was done with 40 w% MEG, only calcite and aragonite were created. The calcite seems to lie in layers, while the aragonite looks uncontrolled and as if it has grown in all kinds of directions.

Olderøy et al. recorded morphologies of flower-like vaterite in 2010 when they investigated polymorph switch in a calcium carbonate system with alginate present in the solution. The flowers appeared at conditions of 40 °C and no alginate present. Also Andreassen et al. observed morphologies of flower-like vaterite, when these types of structures could be created in absence of biomolecule additives (2012b). A third recording of flower-like morphology of vaterite was made by Wang et al., when these structures appeared when two preheated solutions of CaCl₂ and urea was rapidly mixed together at 90 °C (1999). It was concluded that the reason of these shapes was due to the rapid mixing procedure. This could be the reason of the flower-shapes in this master thesis as well, because the solutions were rapidly mixed together, and kept at a constant mixing at 500 rpm throughout the experiment. Wang et al. assumed that the developed flower-shape of vaterite occurred instantaneously when the two solutions were mixed together, but the SEM pictures from the experiments done in this thesis show another result.

A figure was made to show the development of the morphology of flower-like vaterite during one experiment at 40 °C. The 30-40-0 experiment was chosen on the basis of the good SEM pictures obtained from this experiment. The pictures showing the development of vaterite can be seen in Figure 4.6. The settings are the same in all the SEM pictures and the magnification is 3200x, resulting in a scalebar of 10 µm.

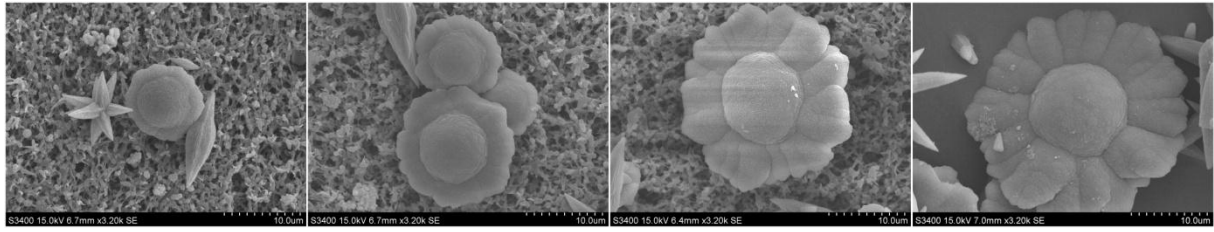


Figure 4.6: Development of morphologies of the flower-like vaterite in the 30-40-0 experiment, pictures taken at 10, 15, 20 and 25 minutes from the left

From the pictures in Figure 4.6, it looks like vaterite crystals may have started out as a more spherical crystal or a *floret*, and then grown into a flower by time. The vaterite crystal grew bigger and the flower petals became more extended towards the end of the experiment. Hence, the full developed flower-shape of vaterite is not just a result of the mixing procedure, also a result of growth at a decreasing supersaturation during an experiment at certain conditions.

Beck and Andreassen introduced a theory in 2012 when they showed that these flower-structures could be created from *hexagonal monocrystalline plates* of vaterite expressing the basal (001) faces to dendritic flower shapes, as a function of supersaturation and/or temperature. This field is not widely investigated by date, but there is ongoing work accepted in Faraday Discussions presenting these morphologies of the flower-like vaterite (Andreassen et al., 2012b).

A collage showing the polymorphism for all experiments at 70 °C can be seen in Figure 4.7. The SEM pictures are taken with the same settings and a magnification of 1000x, resulting in a scalebar of 50 μm.

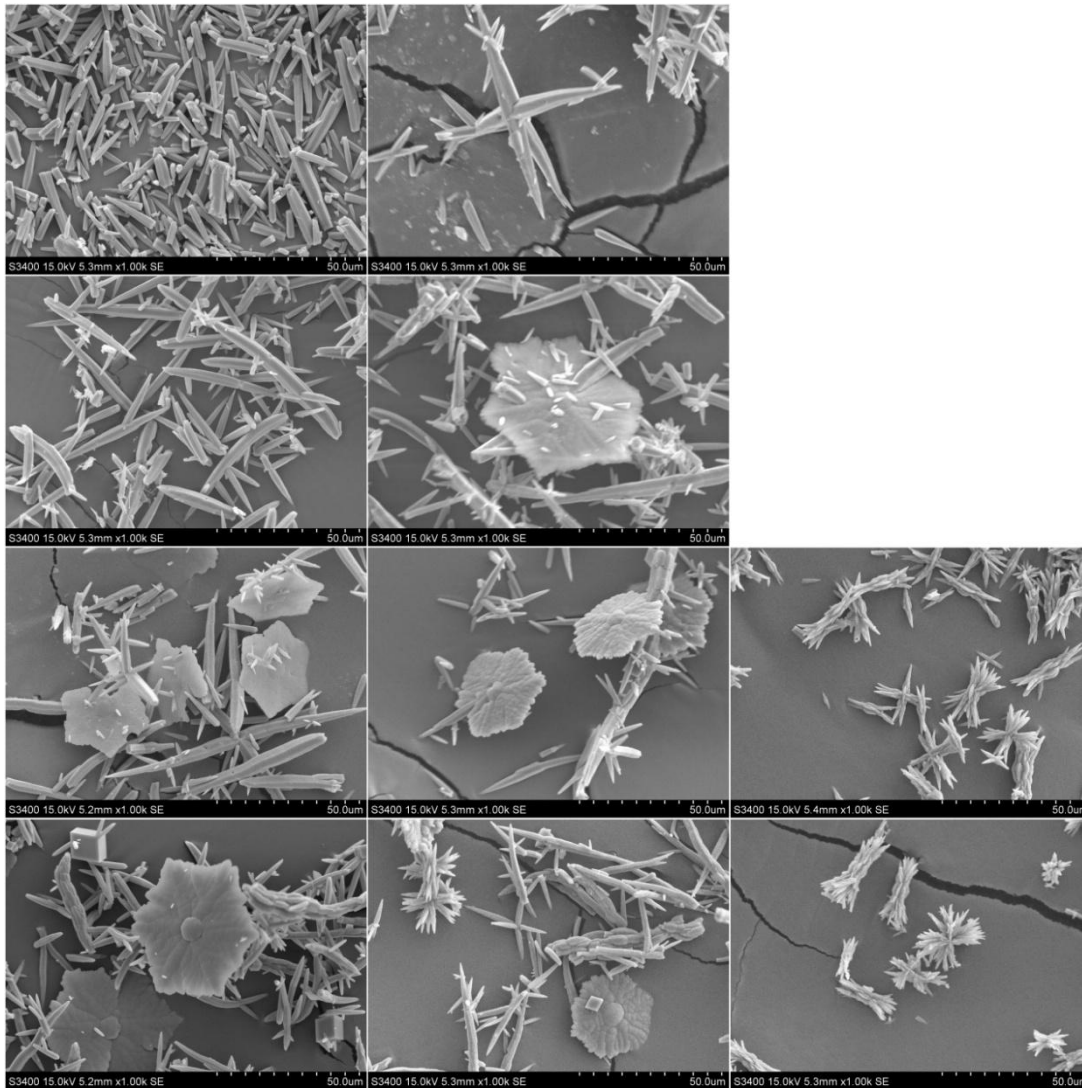


Figure 4.7: Polymorphism in all experiments at 70 °C, showing increasing SR downwards (SR=20, 30, 40 and 70) and increasing MEG content rightwards (0, 40 and 80 w% MEG)

At the elevated temperature of 70 °C, aragonite was the main polymorph precipitated. This effect can be described by thermodynamic control; aragonite is the stabilized polymorph at high temperatures, see Figure 2.12. Flaten et al. also found that *kinetics* favor aragonite; the growth rates of aragonite are higher than for the other two polymorphs (2009). When the supersaturation was increased from 20 to 30, vaterite started to appear (not seen in the picture in Figure 4.7 for SR=30).

The *supersaturation effect* is not very clear from Figure 4.7, as the appearances of the polymorphs are about the same at the different supersaturations. But when comparing the flower-like vaterite obtained at SR=40 and 40 °C, with the *star-like* vaterite obtained at

SR=40 and 70 °C, a *temperature effect* can be recognized. The morphology of the flower-like vaterite changes from flower to star when increasing the temperature from 40 °C to 70 °C.

The effect of MEG on polymorphism is less pronounced at 70 °C than at 40 °C. The most observable effect is that only aragonite and calcite were present at the high MEG content of 80 w%. Earlier studies have shown that MEG seems to stabilize vaterite and aragonite (Flaten et al., 2009). In the experiments performed in this master thesis, vaterite only appeared at 0 and 40 w% MEG and a SR higher than 30, while aragonite was the stabilized polymorph at 80 w% MEG, with the exception of the 40-40-80 experiment.

When the experiments were plotted in the solubility plot in Figure 3.3, it seemed as if an amorphous phase would be created in the beginning of the experiments at a temperature of 70 °C and a supersaturation of 70. No such phase was registered in the start of these experiments, indicating that the solubility curve of Brečević and Nielsen may be too low.

Comparing temperature- and MEG effect

Experiments with MEG contents of 0, 40 and 80 w% were done for two superasturations; namely SR=40 and 70. Combined plots showing the effect of temperature and w% of MEG can be seen in Figure 4.8 for SR=40.

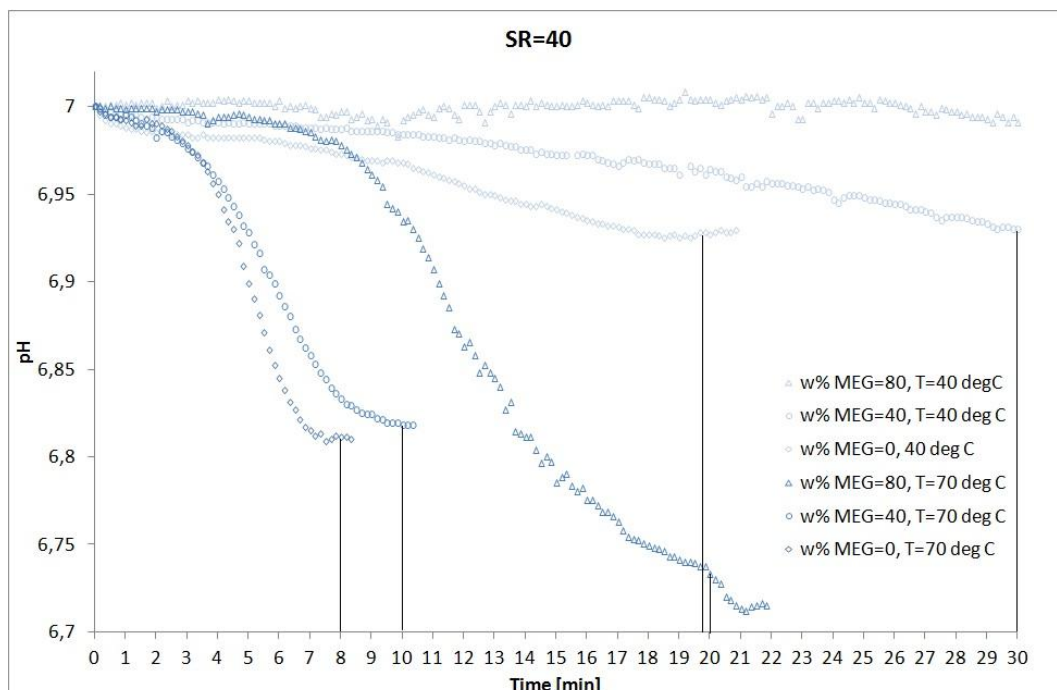


Figure 4.8: Comparing polymorphism at varying temperatures and w% MEG, SR=40

The time when the samples were taken can be seen as black lines in Figure 4.8. The sample from the 40-40-80 experiment was taken after 120 minutes, but this is not shown in Figure 4.8.

From the figure, it can be seen that the induction time and the decrease in pH is more affected by temperature than content of MEG; the pH curves dropped more at 70 °C than at 40 °C. An investigation to see if this observation also applied to the polymorphism will be done in the following paragraph.

The samples taken from the 6 experiments in Figure 4.8 were investigated in SEM. The SEM pictures were taken with the same settings and a magnification of 1500x, resulting in a scalebar of 30 µm. The pictures can be seen in Figure 4.9 for SR=40.

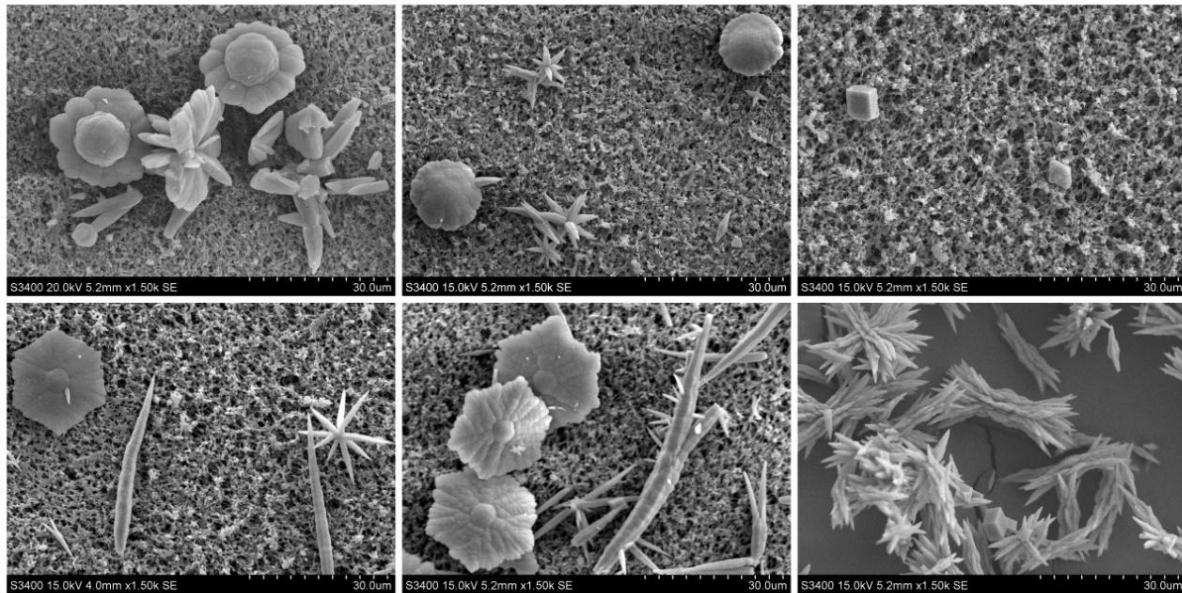


Figure 4.9: Polymorphism at 40 °C in upper grid and at 70 °C in lower grid. Increasing MEG contents towards the right; 0, 40 and 80 w%

As the content of MEG increased, the polymorphs became smaller, indicating a slower growth rate. This effect is greater at 40 °C than at 70 °C.

At 40 °C, morphologies of flower-like vaterite were created at no content of MEG. These flower-like structures can also be seen at 40 w% MEG, but the flower petals are less developed at these conditions. After 120 min in 80 w% MEG, few crystals were created and calcite was the only recognizable polymorph present.

At 70 °C and no MEG content, only polymorphs of vaterite and aragonite were created. All three polymorphs were created at a MEG content of 40 w% (calcite cannot be seen in the picture). At the MEG content of 80 w%, only calcite and aragonite were the polymorphs created. The vaterite created at 70 °C, have a more hexagonal shape and the flower *bud* looks smaller than at 40 °C. These morphologies of vaterite can also be seen at 40 w% MEG. The aragonite created at 70 °C, are longer and more needle-like than at 40 °C. When the content of MEG was increased to 80 w%, the aragonite tended to look like sheaf of wheat.

The trend indicating that temperature seems to have a greater impact on induction time than content of MEG in Figure 4.8, can also be seen in the polymorphism in Figure 4.9. MEG

decreased the size of the particles, but the increase in temperature gave different morphologies of vaterite and aragonite.

Combined plots showing the effect of temperature and w% of MEG can be seen in Figure 4.10 for SR=70.

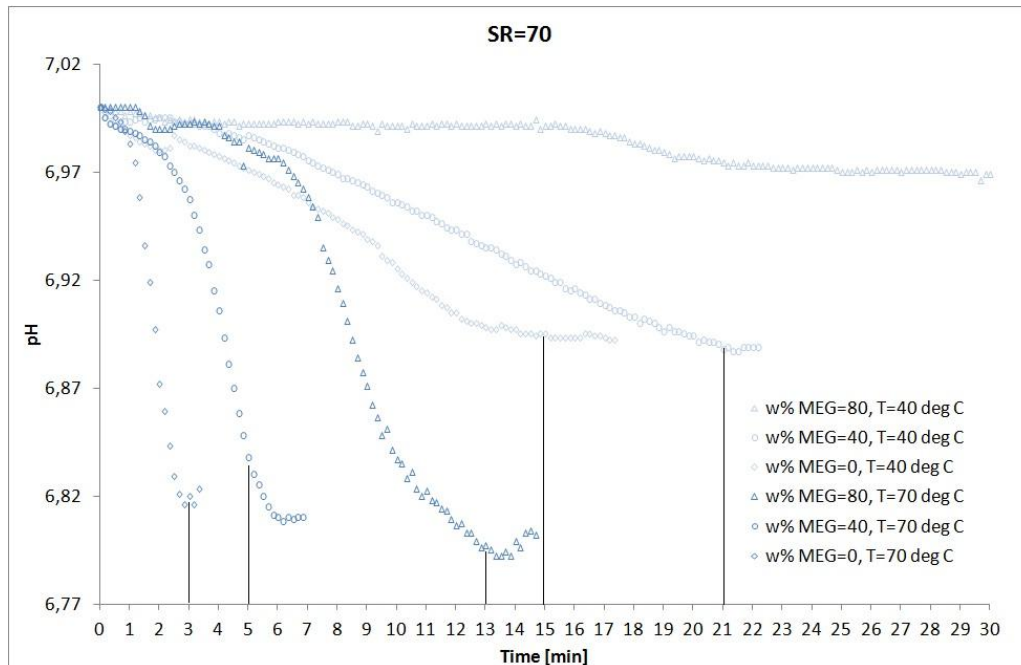


Figure 4.10: Comparing polymorphism at varying temperatures and w% MEG, SR=70

The time when the samples were taken can be seen as black lines in Figure 4.10. The sample from the 70-40-80 experiment was taken after 60 minutes, but this is not shown in Figure 4.10.

Also at SR=70 it can be seen that the decrease in pH was more affected by temperature than content of MEG in the solution.

The samples taken from the 6 experiments in Figure 4.10 were investigated in SEM. The SEM pictures were taken with the same settings and a magnification of 1500x, resulting in a scalebar of 30 μm . The pictures can be seen in Figure 4.11 for SR=70.

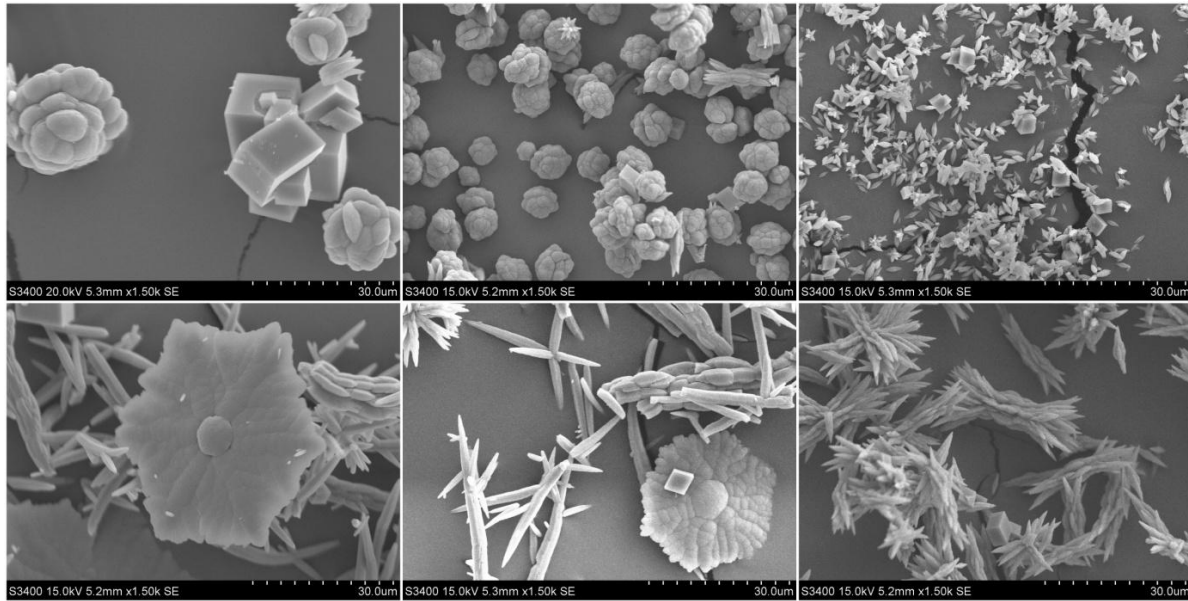


Figure 4.11: Polymorphism at 40 °C in upper grid and at 70 °C in lower grid. Increasing MEG content towards the right; 0, 40 and 80 w%

The same development of growth rate for SR=70 as for SR=40 can be seen from Figure 4.11. When the content of MEG was increased, the growth rate of the particles decreased.

At 40 °C and a supersaturation of 70, the flower-like vaterite looked more gnarled than at SR=40. At MEG contents of 0 and 40 w%, all the three polymorphs can be seen, but vaterite seemed like the more represented polymorph. At 80 w% MEG, only polymorphs of calcite and aragonite were created.

At 70°C and a supersaturation of 70, the flower-like vaterite crystals looked more like stars than at 40 °C. At a MEG content of 0 and 40 w%, all the three polymorphs were created, but aragonite and vaterite were the more represented polymorphs. Aragonite was the polymorph stabilized at 80 w% MEG, and the structures looked like sheaf of wheat.

The trend seen for SR=40 can be recognized at SR=70; temperature seems to have a greater effect on induction time than content of MEG, and this can also be seen in the polymorphism in Figure 4.11. MEG decreased the size of the particles, but the increase in temperature gave different morphologies of vaterite.

4.2.5 Nucleation rates in the experiments

The nucleation rates were calculated using Equation (2.40). The value t_{ind} was found experimentally, and can be seen in Table 4.1. The value of α is obtained from earlier studies to be 10^{-8} (Verdoes et al., 1992). The growth rate, G , depends on temperature, supersaturation, w% MEG and which polymorph that is created in the solution. The polymorphism in each experiment can be seen in Table 4.3. At least two polymorphs were present in almost every experiment. This made it challenging to choose which polymorph the growth rate should be based on.

Growth rate and nucleation rate with respect to vaterite

The growth rate expression based on vaterite is obtained from earlier studies by Flaten where the growth of vaterite was studied at different temperatures and contents of MEG (2010), see Equation (2.48). It was assumed a growth rate order of 2 which made it possible to use the growth rate data from Flaten. A growth rate order of 2 gives a parabolic growth mechanism (reaction controlled mechanism). The growth rate with respect to vaterite was chosen to count for all experiments where vaterite was present. The growth rates and nucleation rates in the experiments where vaterite was present can be seen in Table 4.4.

Table 4.4: Nucleation rates for experiments with vaterite present

Experiment	S_{vaterite}	Polymorphism	Growth rate vaterite, G_v [nm/s]	Nucleation rate vaterite, J_v [#/m ³ s]
30-40-0	2,9	c + v + a	11,83	$1,56 \cdot 10^4$
35-40-0	3,1	c + v + a	14,91	$1,07 \cdot 10^4$
40-40-0	3,3	c + v + a	18,10	$1,99 \cdot 10^5$
70-40-0	4,4	c + v + a	38,67	$2,04 \cdot 10^8$
30-40-40	2,9	c + a	8,57	$7,80 \cdot 10^3$
40-40-40	3,3	c + v	13,11	$3,27 \cdot 10^4$
70-40-40	4,4	c + v + a	28,01	$3,36 \cdot 10^7$
40-70-0	3,3	v + a	22,33	$2,83 \cdot 10^6$
70-70-0	4,4	c + v + a	47,70	$1,09 \cdot 10^8$
40-70-40	3,3	c + v + a	17,34	$3,62 \cdot 10^6$
70-70-40	4,4	c + v + a	37,04	$2,87 \cdot 10^6$

Calculations concerning growth rate and nucleation rate can be studied in Appendix F. Also the relation between SR and the respective supersaturations with respect to each of the different polymorphs can be seen there.

The results from Table 4.4 can be seen in Figure 4.12.

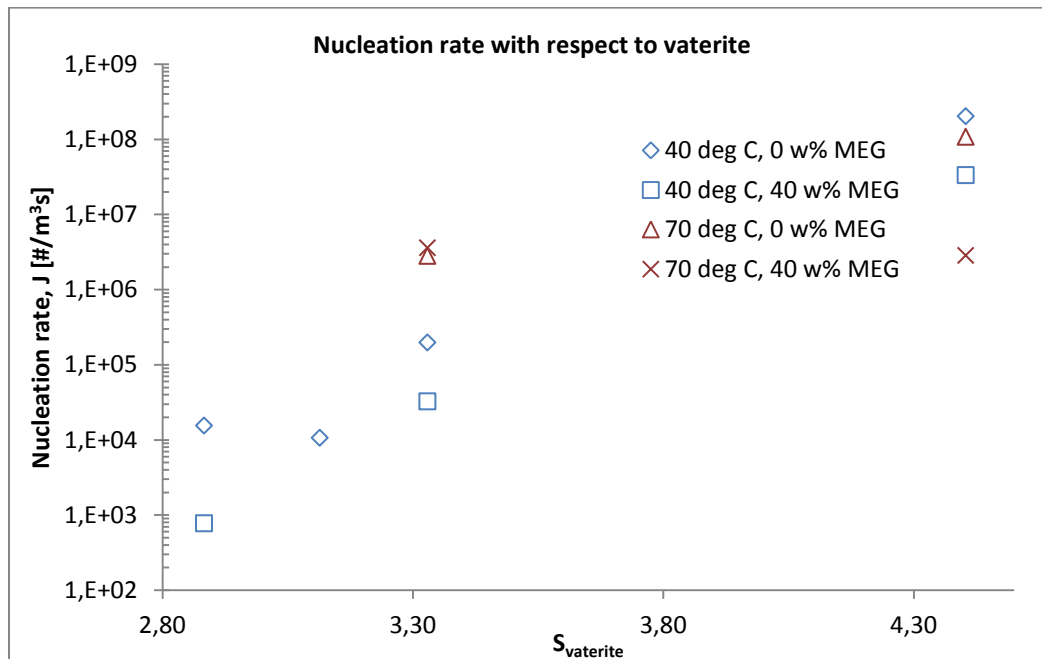


Figure 4.12: Nucleation rates with respect to vaterite

The nucleation rate in Figure 4.12 was written in a logarithmic scale. From the results in the figure, it can be seen that in most experiments, the nucleation rate increased as the supersaturation increased. When increasing the content of MEG in the solution, the nucleation rates in some cases decreased and in some cases increased. These results are incompatible and not giving a clear indication of how MEG affected the nucleation rate. As shown in earlier studies, the growth rate decreased with increasing content of MEG, and consequently the nucleation rates are likely to be underestimated to a larger extent at increasing contents of MEG (Flaten et al., 2010a).

Flaten used the same nucleation rate expression as used in this master thesis, and a nucleation rate with respect to vaterite of $7 \cdot 10^6$ #/m³s for a 70-70-50 experiment was obtained (2010). The most comparable experiment done in the current thesis, was the 70-70-40 experiment, and the nucleation rate obtained at these conditions, was $3 \cdot 10^6$ #/m³s, see Table 4.4. There is a factor of 2 in difference, but the two nucleation rates are raised to the same power. This shows that this nucleation rate found in this master thesis correlates with the nucleation rate in MEG from earlier studies and indicates that the induction times obtained from the pH plots are within usable limits. The nucleation rates from the other experiments may correlate as well, but no nucleation rates from earlier literature could be obtained to compare the results.

From earlier studies by Flaten et al., they claimed that the nucleation rate *increased* with *increasing* content of MEG in the solution (2010b). Mullin has a theory giving the opposite result. From Equation (2.34) it can be seen that the nucleation rate *decreases* as the viscosity in the solution *increases*. There are earlier studies supporting this theory, done by Mullin and

Leci in 1969. They did experiments on nucleation in aqueous citric acid solutions, claiming that the nucleation rate decreased as a result of the increased *viscosity* in the solution. Experiments showing these types of results have mainly been confined to melts. But because MEG increases the viscosity in a solution, the theory of Mullin and Leci could apply to the findings done in this master thesis, saying that the nucleation rate decreased with increasing content of MEG in some of the experiments.

The conflicting results shown in Figure 4.12 may also be an effect of the assumption made in this master thesis, saying that the growth rate with respect to vaterite can be used, even if other polymorphs are present in the solution.

Growth rate and nucleation rate with respect to calcite

Kralj et al. did studies on growth of calcite in water at 40 °C. The growth rates based on calcite are obtained from these studies (1996). The growth rate found was based on the initial supersaturation in the experiment. The growth rate order, g , was set to be 2, to be able to use the growth rate data from Kralj et al. This gives a parabolic growth mechanism (reaction controlled mechanism). The growth rate with respect to calcite was chosen to count for the experiments done at 40 °C where calcite and aragonite were present. The nucleation rates in the experiments where calcite was created in absence of MEG can be seen in Table 4.5.

Table 4.5: Nucleation rates for experiments with calcite and aragonite present

Experiment	Polymorphism	Growth rate calcite, G_c [nm/s]	Nucleation rate calcite, J_c [#/ m^3s]
20-40-0	c + a	0,90	$4,35 \cdot 10^5$
25-40-0	c + a	1,21	$9,41 \cdot 10^6$

As seen from Table 4.5, the growth rate of calcite increased with increasing supersaturation and so did the nucleation rate. The nucleation rate increased with increasing supersaturation, because the driving force of nucleation increases with supersaturation, see Equation (2.30). These observations match earlier studies done by among others Flaten (2010) and Wolthers et al. (2012).

Flaten determined some growth rates with respect to aragonite at 40 °C, but there were no experiments in this thesis that only contained aragonite at this temperature. Moreover are the growth rate constants found by Flaten based on experiments with $S_a < 3$, a much lower S_a than used in this thesis (2010).

Variables in the nucleation rate expression

As seen from Equation (2.40), the nucleation rate is based on three variables, namely the α -value, the induction time, t_{ind} and the growth rate, G . From the expression, it can be seen that the α -value is raised to the power of 1, while G and t_{ind} are raised to the power of 3 and 4, respectively. This indicates that the growth rate and the induction time are factors that should be determined accurately to give the correct nucleation rate.

A plot was made to show how the nucleation rate changes if the three variables are changed by $\pm 10\%$ in the 40-40-0 experiment. The result can be seen in Figure 4.13.

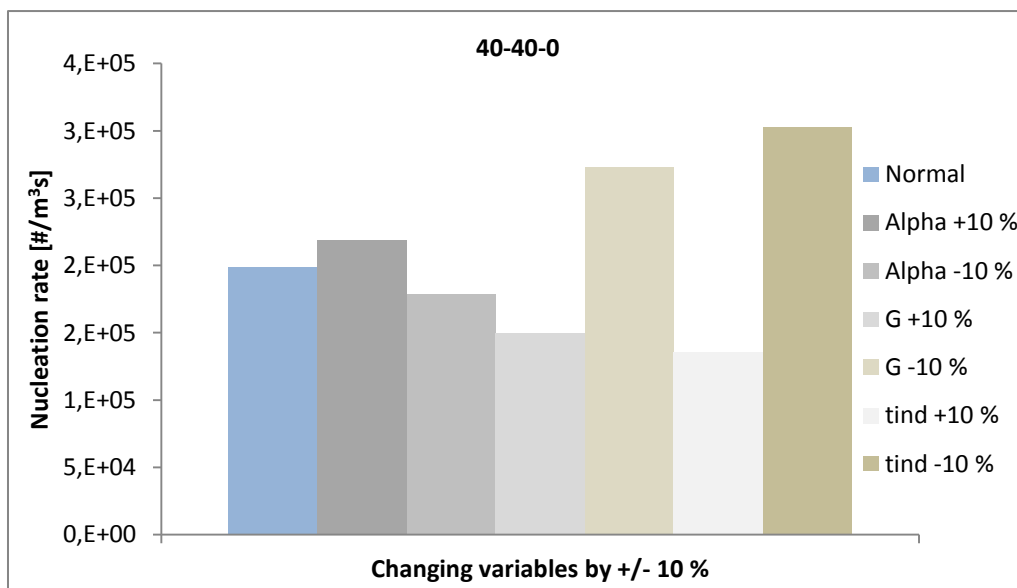


Figure 4.13: Changing the variables with $\pm 10\%$ in the nucleation rate expression for the 40-40-0 experiment

From Figure 4.13 it can be seen that the nucleation rate changes the most when the induction time is decreased by 10% and when the growth rate is decreased by 10%. A table was made to see the change in nucleation rate in percent from normal, see Table 4.6.

Table 4.6: Change of 10% of variables affecting nucleation rate for the 40-40-0 experiment

Change	J [# / m ³ s]	Change from normal [%]
Normal	$1,99 \cdot 10^5$	
α +10 %	$2,19 \cdot 10^5$	10
α -10 %	$1,79 \cdot 10^5$	-10
G +10 %	$1,49 \cdot 10^5$	24,9
G -10 %	$2,73 \cdot 10^5$	-37,2
t_{ind} +10 %	$1,36 \cdot 10^5$	31,7
t_{ind} -10 %	$3,03 \cdot 10^5$	-52,4

As seen from Table 4.6, the nucleation rate is most changed when the induction time is decreased by 10%. The preceding analysis confirms that induction time and growth rates are the factors affecting nucleation time the most.

Uncertainties in the variables in the nucleation rate expression

As described in section 4.2.5, the value chosen for α , was 10^{-8} . But as mentioned in section 2.2.3, the α -value usually lies between 10^{-8} and 10^{-6} . The α -value will change a lot with the supersaturation, and can be expected to be as low as 10^{-5} (Flaten, 2010). By choosing an α -value of 10^{-5} , the nucleation rate increases with a factor of 1000. But because the α -value is the same in all calculations, this uncertainty can be neglected, since the main area of interest is the nucleation rates *compared to each other*. But it is important to evaluate this factor if the exact value of the nucleation rate is the interesting target.

The growth rates are as mentioned before, obtained from earlier studies by Flaten et al. (2010a) and Kralj et al. (1996). It was assumed that these growth rates were valid for the use in this master thesis. It is important to remember, though, that the growth rates they determined were with respect to *one* polymorph, and not a mixture as was the case in the current experiments.

Induction time is the factor affecting the nucleation rate mostly, and this was the value found experimentally in this master thesis. When working with experimental data there will always be different sources of errors, leading to uncertainty in the documented data. Uncertainties associated with the induction times degenerate from the reading method when determining the induction times from pH plots and the variation within one experiment. Other experimental errors can be investigated in Appendix D.

To investigate the experimental errors regarding the determining of induction times from pH plots, 5 parallels were done for the 40-40-0 experiment. The same method was used to determine the induction times as in section 4.2.3. The resulting induction times are displayed in Table 4.7.

Table 4.7: Precision in the reading method to determine induction times for the 40-40-0 experiment

Experiment (date)	Initial pH	Induction time [min]	Deviation [\pm min]	Deviation [%]	Mean deviation [%]
09.03.12	7,052	6	0,8	13,3	11,4
13.03.12	7,054	1	0,15	15,0	
19.03.12	7,103	5	0,3	6,0	
27.13.12	7,087	5	0,5	10,0	
29.03.12	7,115	8	1	12,5	

The pH plots used to determine the induction times in Table 4.7 can be seen in Appendix D.

On the basis of the *reading method*, the induction times determined for the 40-40-0 experiment varied between 1 and 8 minutes, with a mean percentage deviation of 11,4 %. This was a measure of the error that occurred from the experimental method of determining the induction time. This error was assumed to be the same for all experiments, independent

of the varying conditions. This error may vary at other conditions, but for this work it was only going to give an impression of how much deviation the reading method gave.

As seen from Table 4.7, the initial pH in the experiments varied from each other and they also varied from the theoretical value of 7,123 (see Table 3.1). This may indicate that the two start solutions were not entirely at equilibrium when mixing them together. This will have some effect on the precipitation rate in the experiments, as the equilibrium equations then are shifted. This uncertainty is further described in Appendix D, where also the differences in pH during each of the experiments are considered. This uncertainty was nevertheless considered minimal.

The effect of random errors can be reduced by using the average values of a sufficient amount of independent experimental data. Then the precision will increase with increasing amount of parallel experiments performed (Førland, 2001). By assuming that the 5 parallels done for the 40-40-0 experiment were a representative range of values following a normal distribution, the mean induction time and standard deviation could be found. The result of this analysis is displayed in Table 4.8.

Table 4.8: Reproducibility in one experiment, 40-40-0

Mean induction time, t_{ind} [min]	Standard deviation [\pm min]	Standard deviation [\pm %]
5,0	2,6	51,1

All experimental errors were included in the standard deviation of 51,1 % from Table 4.8. This large deviation made the determination of induction times from experimental data the largest source of error in this master thesis. This deviation was concerning the 40-40-0 experiments. Only two parallels were done for the respective experiments, and therefore they are too few to give sufficient results on reproducibility. But one example of the standard deviation when the temperature was 70 °C can be seen in Table 4.9.

Table 4.9: Standard deviation for the 40-70-0 experiment

Experiment (date)	Induction time [min]	Mean induction time, t_{ind} [min]	Standard deviation [\pm min]	Standard deviation [\pm %]
25.04.12	3,6	3,0	1,1	36,0
30.04.12	2,2			

As seen in Table 4.9, the standard deviation was smaller at the 40-70-0 experiments than at the 40-40-0 experiment. This may indicate that the reproducibility was more accurate at 70 °C than at 40 °C, but as mentioned earlier in this paragraph, the experiments were not reproduced a sufficient number of times to conclude with any trends.

The calculations concerning the mean induction time and standard deviation can be seen in Appendix F.

When the standard deviation of $\pm 51,1 \%$ was included in the induction time in Equation (2.40), the nucleation rate changed and can be seen in Table 4.10.

Table 4.10: Change from normal in nucleation rate with standard deviation of induction time

Change	J [#/ m^3s]	Change from normal [factor]
Normal	$1,99 \cdot 10^5$	
$t_{ind} +51,1 \%$	$3,81 \cdot 10^4$	0,19
$t_{ind} -51,1 \%$	$33,48 \cdot 10^6$	17,5

The big changes in nucleation rate displayed in Table 4.10 conclude that the experimental uncertainties in the induction times were the biggest source of error when determining the kinetics in this master thesis.

This standard deviation may be decreased by doing more parallels of the same experiment, but there will always be a certain spread in the experiments due to the stochastic variable in the nucleation mechanism (Jiang and Horst, 2011).

4.3 Variation of stoichiometry

The activity ratio between calcium and carbonate was varied in the 40-40-0 experiment, to investigate whether this variable affected the induction time and polymorphism in the experiments.

4.3.1 Induction times and polymorphism in CO₂-bubbling experiments

The pH plots from the experiments done with CO₂-bubbling can be seen in Figure 4.14.

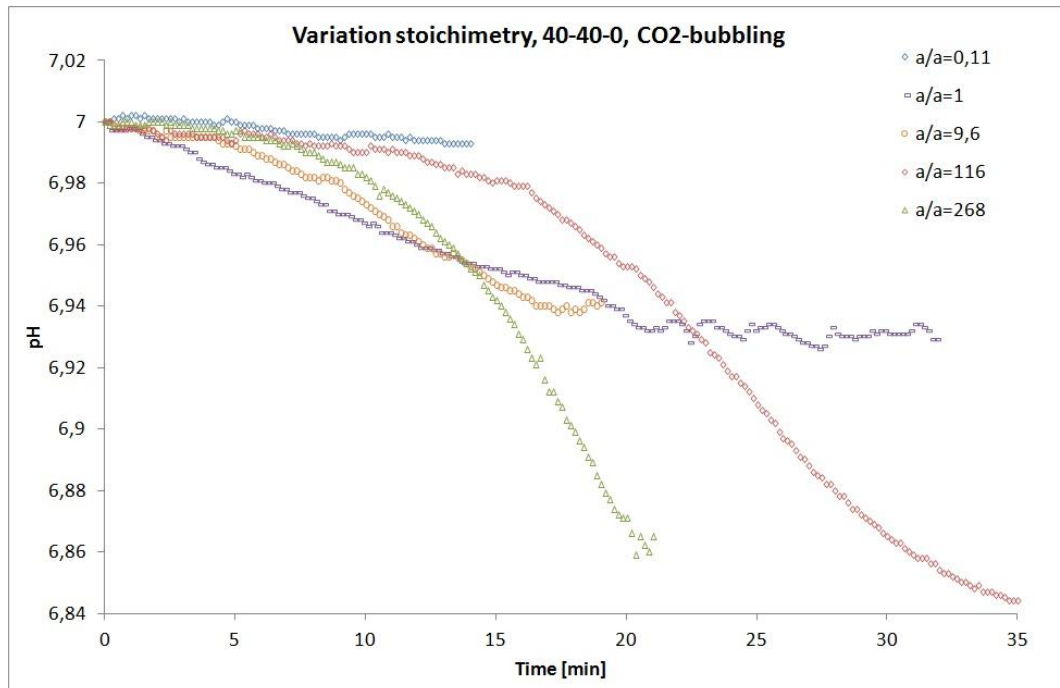


Figure 4.14: Variation stoichiometry, 40-40-0, CO₂ -bubbling

When the ratio between the activities ($a_{Ca^{2+}}/a_{CO_3^{2-}}$) increased, the difference in pH during an experiment also increased. This is because when the ratio was high, there was a lot of calcium available in the solution. Predominance of calcium in the solution made the equilibrium equation (2.12) go towards the right, and CO₃²⁻-ions and H⁺-ions were released. Consequently, a lot of carbonate was consumed to create calcium carbonate. As mentioned in section 2.1.3, the pH decreases during the precipitation of calcium carbonate.

To compare the area where the pH started to decrease, a plot with relative pH was made to more easily compare this area in the different experiments. This plot can be seen in Figure 4.15.

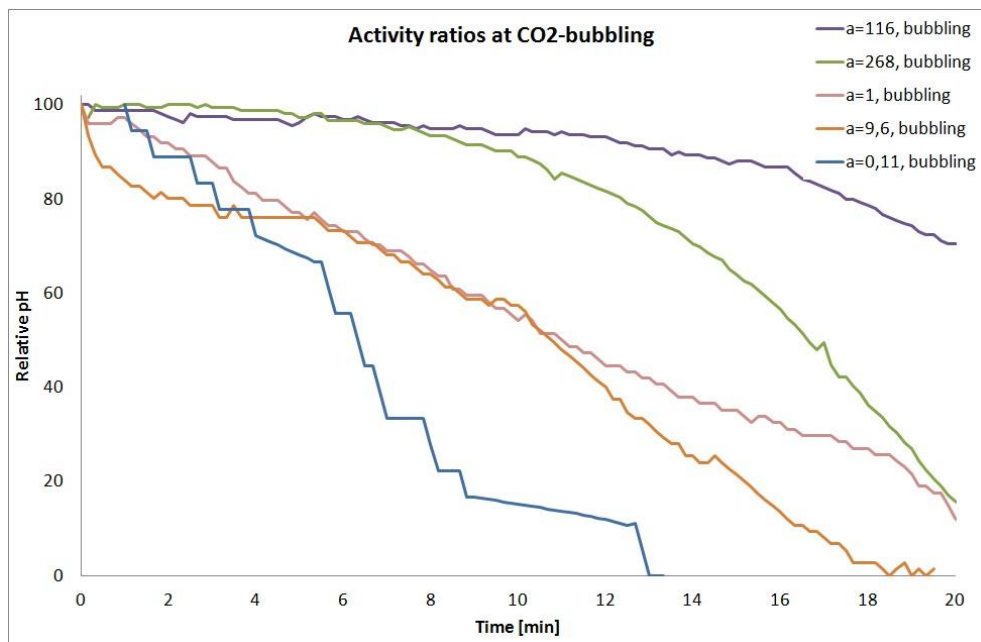


Figure 4.15: Variation stoichiometry, $a_{Ca^{2+}}/a_{CO_3^{2-}}$, CO_2 -bubbling experiments

From Figure 4.15 it can be seen that even though the three parameters SR, temperature and w% MEG were the same in all the experiments, the induction time varied as the stoichiometry in the solution varied. When the activity ratio was ≤ 1 , no induction time could be found from the pH plots. It seemed like the precipitation of $CaCO_3$ started right away. At the other activity ratios, the change in pH was more evident and an induction time could be found from the curves.

A trend seen from the figure was that an activity ratio ≤ 1 did not have any induction time, while the induction time became longer as the activity ratio became > 1 . Gómez-Morales et al. did studies on precipitation of calcium carbonate from solutions with varying Ca^{2+} /carbonate ratios (1996). They mixed solutions of $CaCl_2$ and K_2CO_3 at 25 °C and a pH of 9,0 and observed that the induction time was increased when an excess of Ca^{2+} was present in the bulk solution. The procedure of that experiment and the ones shown in Figure 4.15 were different, but it may be the reason why the induction times differed when the stoichiometry was changed, even at a constant supersaturation and temperature. In the next section, experiments more similar to the ones Gómez-Morales et al. did will be presented to more easily compare the results obtained with results from literature.

The polymorphism obtained in the CO₂-bubbling experiments when activity ratio was varied, can be seen in Figure 4.16. The different morphologies of vaterite are shown in the figure, because this was the more represented polymorph in the 40-40-0 experiments. The magnitudes in the pictures were different; the pictures were only meant to give an impression of how the morphology of vaterite changed when the activity ratio was varied.

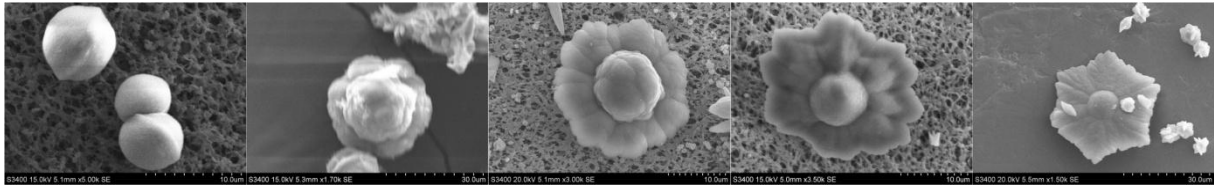


Figure 4.16: Morphologies of vaterite when increasing the activity ratio from the left (0,1, 1, 9,6, 116 and 269). CO₂-bubbling

From Figure 4.16 it seems like the activity ratio affected the extent of the flower petals; as the activity ratio increased, the flower petals of the flower-like vaterite grew larger and larger. When the activity ratio was ≤ 1 , there could not be determined any induction time. In these two experiments, the nucleation rates were probably very high, and this could be the reason for the “underdeveloped” florets; most of the present supersaturation was used for nucleation, and consequently not much was left for the vaterite structures to grow bigger. In Table 4.11, the activity ratios and the shapes of vaterite are shown.

Table 4.11: Morphologies of vaterite from Figure 4.16

Activity ratio [$a_{Ca^{2+}}/a_{CO_3^{2-}}$]	Morphology of vaterite
0,09	Small flower petals – macaroon shape
1,0	Flower petals a bit bigger – small flower
9,6	Flower
116	Flower with large flower petals
269	Hexagonal flower with bud in the middle.

Based on the discovery in the preceding paragraph about how activity ratio affected the shape of vaterite, a figure was made to compare the shape of vaterite in experiments performed with CO₂-bubbling at 40 °C and no content of MEG, when *both* SR and the activity ratio were varied. This can be seen in Figure 4.17.

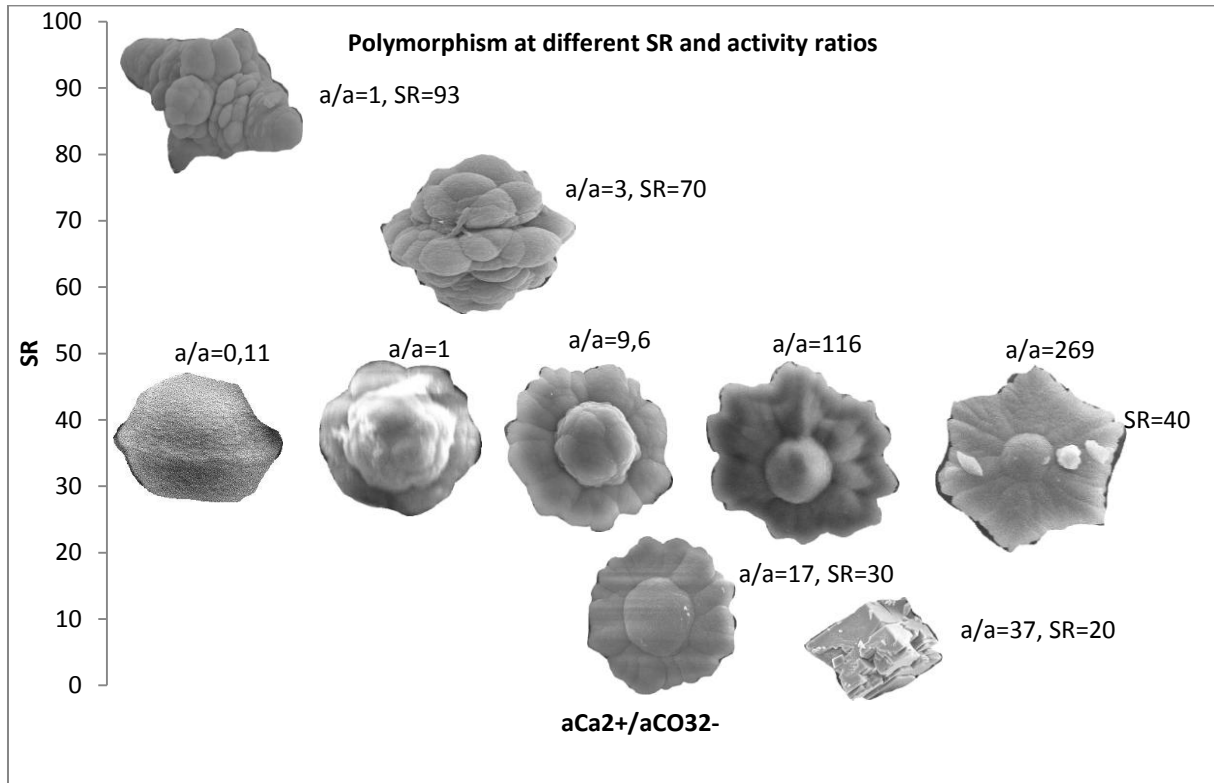


Figure 4.17: Comparison of experiments performed with CO₂-bubbling at 40 °C and no content of MEG. Increasing SR on the y-axis and increasing activity ratio on the x-axis

Vaterite was created in all experiments with an exception when the SR was 20. A general observation is that the increasing activity ratio affected the size and extent of the flower petals, while the increasing SR affected the extent of the flower bud in the middle. The activity ratios at the other supersaturations were calculated the same way as shown for SR=40 in Appendix F.

4.3.2 Induction times and polymorphism in high pH experiments

Four experiments were performed with Na_2CO_3 as the source of carbonate. This was done to evaluate if the source of carbonate affected the induction times and polymorphism from the results obtained in the previous section. To compare the area where the pH started to decrease, a plot with relative pH was made, as in the preceding section. The curves from these experiments can be seen in Figure 4.18.

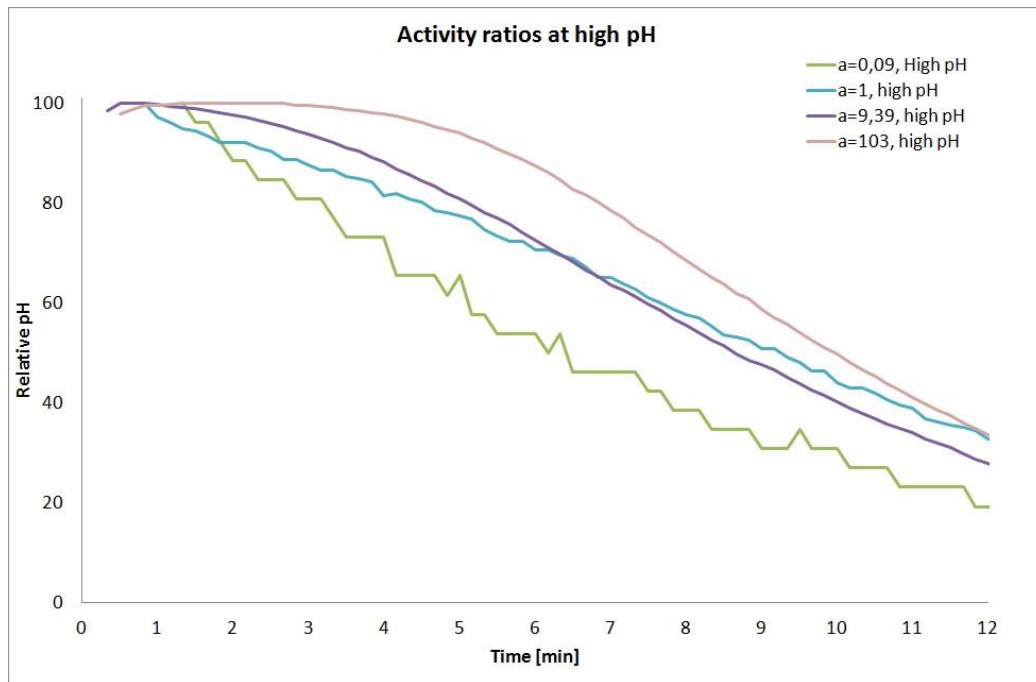


Figure 4.18: Variation stoichiometry, $a_{\text{Ca}^{2+}}/a_{\text{CO}_3^{2-}}$, high pH experiments

The same trend found in the CO_2 -bubbling experiments can also be seen here in the high pH experiments; when $a_{\text{Ca}^{2+}}/a_{\text{CO}_3^{2-}} \leq 1$, no induction time could be determined. As the activity ratio became larger, the induction time became longer. These experiments were similar to the experiments performed by Gómez-Morales et al., and in this master thesis it is concluded that the induction time increases with increasing excess of Ca^{2+} in the solution. This conclusion supports the theory of Gómez-Morales et al. (1996).

The pictures taken in SEM can be seen in Figure 4.19. All the pictures were from samples taken after 20 minutes. The settings for the pictures were the same and the magnification was 2500x.

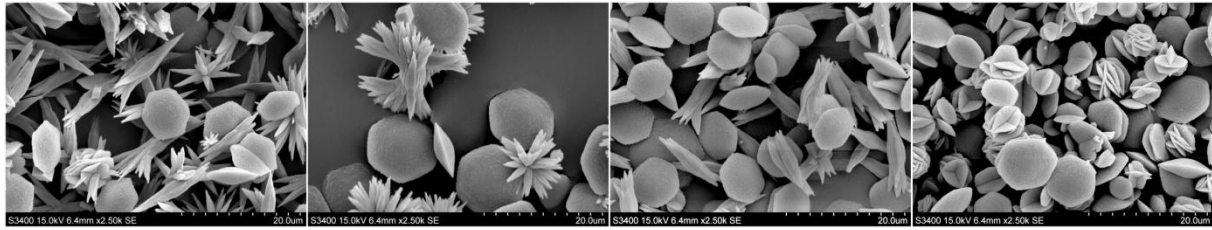


Figure 4.19: Morphologies of vaterite when increasing the activity ratio from the left (0,1, 1,0, 9,4 and 103). High pH

When the activity ratio was < 10 in the high pH experiments, the shape of vaterite did not seem to change much even though the activity ratio was changed. Hexagonal discs could be seen at activity ratios of 0,09, 1 and 9,39. When the activity ratio was increased to 103, the vaterite started to lie in cross, often in several layers, like *desert flowers*. This can be an indication that increased activity ratio between calcium and carbonate in high pH experiments increase the lamination of vaterite discs, resulting in morphologies like desert flowers. Aragonite appeared when the activity ratio < 10 , but not when the activity ratio was 103.

In Table 4.12, the activity ratios, initial pH and the morphologies of vaterite in high pH experiments are shown.

Table 4.12: Morphologies of vaterite from Figure 4.19

Activity ratio [$a_{Ca^{2+}}/a_{CO_3^{2-}}$]	Initial pH	Morphology of vaterite
0,09	10,4	Hexagonal discs
1,0	10,1	Hexagonal discs
9,4	9,9	Hexagonal discs
103	9,6	Discs and desert flower shapes

Another finding done by Gómez-Morales et al. was that the induction time and nucleation rate were affected by the initial pH in experiments where solutions of $CaCl_2$ and K_2CO_3 were mixed together. They discovered that at a initial pH between 9,5 and 10 gave an induction time, while experiments with an initial pH of 10 did not give an induction time at all (1996). This agrees with the observations done in the high pH experiments performed in this master thesis; an activity ratio ≤ 1 and initial pH between 9,5 and 10, did not have an induction time, while an activity ratio > 1 and an initial pH ≥ 10 did have an induction time, see Figure 4.18. The relationship between activity ratio and initial pH in the experiments can be seen in Table 4.12.

5 Conclusions

The induction times were found experimentally and pH was used as the measurement method to detect precipitation in the supersaturated calcium carbonate system. Increase in supersaturation and/or temperature decreased the induction time, while an increase of MEG in the solution increased the induction time. The induction time determined for the experiment performed at 40 °C and SR=40 was 5, 10 and >120 min for respectively 0, 40 and 80 w% MEG. The induction time decreased from 39 to 0 min when the SR was increased from 20 to 93 at 40 °C and no MEG. The induction time decreased from 5 to 2,2 min when the temperature was increased from 40 to 70 °C at SR=40 and no MEG. Content of MEG in the solution affected the induction time most, especially at the lower temperature of 40 °C. When the activity ratio between calcium and carbonate was varied in the 40-40-0 experiment, it was found that the induction time increased when the ratio became > 1.

The polymorphism in the solution was more dependent on supersaturation and temperature than content of MEG. MEG in the solution mainly resulted in smaller particles. The effect of MEG on particle size was more pronounced at 40 °C than at 70 °C. Morphologies of flower-like vaterite were found in all of the experiments at 40 °C and a supersaturation ≥ 30 . As the supersaturation increased, the flower buds became more gnarled. At a temperature of 70 °C, the morphologies of vaterite appeared at supersaturations ≥ 30 , and looked more like stars than flowers. Increased supersaturation in the experiments gave increased growth of vaterite in the flower bud, while increased activity ratio gave increased growth of vaterite in the flower petals. For the experiments done at 70 °C, aragonite was the main polymorph created. Aragonite was stabilized especially at 80 w% MEG and 70 °C, and SR=20 and 70 °C. The aragonite created at SR=93 and 40 °C, appeared like sheaf of wheat. Calcite was created in most experiments.

A standard deviation of 51,1 % in the induction time measurements was found for the 40-40-0 experiment, showing that this was the main uncertainty when determining the kinetics in this master thesis. Induction time impacts the nucleation rate most, and consequently, this big uncertainty was transferred to the nucleation rates. The nucleation rates increased with a factor of 17,5 when the induction time decreased with 51,1 %.

The nucleation rates calculated with respect to vaterite at 40 °C and no content of MEG varied from $1,56 \cdot 10^4 \text{ \#/m}^3\text{s}$ when the supersaturation was 30 to $2,04 \cdot 10^8 \text{ \#/m}^3\text{s}$ when the supersaturation was 70. The nucleation rate with respect to calcite increased from $4,35 \cdot 10^5 \text{ \#/m}^3\text{s}$ to $9,41 \cdot 10^6 \text{ \#/m}^3\text{s}$ when the supersaturation was increased from 20 to 25 at 40 °C and no content of MEG. The nucleation rates increased with supersaturation and temperature. The effect of MEG on nucleation rate was incompatible.

6 Further recommendations

In this master thesis, the parameters supersaturation, temperature, content of MEG and activity ratio between calcium and carbonate was varied. Further investigation of the stoichiometry should be done, as this variable often is neglected when determining kinetics and polymorphism in a calcium carbonate system. Since both induction time and polymorphism changed when the activity ratio in the 40-40-0 experiment was varied, further investigations should be done when also SR and temperature are varied. The effect of MEG on stoichiometry would be interesting to investigate, to reflect real conditions in natural gas production better.

As seen from the uncertainty section, the experimental error concerning the induction time was very large. A better method to measure the induction time should be developed for further experiments, to minimize the experimental uncertainties. If the uncertainty found lies in the nucleation mechanism itself, it is not easy to get a good reproducibility in the experimental values. But a suggestion is to do several parallels to minimize the experimental errors, and try to isolate the uncertainty in the nucleation mechanism. The parallels could be done at two different temperatures, so that the uncertainty associated with this variable could be measured as well.

The uncertainty in the induction time consequently gave large uncertainties in the nucleation rates, as the induction time was included in the nucleation rate expression. Different methods to determine the nucleation rate should be done in parallel with the used method in this master thesis, to compare the results obtained. Also the α -value in the expression calculating the nucleation rate should be estimated for the certain experimental method.

Also the growth rate is included in the expression for calculation of the nucleation rate. The growth rates used in this master thesis were obtained from earlier studies and were based on each of the different polymorphs. It was probably not right to assume that this growth rate was valid for the experiments with a mix of polymorphs present. There should be done an analysis measuring the percentage of the different polymorphs present in an experiment, and then see if this percentage can be used on the growth rates based on each of the polymorphs. In general, more growth rates with respect to the polymorphs aragonite and calcite should be done for solutions containing MEG.

7 References

Andreassen, J.-P. Short course in crystallization and precipitation from solution.

Andreassen, J.-P., 2010. Lecture notes: Introduction. Trondheim. NTNU.

Andreassen, J.-P., R. Beck, and M. Nergaard. , 2012a. Biomimetic type morphologies of calcium carbonate grown in absence of additives. *Faraday Discussions*. <http://dx.doi.org/10.1039/C2FD20056B> (accessed)

Andreassen, J.-P., R. Beck, and M. Nergaard. , 2012b. Biomimetic type morphologies of calcium carbonate grown in absence of additives. *Excepted in Faraday Discussions*:

Beck, R., and J.-P. Andreassen. , 2011. The Influence of crystallization conditions on the onset of dendritic growth of calcium carbonate. *Crystal Research and Technology* 47: 404-408.

Brecevic, L., and A. E. Nielsen. , 1989. Solubility of Amorphous Calcium-Carbonate. *Journal of Crystal Growth* 98 (3): 504-510.

Clarkson, J. R., T. J. Price, and J. C. Adams. , 1992. Role of Metastable Phases in Spontaneous Precipitation of Calcium-Carbonate *Journal of the Chemical Society - Faraday Transactions* 88 (2): 243-249.

Flaten, E. M., 2010. The effect of MEG on the precipitation kinetics of calcium carbonate related to natural gas production from subsea wells, NTNU, NTNU, Trondheim

Flaten, E. M., M. Seiersen, and J.-P. Andreassen. , 2009. Polymorphism and morphology of calcium carbonate precipitated in mixed solvents of ethylene glycol and water. *Journal of Crystal Growth* 311: 3533-3538.

Flaten, E. M., M. Seiersen, and J.-P. Andreassen. , 2010a. Growth of the calcium carbonate polymorph vaterite in mixtures of water and ethylene glycol at conditions of gas processing. *Journal of Crystal Growth* 312: 953-960.

Flaten, E. M., M. Seiersen, and J.-P. Andreassen. , 2010b. Induction time studies of calcium carbonate in ethylene glycol and water. *Chemical Engineering Research and Design* 88: 1659-1668.

Førland, K. S., 2001. *Kvantitativ Analyse*. 2nd ed. Trondheim: Tapir Akademisk Forlag.

Gómez-Morales, J., J. Torrent-Burguès, A. López-Macipe, and R. Rodríguez-Clemente. , 1996. Precipitation of calcium carbonate from solutions with varying Ca²⁺/carbonate ratios. *Journal of Crystal Growth* 166: 1020-1026.

Gómez-Morales, J., J. Torrent-Burguès, and R. Rodríguez-Clemente. , 1996. Nucleation of calcium carbonate at different initial pH conditions. *Journal of Crystal Growth* 169: 331-338.

- Helbæk, M., and S. Kjelstrup. , 2006. *Fysikalsk Kjemi*. 2nd ed: Fagbokforlaget.
- Jiang, S., and J. H. t. Horst. , 2011. Crystal Nucleation Rates from Probability Distributions of Induction Times. *Crystal Growth & Design* 11: 256-261.
- Kaasa, B., 1998. Prediction of pH, mineral precipitation and multiphase equilibria during oil recovery, Institute of Inorganic Chemistry, NTNU, NTNU Trondheim
- Kaasa, B., K. Sandengen, and T. Østvold. , 2004. Thermodynamic predictions of scale potential, pH and gas solubility in glycol containing systems. *SPE 95075*:
- Kashchiev, D., and G. M. v. Rosmalen. , 2003. Review: Nucleation in solutions revisited. *Cryst. Res. Technol.* 38 (7-8): 555-574.
- Konopacka-Lyskawa, D., and M. Lackowski. , 2010. Influence of ethylene glycol on CaCO₃ particles formation via carbonation in the gas-slurry system. *Journal of Crystal Growth* 321 (2011): 136-141.
- Kralj, D., L. Brecevic, and J. Kontrec. , 1996. Vaterite growth and dissolution in aqueous solution III. Kinetics of transformation. *Journal of Crystal Growth* 177: 248-257.
- Lindenberg, C., and M. Mazzotti. , 2009. Effect of temperature on the nucleation kinetics of alfa L-glutamic acid. *Journal of Crystal Growth* 311: 1178-1184.
- Mullin, J. W., 2001. *Crystallization*. 4 ed: Butterwoth-Heinemann.
- Mullin, J. W., and G. L. Leci. , 1969. Some nucleation characteristics of aqueous citric acid solutions. *Journal of Crystal Growth* 5: 75-76.
- Ohtaki, H., 1998. *Crystallization Processes*. 3 vols. Vol. 3: John Wiley & Sons.
- Olderøy, M., M. Xie, B. Strand, K. Draget, P. Sikorski, and J.-P. Andreassen. , 2010. Polymorph Switching in the Calcium Carbonate System by Well-Defined Alginate Oligomers. *Crystal Growth & Design* 11: 520-529.
- Plummer, L. N., and E. Busenberg. , 1982. The solubilities of calcite, aragonite and vaterite in CO₂-H₂O solutions between 0 and 90°C, and an evaluation of the aqueous model for the system CaCO₃-CO₂-H₂O. *Geochimica et Cosmochimica Acta* 46: 1011-1040.
- Sandengen, K., 2006. *Prediction of Mineral Scale formation in wet gas condensate pipelines and in MEG Regeneration Plants*. Department of Materials Science and Engineering, NTNU.
- Sunagawa, I., 2005. *Crystals: Growth, Morphology and Perfection*: Cambridge University Press.
- Uyeda, J., and K. Kikuchi. , 1990. Low temperature type snow crystals with capped dendrites or plates. *Journal of Crystal Growth* 98 (1-4): 1238-1241.

- Verdoes, D., D. Kashciev, and G. M. Rosmalen. , 1992. Determination of nucleation growth rates from induction times in seeded and unseeded precipitation of calcium carbonate. *Journal of Crystal Growth* 118: 401-413.
- Wang, L., I. Sondi, and E. Matijevic. , 1999. Preparation of Uniform Needle-Like Aragonite Particles by Homogeneous Precipitation *Journal of Colloid and Interface Science* 218: 545-553.
- Wolthers, M., N. Gernot, J. P. Gustafsson, and P. v. Cappellen. , 2012. Calcite growth kinetics: Modeling the effect of solution stiochimetry. *Geochimica et Cosmochimica Acta* 77: 121-134.
- Zeppenfeld, K., 2010. Calcite precipitation from aqueous solutions with different calcium and hydrogen carbonate concentrations. *Journal of Water Supply: Research and Technology - AQUA* 59.8: 482-491.
- Zumdahl, S. S., 2005. *Chemical Principles*. 5 ed: Houghton Mifflin Company.

List of symbols

Symbol	Unit	Name
A	m^2	Surface area
	varies	Pre-exponential kinetic parameter
a	-	Activity
a_{\pm}	-	Mean ionic activity
a^*	-	Activity at equilibrium
c	mol/L	Concentration
c^*	mol/L	Equilibrium concentration
C_l	mol/L	solute concentration
C_p	J/K,mol	Heat capacity
E	v	Electrode potential
E_0	v	Standard electrode potential
G	m/s	Growth rate
	J/mol	Gibbs free energy
ΔG_s	J/mol	Excess free surface energy
ΔG_v	J/mol	Excess free volume energy
ΔG_{crit}	J/mol	Gibbs free energy according to a critical radius
g	-	Order of growth
IAP	$(mol/L)^2$	Ionic activity product
J	$mol/m^3,s$	Nucleation rate
	$\#/ m^3,s$	
K_G	-	Overall mass growth rate
K_d	-	Mass transfer coefficient by diffusion
K_d	-	Mass transfer coefficient by reaction
K_{sp}	mol/L	Equilibrium solubility product
K_r	m^3/s	Growth rate constant
k	J/K	Boltzman constant
L	m	Length of a nucleus
M	g/mol	Molecular weight
m	g	Mass
n	mol	Mole
R	J/mol,K	Universal gas constant
r	m	Radius
S	-	Supersaturation ratio
SR	-	Supersaturation ratio
T	K/ °C	Temperature
t	s	Time
t_g	s	Time it takes to grow to detectable size

t_{ind}	s	Induction time
t_n	s	Time to form a stable nucleus
t_r	s	Relaxation time
V	m^3	Volume
v	m^3/mol	Molecular volume
z_i	-	Charge number of specie i
IAP	-	Ion activity product
α	-	Parameter describing ratio of the first observable particle
	-	Activity coefficient
γ	N/m	Interfacial tension between liquid and crystal
γ_{\pm}	-	Mean activity coefficient
ϕ	-	Factor between G for homogeneous and heterogeneous nucleation
μ	J/mol	Chemical potential
ν	-	Number of moles in one mole electrolytic solution
τ	s	Residence time
θ	$^{\circ}$	Contact angle
#	-	Number of particles

Appendix A: Raw data for all experiments

All concentrations have the denomination *mmol/kg solvent* and were found by using MultiScale.

Table appendix 1: Raw data for experiments with CO₂-bubbling and an initial concentration of Ca²⁺ of 5 mmol/kg solvent

Experiment	SR exact	C _{NaOH}	C _{CaCl2}	Alkalinity	Initial pH	Temperature [°C]	w% MEG
20-40-0	20,03	118,0	5	118,0	6,90	40	0
25-40-0	24,98	141,0	5	141,0	6,97	40	0
30-40-0	30,04	164,5	5	164,5	7,03	40	0
35-40-0	34,94	187,5	5	187,5	7,08	40	0
40-40-0	40,00	211,5	5	211,5	7,12	40	0
70-40-0	69,99	363,5	5	363,5	7,33	40	0
93-40-0	93,65	498,5	5	498,5	7,44	40	0
20-40-40	19,92	74,0	5	74,0	7,01	40	40
30-40-40	29,96	100,5	5	100,5	7,13	40	40
40-40-40	39,99	126,5	5	126,5	7,22	40	40
70-40-40	69,96	206,0	5	206,0	7,40	40	40
99-40-40	99,89	292	5	292	7,54	40	40
40-40-80	40,09	60,5	5	60,5	7,48	40	80
70-40-80	69,88	92,2	5	92,2	7,65	40	80
20-70-0	19,90	38,5	5	38,5	6,79	70	0
30-70-0	29,98	51,5	5	51,5	6,91	70	0
40-70-0	40,01	64,1	5	64,1	7,00	70	0
70-70-0	70,00	102,9	5	102,9	7,18	70	0
20-70-40	19,77	23,6	5	23,6	6,90	70	40
30-70-40	30,03	31,0	5	31,0	7,01	70	40
40-70-40	40,07	37,8	5	37,8	7,09	70	40
70-40-40	70,04	57,4	5	57,4	7,26	70	40
40-70-80	40,01	19,95	5	19,95	7,36	70	80
70-70-80	70,05	29,1	5	29,1	7,51	70	80

Table appendix 2: Raw data for 40-40-0 experiment with CO₂-bubbling and varying activity ratio of Ca²⁺ and CO₃²⁻

SR exact	Initial pH	C _{CaCl2}	C _{Ca²⁺, free}	a _{Ca²⁺}	C _{NaOH}	C _{CO3²⁻}	a _{CO3²⁻}	γ	a _{Ca²⁺} /a _{CO3²⁻}
40,13	7,64	1,38	1,14	0,11	850,0	10,36	0,96	0,09	0,11
40,07	7,39	2,46	2,22	0,32	424,0	2,22	2,32	0,14	1,00
40,00	7,12	5,00	4,76	0,98	211,5	0,50	0,10	0,21	9,60
39,98	6,83	13,00	12,76	3,42	103,5	0,11	0,03	0,27	116
40,14	6,74	20,00	19,76	5,21	81,5	0,07	0,02	0,26	269

Table appendix 3: Raw data for the 40-40-0 experiment with high pH and varying activity ratio of Ca²⁺ and CO₃²⁻

SR exact	Initial pH	C _{CaCl2}	C _{Ca²⁺, free}	a _{Ca²⁺}	C _{Na2CO3}	C _{CO3²⁻}	a _{CO3²⁻}	γ	a _{Ca²⁺} /a _{CO3²⁻}
40,34	10,43	0,38	0,14	0,10	2,51	1,55	1,06	0,68	0,09
40,07	10,12	0,66	0,42	0,32	1,09	0,42	0,32	0,75	1,00
40,08	9,88	1,60	1,14	0,97	0,63	0,15	0,10	0,72	9,39
39,93	9,61	6,00	5,77	3,23	0,44	0,06	0,03	0,56	103

K_{sp} at 40 °C is 2,52·10⁻⁹ mol/kg, obtained from MultiScale.

Appendix B: Chemical data and lab calculations

Table appendix 4: Chemical data and supplier

Chemical	Formula	Purity	Supplier
Calcium carbonate dihydrate	CaCl ₂ ·2H ₂ O	99-103	Fluka
Sodium hydroxide	NaOH		
Sodium carbonate anhydrous	Na ₂ CO ₃	≥99 %	Fluka
Hydrochloric acid (used diluted)	HCl	37 %	Merck

It was assumed that 1 L of the parent solution had a density of $\approx 1000 \text{ kg/m}^3$.

Table appendix 5: Data to calculate mother solutions used in the experiments

	CaCl ₂ ·2H ₂ O	NaOH	Na ₂ CO ₃
Molar mass [g/mol]	147,02	40,00	105,99
Volume parent solution [L]	2	2	1
Concentration [mmol/kg solvent]	100	1000	50
Amount solid to make parent solution [g]	29,40	80,00	5,30
Volume start bulbs [mL]	500	500	500

Appendix C: Extended results

Conductivity measurements versus pH measurements

Plots showing results from both conductivity- and pH measurements for the 40-40-0 experiment can be seen in Figure appendix 1 for the CO₂-bubbling experiment and in Figure appendix 2 for the high pH experiment.

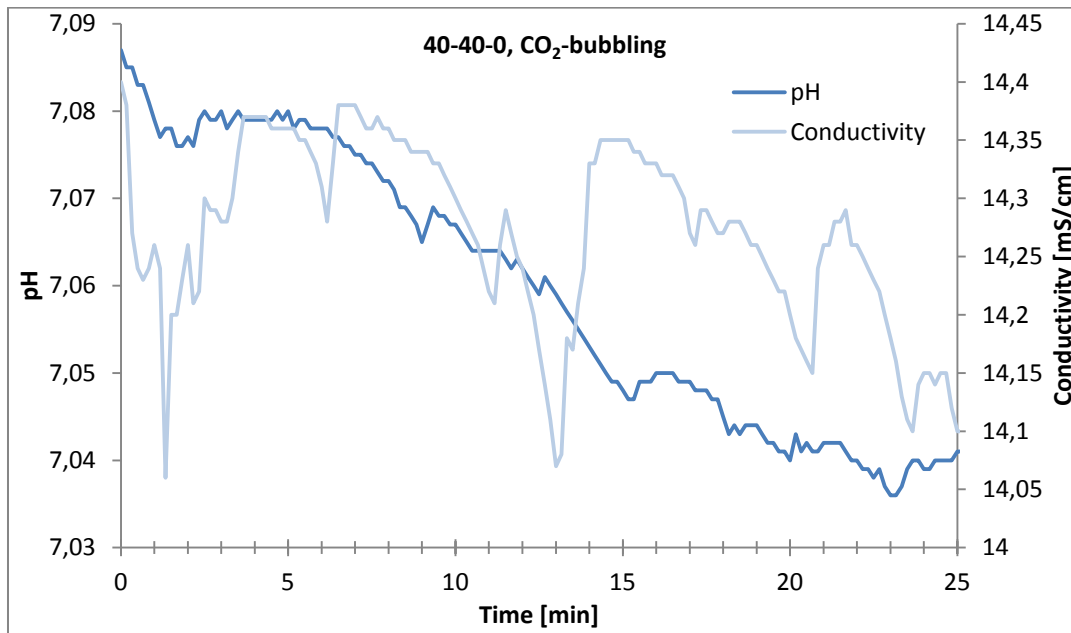


Figure appendix 1: Conductivity measurements versus pH measurements in a 40-40-0 experiment. CO₂-bubbling

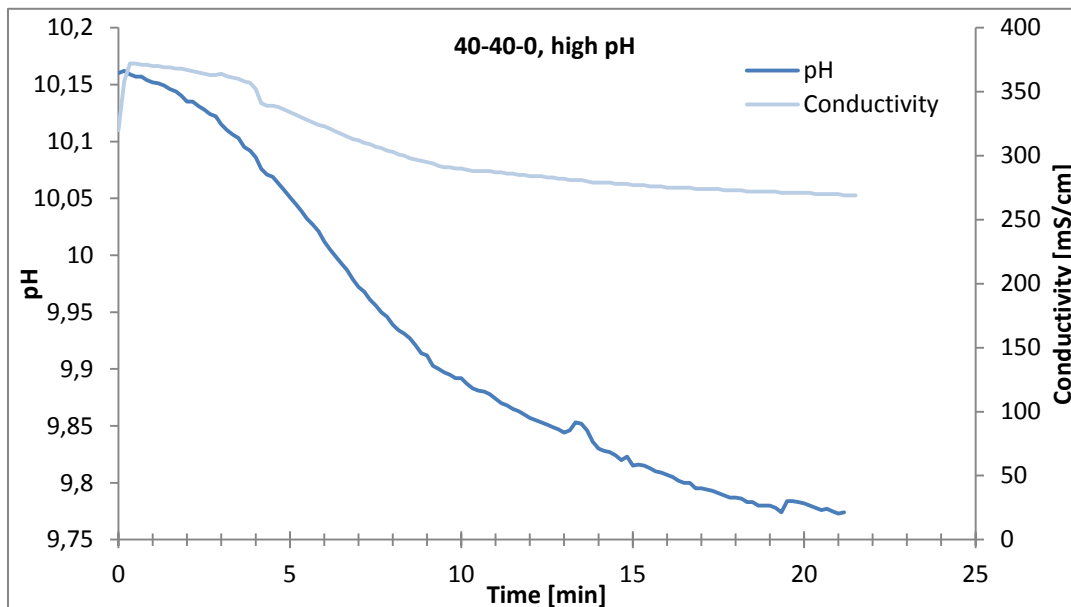


Figure appendix 2: Conductivity measurements versus pH measurements in a 40-40-0 experiment. High pH

Conductivity measurements were more stable for the experiment at high pH than the experiment with CO₂-bubbling. This indicates that CO₂-bubbling in the reactor disturbs the conductivity measurements. The pH measurements were more stable, and an induction time could be determined.

Raw data showing pH plots

A plot obtained directly from the computer logging program is shown in Figure appendix 3.

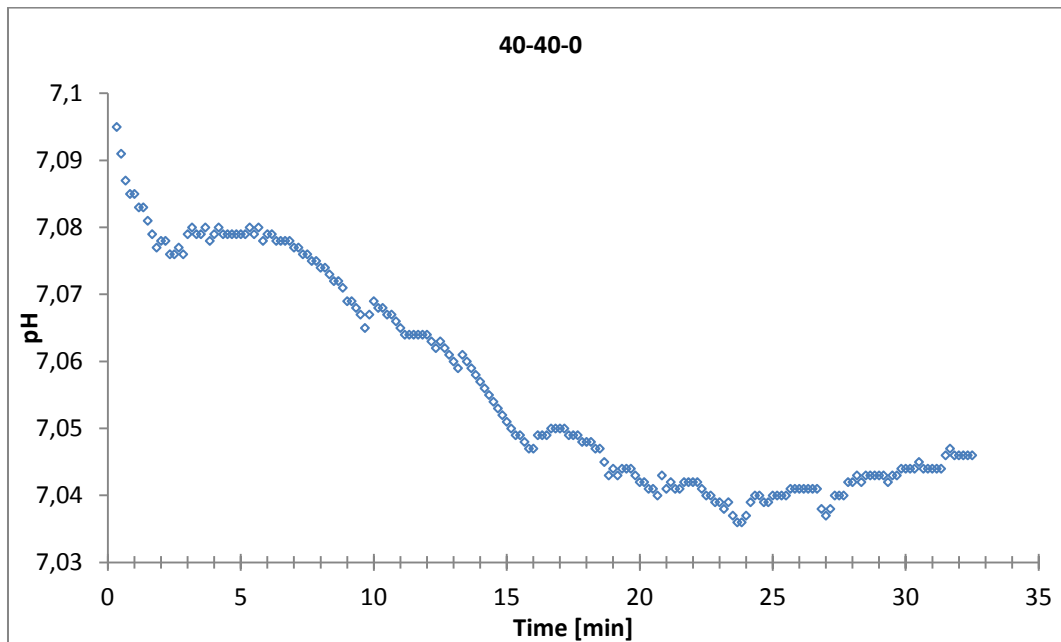


Figure appendix 3: Raw data showing the pH plot for the 40-40-0 experiment

There was a rapid fall in pH in the beginning of the experiment; this was understood as the *mixing time* of the two solutions. Then a plateau appeared, and then the pH started to decrease, indicating that the precipitation had begun. After about 24 minutes, the curve started to flatten out, indicating that the supersaturation in the solution was consumed. After 26 minutes, the pH curve started to increase again. This may be because of how the equilibrium changed when the supersaturation was consumed.

The experiments done in this master thesis were stopped when the curve flattened out.

Induction times with varying SR, temperature and w% MEG

The pH plots used to determine the induction times at the different conditions can be seen in Figure appendix 4-Figure appendix 8.

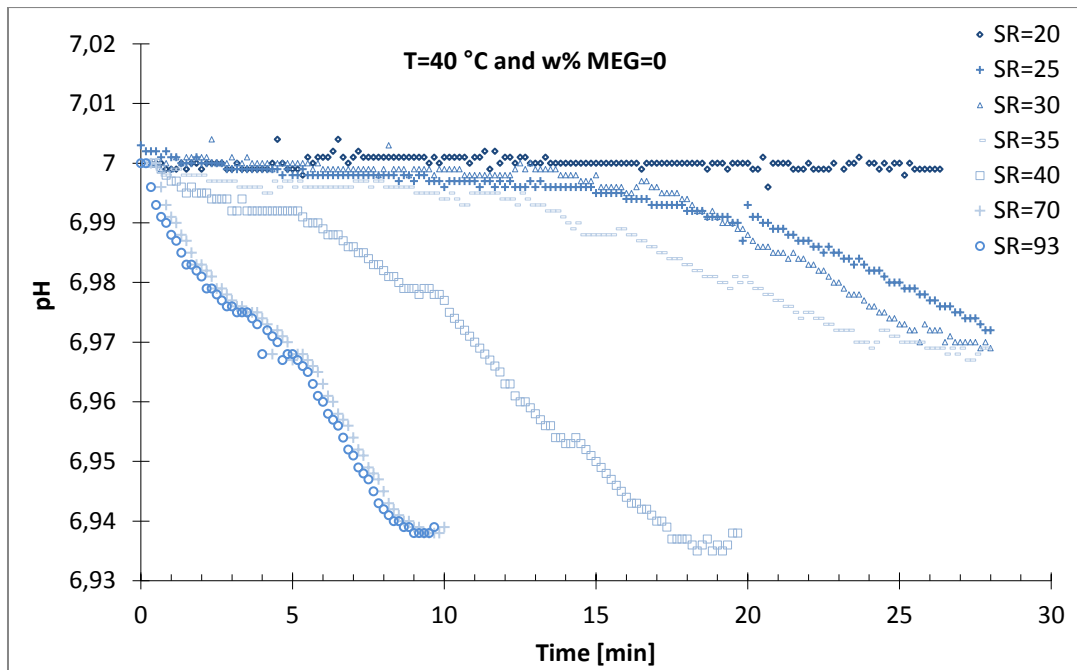


Figure appendix 4: Drop in pH at 40 °C and w% MEG=0

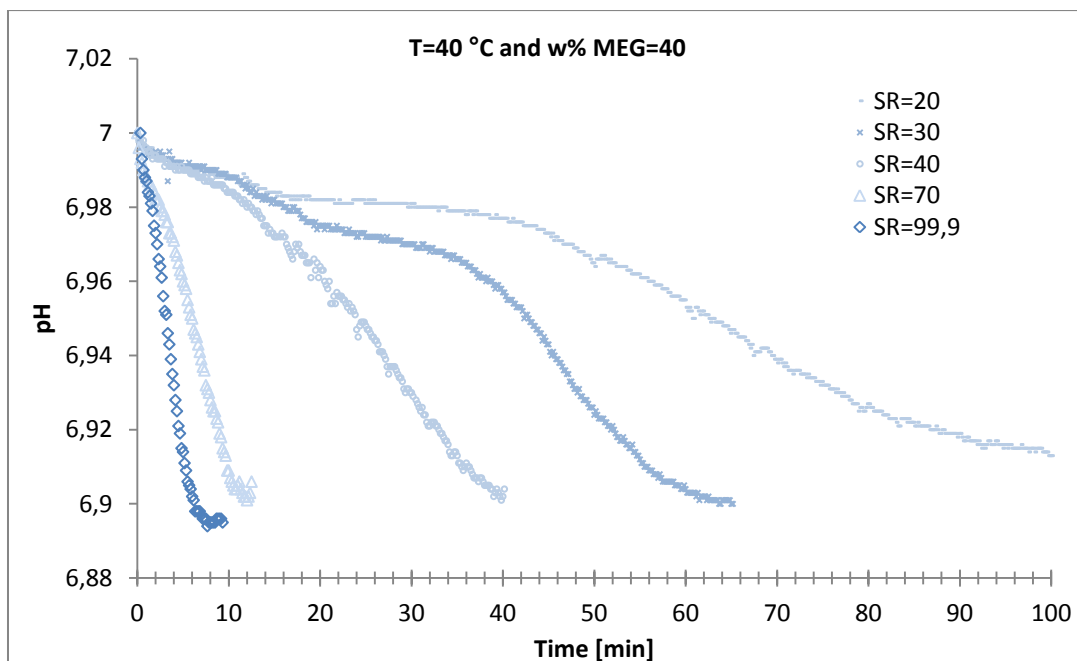


Figure appendix 5: Drop in pH at 40 °C and w% MEG=40

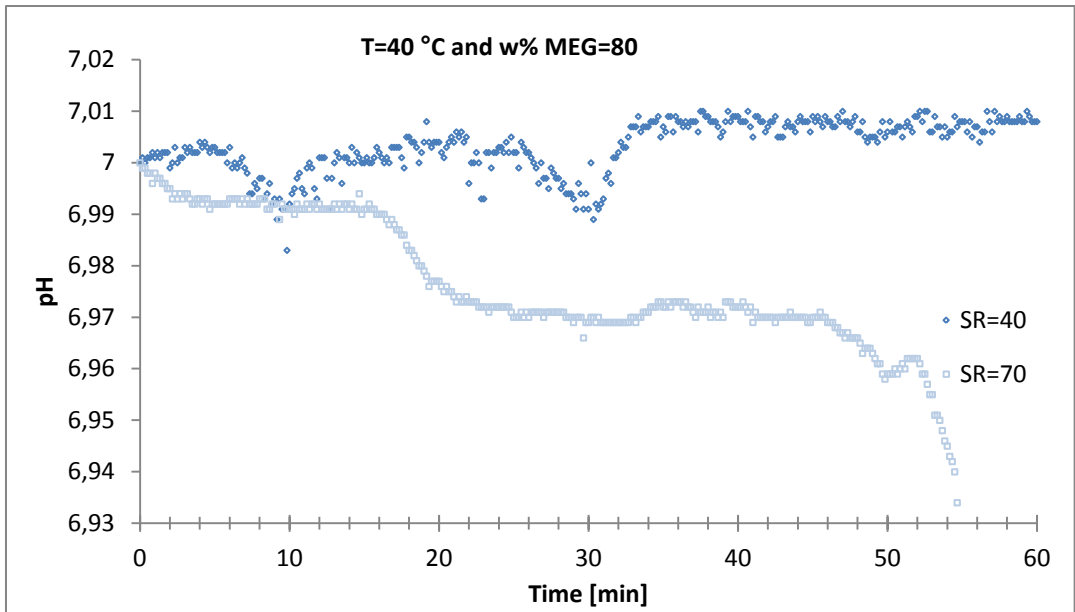


Figure appendix 6: Drop in pH at 40 °C and w% MEG=80

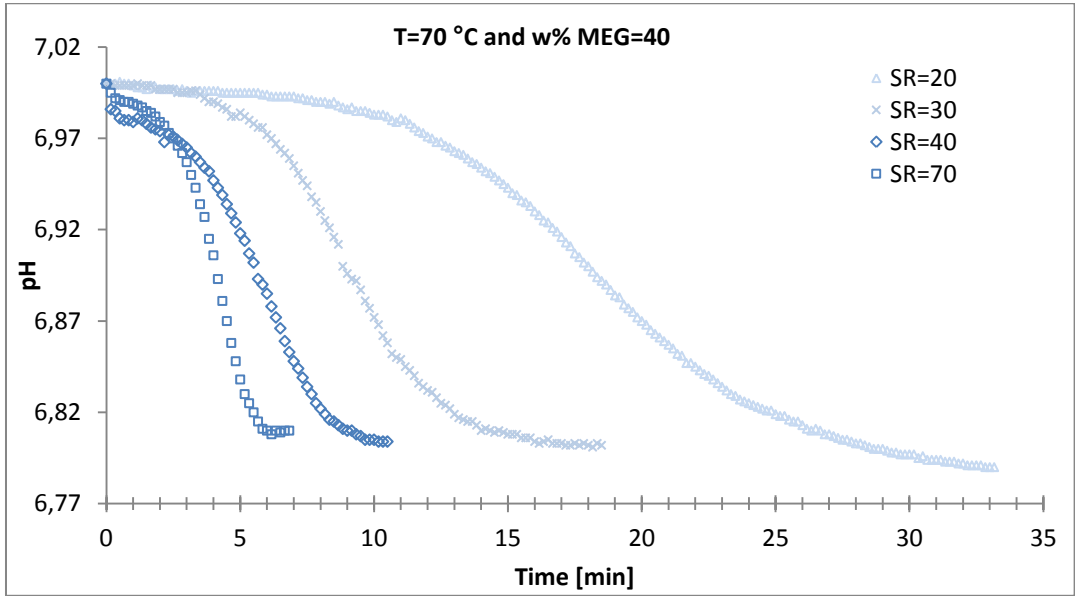


Figure appendix 7: Drop in pH at 70 °C and w% MEG=40

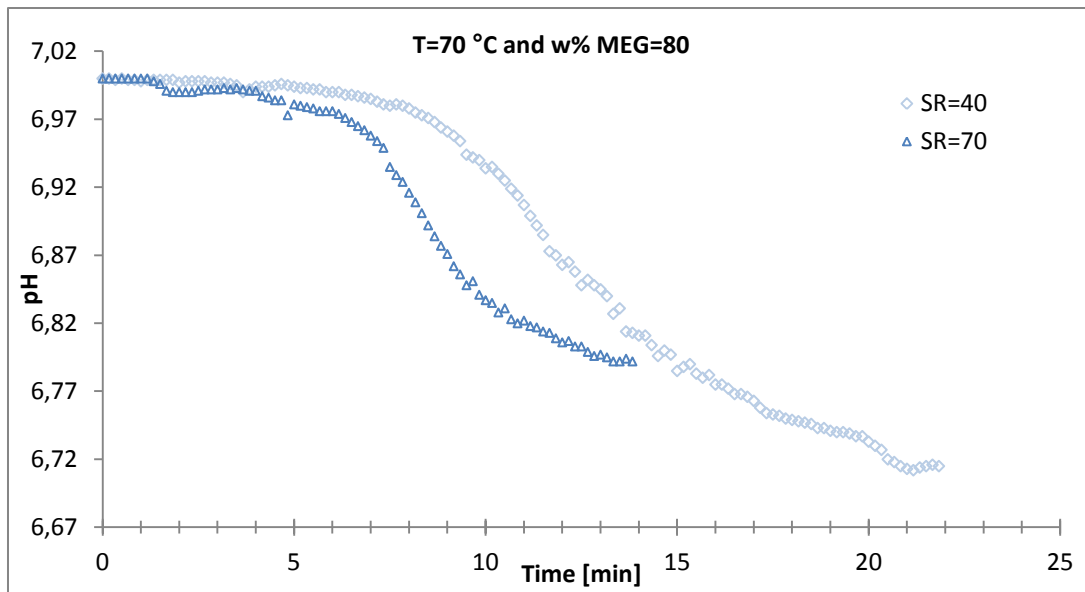


Figure appendix 8: Drop in pH at 70 °C and w% MEG=80

Induction time determination

The induction times were determined based on the method described in section 2.2.3. In Figure appendix 9, the method used to determine the induction time was shown for the 40-70-0 experiment.

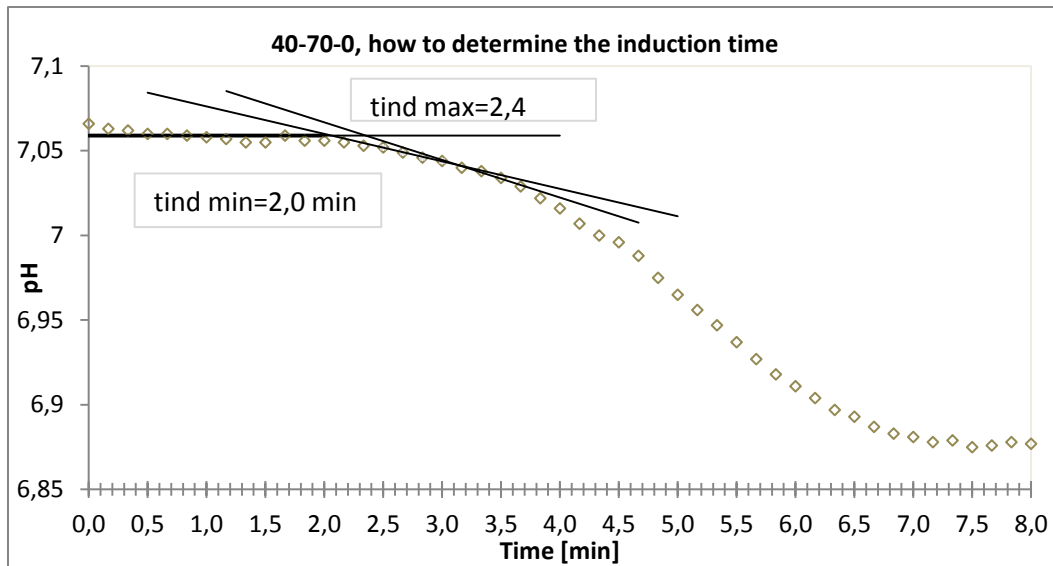


Figure appendix 9: Induction time determination from experimental data

The average induction time determined was 2,2 minutes and the uncertainty in induction time for the current experiment by using this method was $\pm 0,2$ minutes.

Induction times in one plot

All the induction times determined experimentally are shown in Figure appendix 10.

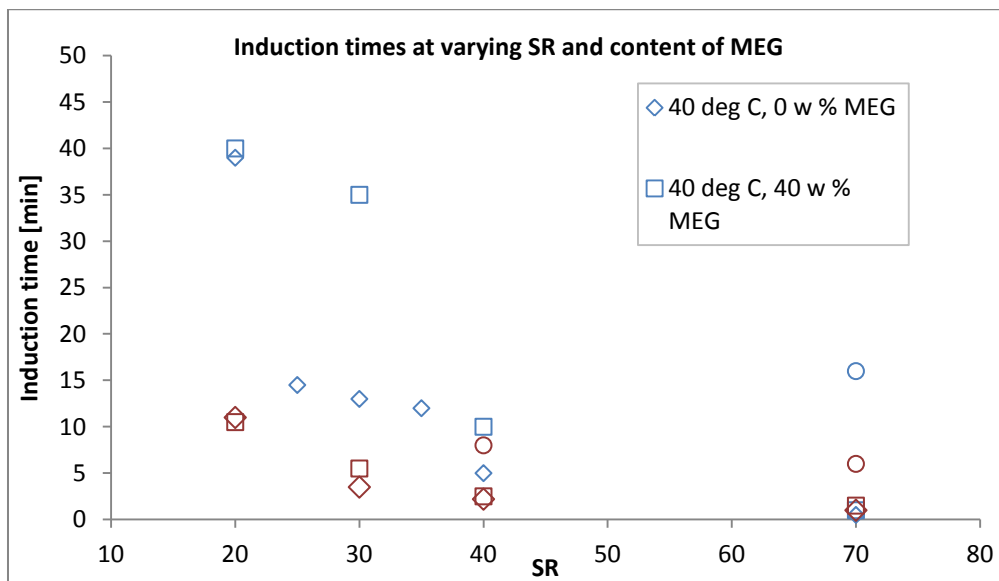


Figure appendix 11: Induction times as a function of SR for all experiments

The induction time set as 120 minutes for the 40-40-80 experiment was left out of Figure appendix 11.

Appendix D: Uncertainties in the experiments

Uncertainty of SR in relation to temperature

As described in the theory, supersaturation is highly dependent on temperature, and in Figure appendix 12 it can be seen how the SR changed when the set-temperature varied with ± 3 °C. The SR at different temperatures was found by using MultiScale.

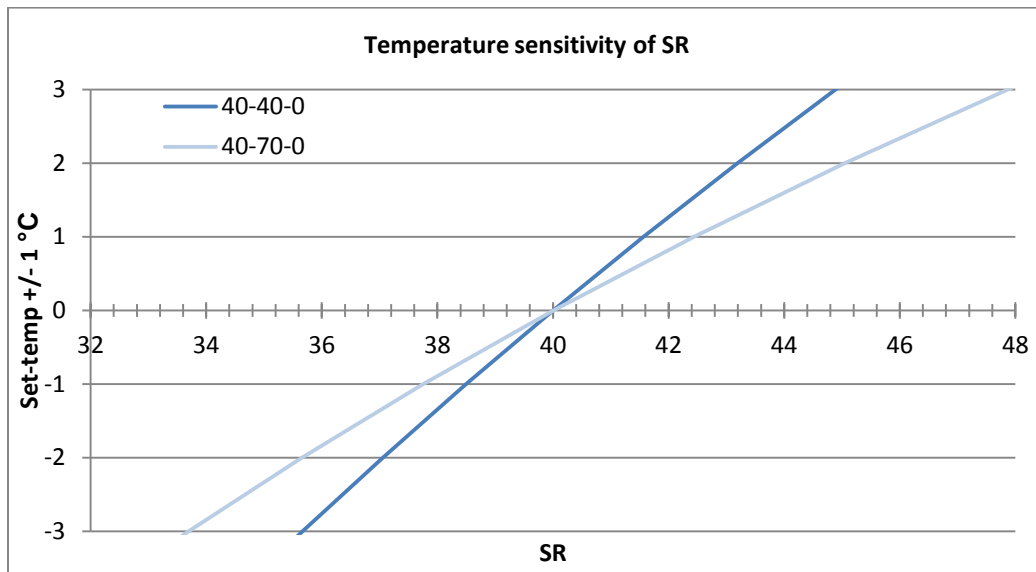


Figure appendix 12: Temperature sensitivity of SR

Two experiments with the wanted supersaturation ratio of 40 and no MEG added can be seen plotted in Figure appendix 12. The dark blue line is for 40 °C, and the light blue line is for 70 °C. As seen from the figure, by varying the temperature with -1 °C, the SR changed from 40 to 38,5 at 39 °C, and from 40 to 37,8 at 69 °C. This shows that temperature control was important in order to get the SR wanted in the experiments.

Figure appendix 12 shows that SR was more sensitive to the temperature at 70 °C, than at 40 °C. This observation follows classical crystallization theory which says that the dependency of SR in relation to temperature increases with increasing temperature (Mullin, 2001).

The temperature development through two experiments were done; one at 40 °C and one at 70 °C. The results can be seen in Figure appendix 13.

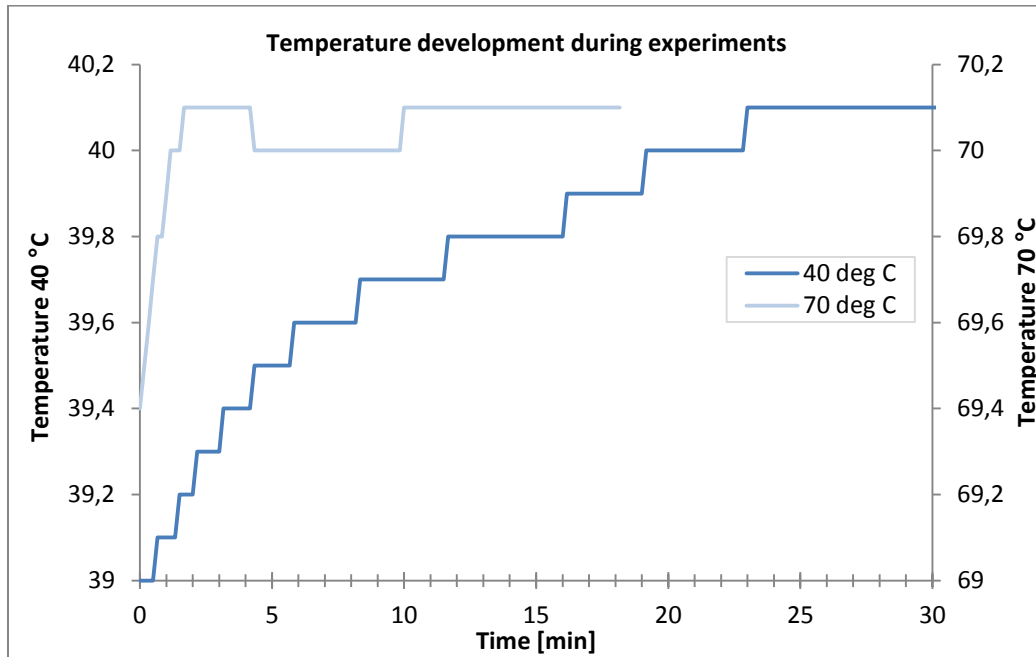


Figure appendix 13: Temperature development in experiments at 40 °C and 70 °C

It was found that the experiments followed the temperature of 40 ± 1 °C and $70 \pm 0,6$ °C. This deviation from set temperature gave some variation in the supersaturation during the experiment. This error was considered minimal, because the change in SR was < 10 % during the experiments. Consequently, this error was neglected.

Absorption of CO₂ in the solution

To verify that the CO₂ in the liquid phase and the CO₂ in the gas phase were at equilibrium, an experiment was done to check if the decrease in pH only was due to precipitation of CaCO₃ or if it was partly because of interactions between CO₂ in the gas phase and in the liquid phase.

One solution of NaOH was prepared as usual for the 40-40-0, experiment, but mixed with water in the reactor instead of CaCl₂. The pH was logged for 25 minutes, and the resulting plot compared to the pH plot for a regular 40-40-0 experiment is shown in Figure appendix 14.

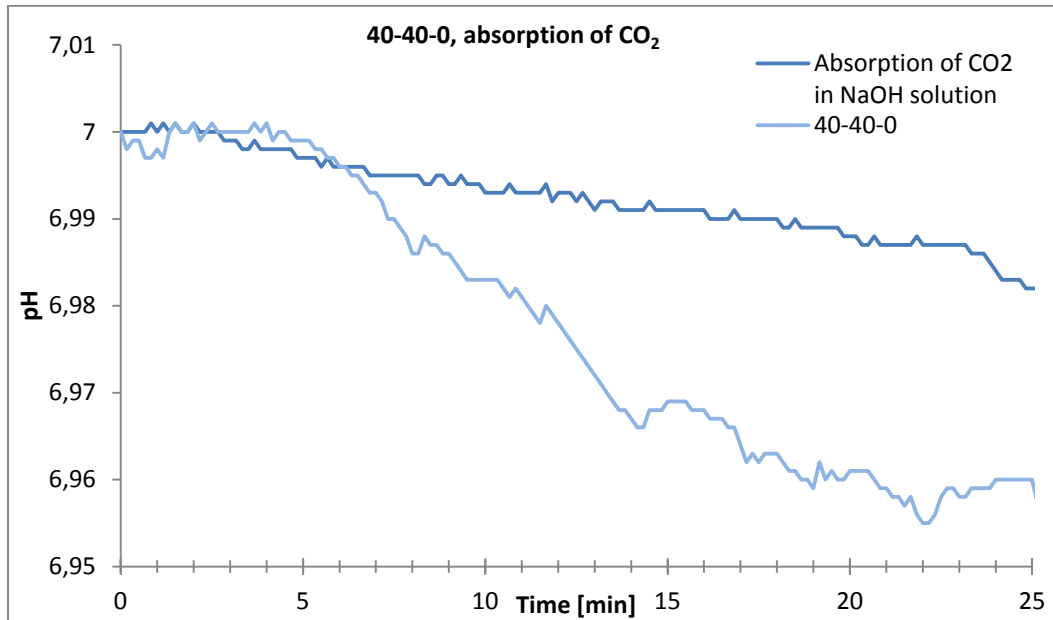


Figure appendix 14: Absorption of CO₂ in the liquid phase

The difference in pH due to atmospheric interactions was 0,018, and the difference in pH in the regular experiment was 0,035. This indicated that as much as 51,4 % of the decrease in pH could be due to absorption of CO₂ in the liquid phase. But because the importance of this master thesis was the *change* in slope to find the induction time, this source of error can be ignored. But it is important to be aware of this uncertainty if the difference in pH between initial- and equilibrium conditions is to be used.

Reproducibility in the 40-40-0 experiment

The experiments were adjusted to start at a pH of 7, to more easily compare the different induction times.

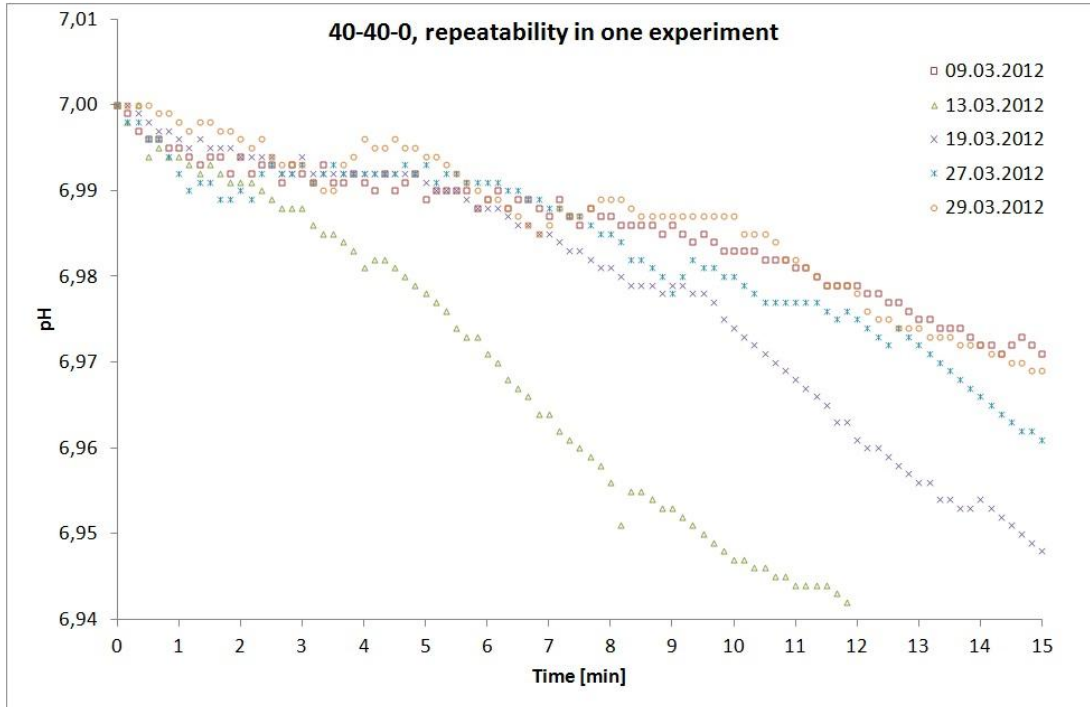


Figure appendix 15: Reproducibility in the 40-40-0 experiment

Comparison of pH-data in the reproducibility experiments are displayed in Table appendix 6.

Table appendix 6: Comparison pH in the repeatability experiments, 40-40-0

Experiment (date)	Initial pH	Equilibrium pH	Δ pH	Theoretical pH_i	Theoretical pH_{eq}	Δ pH theoretical
09.03.12	7,052	7,023	0,029	7,123	7,107	0,016
13.03.12	7,054	6,996	0,058			
19.03.12	7,103	7,038	0,065			
27.13.12	7,087	7,036	0,051			
29.03.12	7,115	7,038	0,067			

The theoretical values of pH were obtained from MultiScale. The difference in pH in the performed experiments was higher than the theoretical difference in pH at these conditions. This indicated that the pH dropped more than expected, probably due to leakage in the reactor giving an increase in the pH drop, as shown in the previous paragraph.

Experimental errors

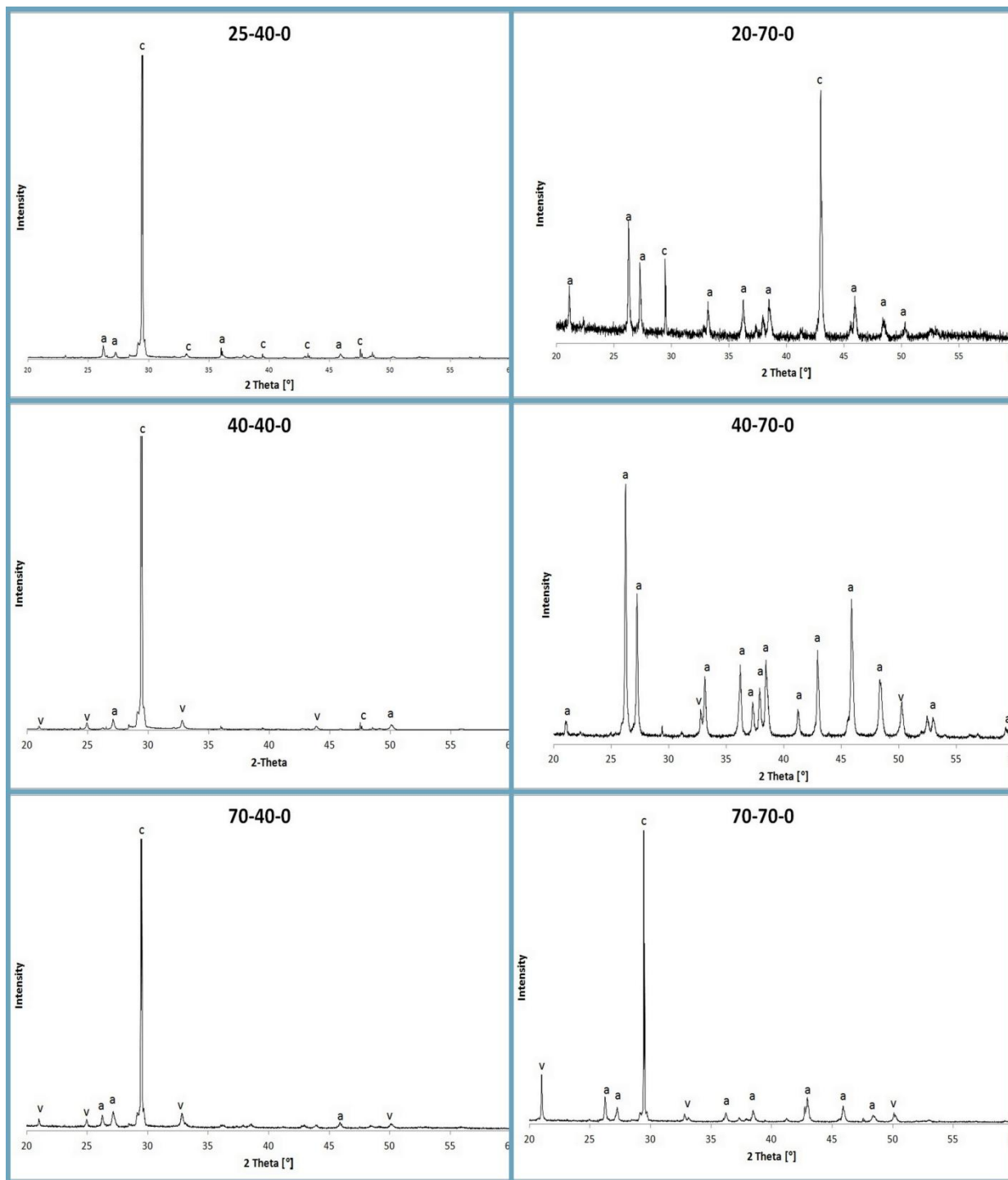
When working with experimental data there will always be different sources of errors, leading to uncertainty in the documented data. In the experiments performed in this master thesis, there were different factors of uncertainty, both experimental and in relation to the nucleation mechanism.

Experimental errors may be systematic or random (Førland, 2001). In this experiment systematic errors have been neglected because the same operator has done all the experiments and any systematic errors can be considered the same for all the experiments.

Random errors give imprecise results and may be differences in concentration, present corrosion in the solution, the stirring of the propeller, uncertainty in the nucleation mechanism or/and treatment of the experimental data. The uncertainty regarding differences in initial concentrations was minimized by using parent solutions as source of calcium and carbonate, see Appendix B. This was done in order to get as accurate concentrations as possible, since weighing out powder gives rise to uncertainty. The uncertainty regarding corrosion was minimized by using equipment made of Teflon in the reactor. The stirring was held constant at a rate of 500 rpm in all experiments. When the intersection between two parts of the pH curve was to be determined, there was an uncertainty regarding the method being used. Because the same operator has determined all the intersections in these experiments, this uncertainty has been considered to be minimized as well.

Earlier studies by Jiang and Horst showed that there is a stochastic variation within the nucleation mechanism in one experiment done in parallels (2011). They concluded that fluctuation in temperature in the experiments impacted the supersaturation in the solution, and further the induction time. This uncertainty was not studied in this master thesis, but the error regarding variation in the nucleation mechanism was a part of the standard deviation.

Appendix E: XRD results



Appendix F: Calculations

Amount extracted from parent solutions

One example of how much that was extracted from the parent solution is shown for the 40-40-0 experiment with CO₂-bubbling and an activity ratio of 9,6. The results are displayed in Table appendix 7.

Table appendix 7: Calculation of how much that was extracted from the parent solutions in the 40-40-0 experiment

	CaCl ₂ ·2H ₂ O	NaOH
In reactor [mmol/kg solvent]	5,0	211,5
Concentration start bulbs [mmol/kg solvent]	10,0	423,0
Taken from parent solution [g]	50,00	211,50
Deionized water added [g]	450,00	288,50
Volume start bulbs [mL]	500	500

1 L parent solution ≈ 1 kg parent solution

Activity ratios between Ca²⁺ and CO₃²⁻

An example of the calculation of the activity coefficient, γ_{\pm} , and the activity ratio between calcium and carbonate, is shown below. The demonstrating experiment is the 40-40-0 experiment with CO₂-bubbling and an initial concentration of Ca²⁺ of 2,46 mmol/kg solvent.

$$\gamma_{\pm} = \sqrt{\frac{K_{sp} \cdot SR}{c_{Ca^{2+}, free} \cdot c_{CO_3^{2-}}}}$$

$$\gamma_{\pm} = \sqrt{\frac{2,52 \cdot 10^{-9} \text{ mol} / \text{kg} \cdot 40,07}{(2,22 \cdot 2,22) \cdot 10^{-3} \text{ mol} / \text{kgsolvent}}} = 0,14$$

$$a_{Ca^{2+}} / a_{CO_3^{2-}} = \frac{a_{Ca^{2+}}}{a_{CO_3^{2-}}} = \frac{(c_{Ca^{2+}, free} \cdot \gamma_{\pm})}{(c_{CO_3^{2-}} \cdot \gamma_{\pm})} = \frac{(2,22 \text{ mmol} / \text{kgsolv} \cdot 0,14)}{(2,22 \text{ mmol} / \text{kgsolv} \cdot 0,14)} = 1,00$$

Growth rate

The growth rate with respect to vaterite was calculated. One example of the 40-40-40 experiment is shown below:

$$G(T, w\% MEG) = (-4,8 \cdot 10^{-9} + 2,6 \cdot 10^{-11} \cdot T - 2,3 \cdot 10^{-11} \cdot w\% MEG) \cdot (S_v - 1)^2$$
$$G = (-4,8 \cdot 10^{-9} + 2,6 \cdot 10^{-11} \cdot (40 + 273) - 2,3 \cdot 10^{-11} \cdot 40) \cdot (3,33 - 1)^2 = 13,11 \text{ nm} / \text{s}$$

The relation between SR and the corresponding supersaturations with respect to each of the polymorphs is displayed in Table appendix 8.

Table appendix 8: Relation between SR and the supersaturations based on each of the polymorphs

SR	S_c	S_v	S_a
20	4,5	2,4	3,8
25	5,0	2,6	4,2
30	5,5	2,9	4,6
35	5,9	3,1	5,0
40	6,3	3,3	5,3
70	8,4	4,4	7,0
93	9,6	5,1	8,1

Nucleation rate based on results in this master thesis

The nucleation rates in the different experiments were calculated, and one example of such a calculation can be seen below for the 70-40-0 experiment where the nucleation rate was calculated with respect to vaterite:

$$J = \frac{3\alpha}{t_{ind}^4 \pi G^3}$$
$$J_{(70-40-0)} = \frac{3 \cdot 10^{-8}}{30 \text{ s}^4 \cdot \pi \cdot (3,88 \cdot 10^{-8} \text{ m} / \text{s})^3} = 2,04 \cdot 10^8 \text{ \#} / \text{m}^3 \text{ s}$$

Standard deviation

The uncertainty in the 40-40-0 experiment was calculated on the basis of the average induction time determined in the 5 parallels. The standard deviation to the mean average induction time was found:

$$t_{ind}(average) = \frac{\sum_{i=1}^n t_{ind_i}}{n}$$

$$t_{ind}(average) = \frac{(6+1+5+5+8) \text{ min}}{5} = 5 \text{ min}$$

$$\sigma = \sqrt{\frac{1}{n-1} \left(\sum_{i=1}^n (t_{ind_i} - t_{ind_{average}})^2 \right)}$$

$$\sigma = \sqrt{\frac{(6-5)^2 + (1-5)^2 + (5-5)^2 + (5-5)^2 + (8-5)^2}{4}} = 2,6 \text{ min}$$

Appendix G: Analysis equipment

MultiMEGScale7.0

MultiMEGScale, referred to as MultiScale in the report, is a simulation tool working with respect to equilibrium between compounds. MultiScale is based on the Pitzer model and solubility measurements of calcite. It was designed to predict pH, multiphase equilibrium and possible scale formation during oil and gas recovery and transport. The input data is temperature, initial concentrations, content of MEG and alkalinity in the system.

SEM (Scanning Electron Microscope)

For SEM analysis, a Hitachi S-3400 N scanning electron microscope was utilized. For filter samples, a small piece of the filter was fastened to a metal stub by double sided carbon tape. For samples with enough precipitated powder, the powder was poured straight onto the carbon tape. An Edwards Sputter Coater S150B was used to coat the samples with gold. The settings used in SEM were a pressure of 40 Pa, voltage at either 15 or 20 kV, emission current of 35 mA and working distance about 5 mm.


XRD (powder X-Ray Diffraction)

XRD-spectra were made by using a D8-Focus diffractometer. The powder was poured from the filter paper and diluted with ethanol in a mortar. The mix of wetted powder and ethanol was dripped on a single crystal silicon sample holder by using a pipette. The sample was analyzed when the ethanol had vaporized.

Titration unit

Calcium titration with EDTA of the withdrawn bulk samples was performed by a Mettler Toledo DL53 titrator unit. About 5 mL 10 % HCl was added to the sample in order to dissolve eventual precipitated calcium. About 2 mL ammonia/ammonium buffer solution was then added to give a pH about 10. The calcium concentration was determined by amount of EDTA required to reach the titration end point, and the weight of the initial sample.

Appendix H: Risk assessment form

NTNU		Risk assessment			Utarbeidet av		Nummer		Dato	
					HMS-avd.		HMSRV2603		04.02.2011	
HMS/KS					Godkjent av		Side		Erstatter	
Unit:					Kjemisk prosess teknologi		Date:		07.10.2011	
Line manager:					Øyvind Gregersen					
Participants in the identification process (including their function):					Jens-Petter Andreassen, veileder og Astrid Omland Barland, deltaker					
Signatures:									0	
ID no.	Activity from the identification process form	Potential undesirable incident/strain	Likelihood: Likelihood (1-5)	Consequence:			Risk value	Comments/status Suggested measures		
1	HCl	Søl, sprut på hud, klær eller i øye	3	Human (A-E)	Environment (A-E)	Economy/material (A-E)	Human			
2	MEG	Søl, sprut på hud, klær eller i øye	3	A	A		A3	Brak avtrekk		
3	NaOH	Søl, sprut på hud, klær eller i øye	3	A	A		A3			
4	Glassutstyr	Knusing av glass	2	B			B2			
5	Grassylinder med CO2	Trykk overstiger tålegrense for labutstyr	3	A			A3			
6	Vannbad/Gummislanger	Brennskader ved høy temperatur	3	A			A3			
7										
8										